Reduced Cementitious Material in Optimized Concrete Mixtures

NRRA RIGID PAVEMENT TEAM

A pooled fund project administered by the Minnesota Department of Transportation

NRRA Report No. 202102

NRRA National Road Research Alliance

DEPARTMENT OF TRANSPORTATION

To request this document in an alternative format, such as braille or large print, call 651-366-4718 or 1-800-657-3774 (Greater Minnesota) or email your request to ADArequest.dot@state.mn.us. Please request at least one week in advance.

Technical Report Documentation Page

1. Report No.	2.	3. Recipients Accession No.	
NRRA202102			
4. Title and Subtitle Reduced Cementitious Material in Optimized Concrete Mixtures		5. Report Date March 2021 6.	
7. Author(s) Peter Taylor, Seyedhamed Sadati		8. Performing Organization Report No.	
9. Performing Organization Name and Address National Concrete Pavement Technology Center Iowa State University 2711 South Loop Drive, Suite 4700 Ames, IA 50010		10. Project/Task/Work Unit No. 11. Contract (C) or Grant (G) No. (c) 1003320 (wo) 3	
12. Sponsoring Organization Name and Address National Road Research Alliance Minnesota Department of Transportation 395 John Ireland Boulevard, MS 330 St. Paul, Minnesota 55155-1899		13. Type of Report and Period Covered Final Report 14. Sponsoring Agency Code	
15. Supplementary Notes http://mndot.gov/research/reports/2021/NRRA202102.pdf			

16. Abstract (Limit: 250 words)

This document reports the activities and observations of a research team that performed on-site and laboratory testing of concrete mixtures with reduced cementitious materials content placed in two cells at the MnROAD facility in Albertville, Minnesota.

The overall objectives of this research project included investigating the early age characteristics of concrete paving mixes containing reduced cementitious contents as well as their long-term performance.

It was observed that while workability was marginal in the mixture proportioned with 470 lb/yd3, all other properties of the test sections were similar to those of the control section.

17. Document Analysis/Descriptors		18. Availability Statement	
Cement, pavement performance		No restrictions. Document available from: National Technical Information Services, Alexandria, Virginia 22312	
19. Security Class (this report)	20. Security Class (this page)	21. No. of Pages	22. Price
Unclassified	Unclassified	163	

REDUCED CEMENTITIOUS MATERIAL IN OPTIMIZED CONCRETE MIXTURES

FINAL REPORT

Prepared by:

Peter Taylor
Seyedhamed Sadati
National Concrete Pavement Technology Center
Iowa State University

MARCH 2021

Published by:

Minnesota Department of Transportation
Office of Research & Innovation
395 John Ireland Boulevard, MS 330
St. Paul, Minnesota 55155-1899

ACKNOWLEDGMENTS

The research team would like to express its gratitude to the Minnesota Department of Transportation (MnDOT) for sponsoring this research, providing data, and working with the research team. Thanks also go to the National Road Research Alliance (NRRA) for supporting this work.

TABLE OF CONTENTS

LIST OF FIGURES

LIST OF TABLES

EXECUTIVE SUMMARY

Mixture proportioning generally uses a recipe based on a previously produced concrete, rather than adjusting the proportions based on the needs of the mixture and locally available materials. As budgets grow tighter and environmental regulations increase, an emphasis on lowering the carbon footprint is focusing attention on making mixtures that are more efficient in their use of materials yet do not compromise engineering performance. One means of reducing environmental impact is to reduce the amount of binder in the mixture.

This document reports the activities and observations of a research team that performed on-site and laboratory testing of concrete mixtures with reduced cementitious materials content placed in two cells at the MnROAD facility in Albertville, Minnesota. Concrete paving mixtures with "low" cementitious content, i.e., 500 lb/yd3, and "lower" cementitious content, i.e., 470 lb/yd3, were used in two otherwise identical sections in cells 138 and 238. Each cell is about 260 feet long.

The overall objectives of this research project include:

- Investigate the early age characteristics (e.g., placement issues, strength gain rate, cracking risk) of concrete paving mixes containing reduced cementitious contents
- Assess causes of, or potential for, durability issues with reduced cementitious contents
- Identify the effect of reduced cementitious content on long-term serviceability and economics of concrete pavements
- Develop recommended specifications for the use of reduced cementitious content concrete paving mixes

Based on the work conducted, the following findings are noted:

1. Results obtained from the work indicated that all properties were acceptable in the 500 lb/yd^3 section. Workability was marginal in the mixture proportioned with 470 lb/yd^3, although in all other aspects, the section performed satisfactorily.

2. Data from testing using the MIRA indicate that there are no signs of insufficient mixing or structural distress in the different sections.

3. No signs of early age materials related distress were observed that could be attributed to the reduced cementitious materials content. Distress observed in cell 238 was attributed to segregation that exacerbated cracking adjacent to a transverse crack induced by a utility line.

4. Both test sections performed well with respect to Iinternational Roughness Index (IRI) and Load Transfer Efficiency (LTE), and slightly better than the control section, largely due to differences in thickness and age.

5. Comparable wear depth was observed for all three sections. Surface macro texture measurements exhibited comparable numbers for all three cells, with a slightly higher rate of increase for the trafficked lane.

6. Results suggest that given a proper mixture proportioning methodology, it will be possible to develop environmentally friendly concrete mixtures with reduced cementitious materials content, reduced carbon footprint, and reduced cost, without any negative impacts on the quality of construction and long-term durability.

7. A mixture proportioning methodology is suggested to provide long-lasting mixtures without excess cementitious materials in the mixture.

CHAPTER 1: INTRODUCTION

1.1 PROBLEM STATEMENT

Mixture proportioning generally uses a recipe based on a previously produced concrete, rather than adjusting the proportions based on the needs of the mixture and locally available materials. As budgets grow tighter and environmental regulations increase, an emphasis on lowering the carbon footprint is focusing attention on making mixtures that are more efficient in their use of materials yet do not compromise engineering performance. One means of reducing environmental impact is to reduce the amount of binder in the mixture.

This document reports the activities and observations of a research team that performed on-site and laboratory testing of concrete mixtures with reduced cementitious materials content placed in two cells at the MnROAD facility in Albertville, Minnesota. Concrete paving mixtures with "low" cementitious content, i.e., 500 lb/yd3, and "lower" cementitious content, i.e., 470 lb/yd3, were used in two otherwise identical sections in cells 138 and 238. Each cell is about 260 feet long.

The primary goal of this work is to monitor the constructability and longevity of the concrete mixtures with reduced cementitious material content.

1.2 RESEARCH OBJECTIVES

The overall objectives of this research project include:

- Investigate the early age characteristics (e.g., placement issues, strength gain rate, cracking risk) of concrete paving mixes containing reduced cementitious contents
- Assess causes of, or potential for, durability issues with reduced cementitious contents
- Identify the effect of reduced cementitious content on long-term serviceability and economics of concrete pavements
- Develop recommended specifications for the use of reduced cementitious content concrete paving mixes

1.3 PROJECT INFORMATION

The present project investigates the performance of two test cells (138 and 238) constructed with optimized concrete mixtures at the MnROAD pavement research facility. Located in Albertville, 40 miles northwest of Saint Paul, Minnesota, the MnROAD research facility consists of two distinct segments of roadway: the Mainline (ML) and the Low Volume Road (LVR). MnROAD was built in 1993, and comprised 23 original test cells. As of 2016, there were 69 test cells between the Mainline and LVR. A different pavement type and/or design is used in construction of each of these cells.

The Mainline is a 3.5-mile, 2-lane interstate highway that carries live traffic diverted from Westbound Interstate 94 while the LVR is a 2-lane, closed loop with 24 test cells (in 2016) and a total length of 2.5

miles. The traffic on the LVR is restricted to a single 18-wheel, 5-axle tractor with a trailer, which is intended to simulate the traffic conditions on rural roads. Operation of this vehicle is performed by the MnROAD staff according to a controlled schedule that includes 80 laps per day on the inside lane only. The outside lane is subject to environmental loading only, except for the minimal loading from lightweight test vehicles. This restriction is intended to demonstrate the pavement response due to environmental effects versus loading effects.

The low cementitious test cells 138 and 238 are contiguously located on the LVR as presented in Figure 1. A concrete mixture with 500 lb/yd^3 of cementitious materials was used for building cell 138 and designated as the low cementitious mixture, while another similar mixture proportioned with 470 lb/yd^3 of cementitious materials content was used for cell 238 and designated as the lower cementitious mixture in this report. Data obtained from these two cells were compared to those gathered from testing cell 524 proportioned with 570 lb/yd^3 of cementitious materials, which serves as the reference cell in this study.

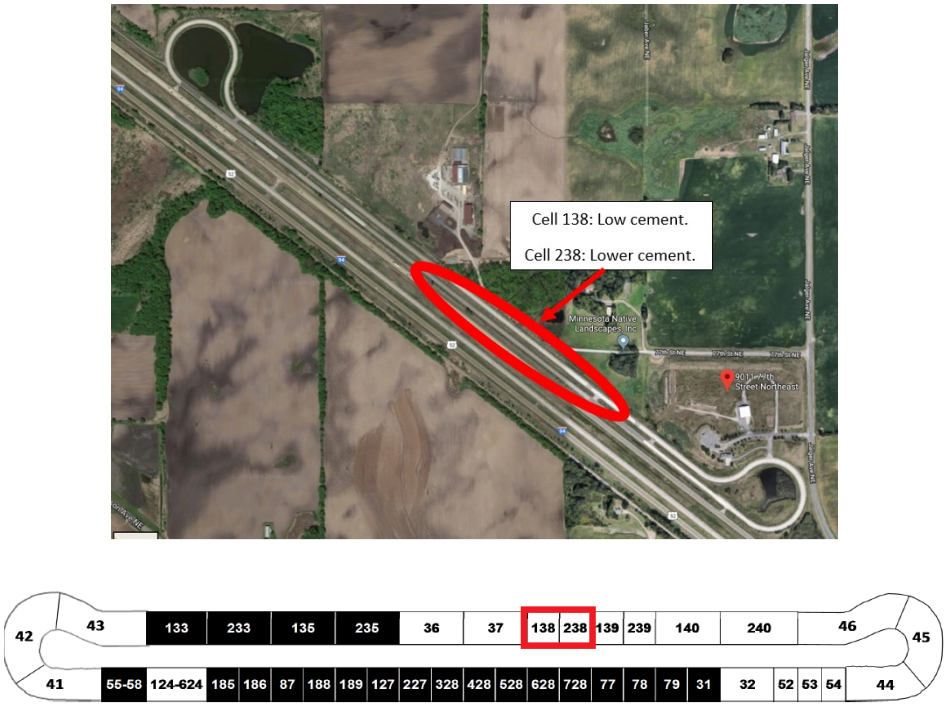

Figure 1. Aerial photo (top) and schematic view (bot.) of the investigated cells

Concrete placement, sampling, and testing for fresh properties took place on July 14, 2017. The construction activities, design details, and research activities of each test cell were identical:

Construction activities

- Remove 258 feet of existing concrete pavement
- Repair existing Class 5 base (if damaged)

- Install sensors, including vibrating wire strain gauges, quarter-bridge strain gauges, thermocouple trees and maturity loggers
- Install T2 plates (for thickness verification)
- Place new concrete layer and conduct tests during paving
- Fabricate research samples (cylinders/beams) for further lab testing
- Place new gravel shoulders

Design details (shown in Figure 2)

- Panel thickness = 8 inches
- Panel size = 12 ft W x 15 ft L driving lane
- Low cementitious mixture with 500 lb/yd^3 of cementitious materials at cell 138 and lower cementitious mixture with 470 lb/yd^3 of cementitious materials at cell 238
- Shoulders = 2-inch thick shoulder gravel
- Dowel bars = 1.25-inch diameter epoxy coated steel in standard MnDOT pattern
- Joints = single 0.125-inch width saw cut, depth = T/4, unsealed
- Base: 5.0-inch Class 5 aggregate base
- Subgrade: clay loam (A-6)

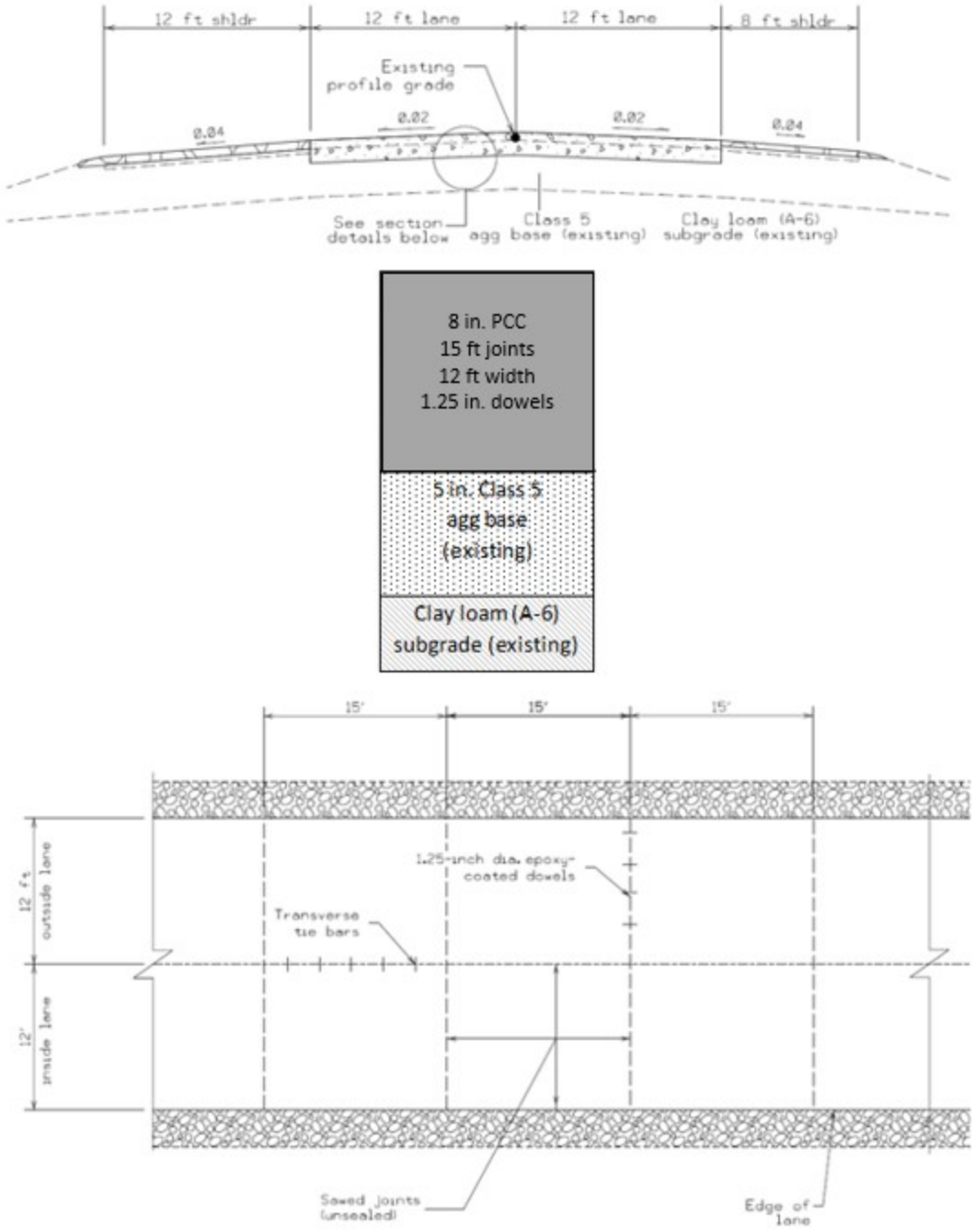

Figure 2. Pavement construction details

Instrumentation was used for evaluating the *in-situ* properties of the concrete as shown in Table 1. Sampling for fresh properties and monitoring the early age characteristics were performed as detailed in Table 2 and Table 3. Moreover, specimens were cast for investigating the hardened properties in the laboratory as detailed in Table 4 .Results are discussed in the following chapters.

Table 1. Pre-paving activities

Pre-Paving				
Project Test Matrix	**Test Ages**	**Number of Sensors**	**Cure Procedure**	**Conducted by**
Vibrating Wire Strain Gauges	On-site sensor installation /Continuous	4	In the pavement	MnDOT
Quarter-bridge Strain Gauges		8		
Thermocouple Trees		2		
Maturity Logger		1		
5TE Moisture Sensor		2		

Table 2. Research activities during paving

During Paving					
Project Test Matrix	**Test Age**	**Type of Test Specimens**	**Size of Specimens**	**Number of Specimens**	**Conducted by**
AASHTO PP84, Box Test	Fresh	Cube	9.5 in3	1	MnDOT
AASHTO TP129, VKelly Test	Fresh	Tub	17x15x8 -inch rubber tub	3	ISU
AASHTO PP84, SAM Test	Fresh	Air pot	0.25 cf	1	MnDOT/ISU
AdiaCal Calorimetry: semi-adiabatic measurement on concrete temperature	up to 1 day	Cylinders	4x8-inch	2	ISU
AASHTO T318, Microwave w/cm ratio	Fresh	Bowl	~2,000 g	1	ISU
ASTM C138, Unit Weight	Fresh	Air pot	0.25 cf	1	MnDOT/ISU

Table 3. Early research activities

Early Research Activities		
Test	**Location**	**Conducted by**
Monitor maturity	Paving cell/In the pavement	MnDOT
Conduct early-age warp and curl tests		MnDOT
Monitor joint deployment using MIRA		ISU
Baseline FWD and truck load tests		MnDOT

Table 4. Hardened concrete testing plan for laboratory

Post-Testing							
Project Test Matrix	**Test Age (day)**	**Type of Test Specimens**	**Specimen Size**	**Number of Specimens**	**Curing**	**Cure Time**	**Conducted by**
ASTM C39, Compressive Strength	2 , 3 , 7 and 28 days	Cylinders	6x12-inch 2 per test	8	Moist Room	Per test age	MnDOT
ASTM C78, Flexural Strength	2 , 3 , 7 and 28 days	Beams	6x6x20-inch 1 per test	4	Lime-water	Per test age	MnDOT
ASTM C666, Proc. A Freezing and Thawing in Water	14 days	Cores	3x3x11¼-inch, set of three beams	3 beams	Lime-water	14 days	MnDOT
AASHTO T336, Coefficient of Thermal Expansion	28 days	Cylinder	4x8-inch	1	Moist Room	28 days	MnDOT
ASTM C469, Modulus of Elasticity and Poisson's	28 days	Cylinder	6x12-inch	1	Per test method	28 days	MnDOT
ASTM C215, Dynamic Modulus	7 and 28 days	Cylinder	4x8-inch	1	Moist Room	28 days	MnDOT
Wenner Probe Resistivity	28 days	Cylinder	4x8-inch	2	Per test method	28 days	MnDOT/ISU
ASTM C856, Brief Petrographic Examination of Hardened Concrete:	After ASTM C666 testing	Tested freeze-thaw beam	3x3x11¼ inch	1	Lime-water	14 days	MnDOT

estimated air content; degraded air system; microcracking							
ASTM C457, Air Void Analysis of Hardened Concrete	at least 14 days	Tested freeze-thaw beam	4x8-inch cylinder	1	At least 14 days moist cure	14 days moist cure	MnDOT
ASTM C157, Drying Shrinkage	56 days	Beams	4x4x11¼-in beams with pins	1	28 days lime-water	28 days	MnDOT
AASHTO PP84, Bucket Test	14 days up to 90 days	Cylinders	4x8-inch	3	lime-water	60 days	ISU
Modified ASTM C29, Dry Rodded Unit Weight and Voids in Combined Aggregate Systems	-	Aggregates	80 lbs	3	-	-	ISU
AASHTO PP84, Low Temperature Differential Scanning Calorimetry (LT-DSC)	after 28 days	Cylinder	4x8-inch	1	50C sealed oven cure	28 days	ISU

1.4 REPORT ORGANIZATION

This report is presented in six chapters, including this introductory chapter. Chapter 2 presents a summary of existing literature on factors affecting the cementitious materials content in concrete mixtures and discusses the effect of cementitious materials content on fresh and hardened concrete properties. Chapter 3 presents details of the experimental program undertaken in this work, including the material properties and concrete mixture proportioning, an overview of field samples collected and evaluated, *in-situ* test results and data obtained from the installed instrumentation, and distress survey results. Chapter 4 presents the effect of reduced cementitious materials content on long-term serviceability of concrete pavements. Chapter 5 presents guidelines for mixture proportioning with reduced cementitious materials content. A summary of the research findings and recommendations for future research are presented in Chapter 6.

CHAPTER 2: LITERATURE REVIEW

This literature review focuses on the reported performance of concrete mixtures prepared with varying quantities of cementitious materials.

A common misconception in concrete mixture design is that increasing cement content increases concrete strength. Based on this perception, a minimum cement content is often specified that can be too conservative and exceeds the amount needed for the desired strength and durability. However, it has been proved that once the cement content reaches an optimum value, using more cement does not result in higher strength for a given water to cementitious materials ratio (w/cm) and may adversely affect other concrete properties. Such mixtures can be too sticky, increasingly permeable, and prone to shrinkage and cracking issues (Taylor et al. 2015). This excess cement may also have a negative impact on cost and the environment for the following reasons (Taylor et al. 2012):

- Cement is the most expensive component in concrete.
- Cement accounts for about 80% of the carbon dioxide (CO_2) burden of a concrete mixture.

Three reasons for imposing minimum cement contents have been identified (Wassermann 2009):

- To achieve a given maximum w/cm. This reason was valid when the only way to control workability was by adjusting water content.
- To maintain a minimum fines content for workability assurance and development of the bond between concrete and reinforcing steel. The minimum fines content can be controlled by controlling the combined aggregate gradation.
- To protect embedded steel in concrete by binding chlorides. This protection can be improved by the use of some supplementary cementitious materials (SCMs).

This review investigates the effects of reducing cementitious content on concrete performance.

2.1 SPECIFICATION REVIEW

Rudy (2009) reviewed the requirements for pavement concrete mixture designs included in specifications from several states and provided mixture proportions for concrete pavements found in the literature and utilized in some projects. The selected states generally experience cold and wet winters followed by hot and humid summers, which results in large temperature and moisture differentials from season to season. The requirements and proportions are summarized in Table 5.

Table 5. Summary of concrete pavement specifications from various regions (After Rudy 2009)

State/Country	Min. cement content (lb/yd^3)				Target air content, %	Max. w/cm	Pozzolan content by weight, %		Slag cement by weight, %		Open to traffic	Other requirements or practices
	Plain	Fly ash C (CFA)	Fly ash F (FFA)	Slag cement			Min	Max	Min	Max		
Illinois (IDOT 2012)	565 (Central mixed); 607 (Truck mixed)	452	480	424	5.0-8.0	0.42	-	20(CFA) or 15(FFA)	-	25	-	Slump between 1/2 and 1.5 in. for slipform paving; Fine to total aggregate 38 to 40%
Indiana (INDOT 2016)	564	451	-	395	5.0-8.0	0.49	-	20 (CFA or FFA)	-	30	Flexural strength (fl)≥550 psi @7 days	Slump between 1.25 and 3.00 in. for slipform paving. Nominal maximum aggregate (NMA) size 3/4 in.
Iowa DOT (Iowa DOT 2008a, 2008b)	564	458	458	372	6.0-10.0	0.45		20 (CFA or FFA)	-	35	fl≥500 psi @7 days	1/2 in.<slump<4 in.; maximum allowed size of coarse aggregate 1 in.
Kansas (KDOT 2015)	564	542	452	391	5.0-8.0	0.50	-	25 (CFA or FFA)	-	40	-	

State/Country	Min. cement content (lb/yd^3)				Target air content, %	Max. w/cm	Pozzolan content by weight, %		Slag cement by weight, %		Open to traffic	Other requirements or practices
	Plain	Fly ash C (CFA)	Fly ash F (FFA)	Slag cement			Min	Max	Min	Max		
Kansas Optimized Mix	521											25% maximum blended SCM; 10% maximum limestone; 50% total combined SCMs.
Michigan (MDOT 2012)	526 (P1 grade)	423	423	338	6.5	0.50	-	30 (CFA or FFA)	-	40	fl≥500 psi @7 days; compression strength (fc)@7days≥2600 psi	Slump <3 in., QA specification: coarse aggregate volume: 65-75%, fc@28days≥4,000 psi
Minnesota (MnDOT 2016)	530	385	385	385	7.0	0.40(with fly ash) or 0.42 (with slag/ternary)	-	33 (CFA or FFA)	-	35	-	Slump: 1/2–3 in. Concrete Grade A. Minimum NMA size of 1 ½".
Missouri (MoDOT 2016)	560	420	420	431	5.0	0.50	-	25 (CFA or FFA)	-	25	-	-
New York (NYSDOT 2016)	605 (C class)	484	484	484	6.5	0.44	15 (FFA)	20 (FFA)	-	20	fc required to open pavement to general traffic is 3,000 psi	NMA size of 1 in., slump rage from 1–3 in.

State/Country	Min. cement content (lb/yd^3)				Target air content, %	Max. w/cm	Pozzolan content by weight, %		Slag cement by weight, %		Open to traffic	Other requirements or practices
	Plain	Fly ash C (CFA)	Fly ash F (FFA)	Slag cement			Min	Max	Min	Max		
Ohio (ODOT 2008)	600	510	510	385	6.0	0.50	-	15 (CFA or FFA)	-	30	-	-
Pennsylvania (PennDOT 2009)	587	499	499	294	6.0	0.50	-	15 (CFA or FFA or Class N)	25	50	-	Class N pozzolan is allowed
Virginia (VDOT 2016)	564 (A3 class)	-	395	282	6.0	0.49	-	30 (CFA or FFA)	35	50	fl required to open pavement to general traffic is 600 psi	Slump: ≤2 in.
Wisconsin (WisDOT 2018)	517 (A3 grade)	395	-	285	7.0	0.47	-	30 (CFA or FFA or Class N)	30	50	fc≥3000 psi	Slump ≤2.5 in.; NMA 3/4 in.; Class N pozzolan is allowed
Canada (Rudy 2009)	-	-	-	-	4.5-7.5	-	-	10 (CFA or FFA)	-	25	fc @28 days: ≥4,350 psi for Ontario; ≥5,100 psi for Quebec	Coarse aggregate has a combined gradation includes aggregates with NMA size 1.5 in. and 3/4 in. aggregates
Germany (Rudy 2009)	540	-	-	-	4.0	0.50	-	-	-	-	fc@28days≥5,400 psi.; fl@28days≥650 psi.	-

State/Country	Min. cement content (lb/yd$^{3)}$				Target air content, %	Max. w/cm	Pozzolan content by weight, %		Slag cement by weight, %		Open to traffic	Other requirements or practices
	Plain	Fly ash C (CFA)	Fly ash F (FFA)	Slag cement			Min	Max	Min	Max		
Austria (Rudy 2009)	Cement content: lower course 594, upper course 675				4.0-6.0	-	-	-	20	25	fc@28days≥5000 psi; fl@28days≥800 psi for lower lift; fc@28days≥5800 psi; fl@28days≥1000 psi top lift	For cement, Blaine fineness cannot be greater than 3500 cm^2/g and Initial setting time>2h
Belgium and Netherlands (Rudy 2009)	540	-	-	-	-	0.55	30	35 (CFA or FFA)	-	60	fc@28days≥6,525 psi	-
China (JTG T F50 2011)	505	421		-	-	0.44	-	30 (CFA or FFA for Type I Cement); 25 (For Type II cement)	-	-	For heavy traffic - fc@28days≥7250 psi; fl@28days≥870 psi	Slump: 1–4 in.

Generally, the minimum amount of cement used for plain concrete mixtures is about 530 lb/yd3 for most US states and 505 lb/yd3 in Chinese specifications. If fly ash (both Class C and F) is used, the minimum cement content is about 450 lb/yd3, depending on the replacement dosage. Minimum cement content may be further reduced with slag cement replacement due to the latter's higher allowable dosage in some locations (up to 60% in Belgium and the Netherlands).

The w/cm is another primary parameter affecting minimum binder contents and the performance of concrete mixtures. The American Concrete Pavement Association (ACPA) handbook (2007) suggests that the maximum w/cm for slip-form paving should not exceed 0.45, and the limit used by states ranges from 0.40 to 0.55. The National Concrete Pavement Technology Center recommends a value of 0.42 for pavements subjected to aggressive de-icing salts. Minnesota limits w/cm to a maximum of 0.40.

Supplementary cementitious materials used in pavements include fly ash and slag cement. The typical range of fly ash substitution in pavement concrete is between 15% to 30%, while slag cement replacement is between 25% and 50%.

The gradation and nominal maximum aggregate (NMA) size of aggregates are other parameters influencing binder content and overall performance. The NMA size ranges from 0.75 to 1.50 in., while the gradation is selected according to standards published by the American Association of State Highway and Transportation Officials (AASHTO) or ASTM International, with the fine-to-total aggregate ratio in the range of 0.4 to 0.6 by mass (IM 529 2007). However, some states, such as Iowa and Minnesota, have developed special guidelines for optimizing aggregate gradation for concrete paving mixtures. More information regarding this topic is provided in the following section.

2.2 FACTORS AFFECTING BINDER CONTENT

Concrete is a heterogeneous and complex material in which there are multiple interactions between the components. It is well documented that overall concrete performance is affected by the nature of the mix components and their quantities (Taylor 2015, Wassermann et al. 2009). Each mix component has an impact on both fresh and hardened concrete properties, albeit at varying levels. Concrete mixture proportioning, therefore, has to be a well-thought-through and iterative process.

A concrete mixture proportioning method proposed by Taylor et al. (2015) defines three decisions: (1) selection of a combined aggregate system, (2) selection of paste quality, and (3) selection of paste quantity. The design procedure is based on evaluating and selecting the paste and aggregate systems separately, followed by an analysis of the interaction between them (Taylor et al. 2015). The fundamental philosophy is that paste quality primarily controls long-term performance (assuming durable aggregates), while paste quantity and the aggregate system are mainly responsible for the workability of the fresh concrete.

A quantitative parameter, paste volume to voids volume in a combined aggregate ratio (Vpaste/Vvoids), was developed for this mix design method in order to correlate the performance of a mixture to the paste volume for a given aggregate system. Vpaste/Vvoids is calculated by calculating the paste volume of the concrete mixture and dividing that value by the volume of voids between the combined

compacted aggregates. The paste volume includes the volume of water, cementitious materials content (CMC), and air in the system. The voids refer to the space between the compacted combined aggregates, which is determined in accordance with ASTM C29. A ratio of 100% indicates that all of the voids available in the combined aggregate system are filled with paste, with no excess (Taylor et al. 2015).

The factors that influence selection of the paste content are discussed in the following sections.

2.2.1 Supplementary Cementitious Materials (SCMs)

SCM types and dosages have varied effects on properties such as water demand and air content, as summarized in Table 6. The table can be used as a reference in slip-form paving mix design.

Table 6. Effects of SCMs on various concrete properties

Properties	Supplementary Cementitious Materials Type					
	Class F Fly Ash (FFA)	**Class C Fly Ash (CFA)**	**Slag Cement (S)**	**Silica Fume**	**Metakaolin**	**Limestone Powder**
Water demand (for a given consistency)	Significantly reduced	Reduced	Slightly reduced	Marginal effect at low dose (<5%); increased at high amounts	Increased, especially at higher dosages	Slightly reduced
Air void system	May be difficult to entrain air with high LOI	Neutral	Neutral	May be difficult to entrain air	May be difficult to entrain air	Neutral
Setting time	Delayed	Slightly delayed	Slightly delayed	Accelerated	Neutral	Neutral
Incompatibility with chemical admixtures	Low risk	Some risk	Low risk	Low risk	Low risk	Low risk
Strength gain	Slower but continues longer	Slightly slower but continues longer	Slightly slower but continues longer	Accelerated initially	Accelerated initially	Neutral
Heat generation	Lower	Slightly lower	Slightly lower	Higher	Slightly higher	Slightly lower
Drying Shrinkage	Neutral	Neutral	Neutral	Increased	Increased	Neutral
Permeability	Lower over time	Lower over time	Lower over time	Lower	Lower	Neutral
Alkali silica reaction	Reduction	Reduction at sufficient dosage (>15% of binder content)	Reduction at high dosage (>25% of binder content)	Reduction	Reduction	Neutral
Sulfate resistance	Increase	Increase at sufficient dosage	Increase at high dosage	Neutral	Neutral	May be worse at high dosages in very cold environments
Corrosion resistance	Slightly increase	Slightly increase	Increase	Increase	Increase	Neutral
Stiffness	Strength related					
Freezing and thawing	Neutral (rely on air void system, strength, w/cm, and quality of aggregate)					
De-icer scaling resistance	Neutral (rely on air void system, w/cm, proper finishing and curing, and bleeding control)					
Properties	**Supplementary Cementitious Materials Type**					

Source: Taylor 2014

Selection of a proper SCM dosage is a compromise between obtaining the benefits desired, such as increased resistance to alkali silica reaction, reduced water demand for a given consistency, and improved durability, and limiting negative effects such as shrinkage and risk of cracking. Recommended dosages in current specifications can be found in Table 5.

In general, the inclusion of fly ash reduces the water demand (by about 1% to 10% at normal dosages for a given slump) and decreases the air content if no further adjustment in the amount of air-entraining admixture (AEA) is made. Fly ash reduces water demand in a manner similar to that of liquid chemical water reducers (Helmuth 1987).

The introduction of slag cement can also result in the reduction of water demand, although the impact is dependent on the slag cement's fineness and is less marked than that of fly ash. For a given slump, slag cement at normal dosages may reduce the water demand up to 3% to 5% compared to ordinary portland cement.

For a given slump, concrete mixtures containing these materials are generally easier to place, consolidate, and finish. These benefits allow for the potential of reducing binder content while maintaining the desired workability.

2.2.2 Chemical Admixtures

AEAs are used to enhance freeze-thaw resistance by stabilizing small bubbles in the paste. The finely distributed network of bubbles also has a significant impact on plastic concrete properties, where improvements in the workability of concrete can be expected, particularly in low-cement concrete mixtures (Kosmatka and Wilson 2016). Cordon (1946) suggested that an air-entrained mixture made with 3% air and natural aggregate with a 1.5 in. slump exhibits the same workability as a non-air-entrained concrete with 1% air and a 3 in. slump, even though less cement is required for the air-entrained mix. Gilkey (1958) quantitatively demonstrated that entrained air can reduce water and thus required binder content, as shown in Figure 3. However, excess AEAs can result in sticky mixtures that are difficult to finish. Moreover, each 1% increase in air content is accompanied by a 5% to 6% reduction in strength, as a rule of thumb (Kosmatka and Wilson 2016).

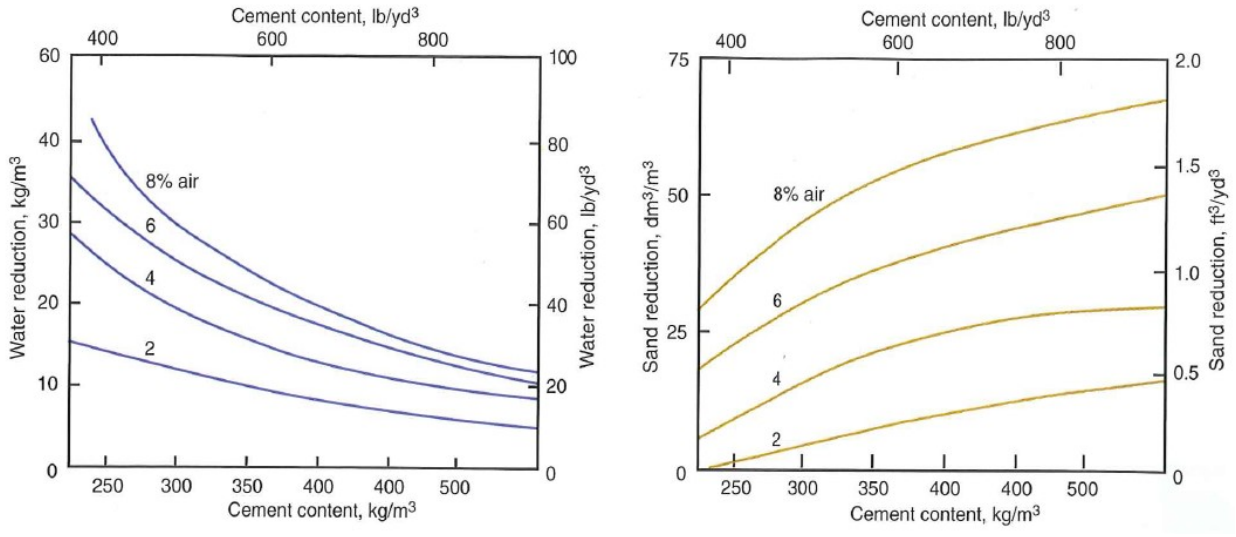

Figure 3. Relationship among cement content, water reduction and sand reduction at various levels of air

Water-reducing admixtures (WRA) are commonly used in pavement concrete mixtures as cement dispersants. These admixtures work primarily through electrostatic and steric repulsive forces to separate cement particles, which in turn increases workability for a given water content. Normal WRAs have the ability to decrease water content by 5% to 10% and increase air content by 0.5% to 1%, while high-range water reducers (superplasticizers) may reduce water content by between 12% and 30% and increase air content by up to 1% (Kosmatka and Wilson 2016). However, according to Whiting and Dziedzic (1992), using a water reducer to reduce the cement and water content of a concrete mixture while maintaining a constant w/cm ratio can result in equal or reduced compressive strength and an increase in slump loss. Other effects caused by the introduction of WRAs are as follows (Kosmatka and Wilson 2016):

- Despite a reduction in water and cement content, WRAs may increase drying shrinkage, but the effect is small when compared to other significant factors.
- WRAs can delay setting time and early strength gain. ASTM C494 Type A WRAs have little effect on setting time at their typical dosages, while Type D WRAs provide water reduction and retardation and Type E WRAs can reduce water content and accelerate setting.
- WRAs can have an air-entraining effect: Lignin-based admixtures may increase air by 1% to 2%, while polycarboxylate-based WRAs are normally formulated as defoamers to minimize additional entrained air.

Calcium chloride-based admixtures have the ability to reduce water content by about 3% and increase air content by about 0.5%.

Other types of chemical admixtures used in pavement concrete mixtures, such as shrinkage-reducing admixtures, alkali-aggregate reactivity inhibitors, coloring admixtures, pumping aids, and bonding admixtures, seem to have marginal effects on water requirements.

2.2.3 Aggregate System

Mixture proportioning is focused on meeting the basic performance specifications of a mixture and producing the most economical concrete. One way to reduce cost is to use as little cementitious paste as possible without compromising the engineering properties. Aggregate properties (e.g., gradation, surface texture, shape, and size) have a strong impact on system workability (Cook et al. 2016, Marc et al. 2010, Dhir et al. 2006, Alexander and Mindess 2005).

In pavement concrete mixtures, enough paste is needed to fill the voids available between the aggregate particles, coat the aggregate particles, and lubricate the aggregates to provide a desired workability (Kennedy 1940). The aggregate system can therefore strongly influence how much paste is required to achieve desired performance.

Practitioners have reported graphical gradation techniques to proportion aggregates to achieve a so-called optimized combined aggregate gradation. These tools include the following:

- The Coarseness-Factor Chart (Shilstone 1990) is based on separating the combined aggregates at the 3/8 in. sieve (Figure 4). Systems that fall within Zone II are reported to be preferred for slip-form paving mixtures (Richardson 2005). However, Cook et al. (2016) considered that this chart is not helpful in understanding the workability behavior of slip-form concrete.

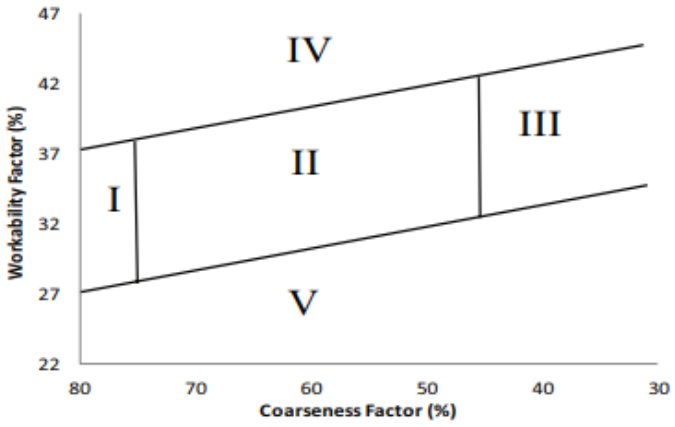

Shilstone 1990

Figure 4. Shilstone chart

- The Power 45 Chart (Kennedy et al. 1940, Fuller and Thompson 1907) plots a combined gradation with the sieve size raised to the 0.45 power on the cumulative percent passing chart (Richardson 2005). The aim is to force the combined gradation to be close to a straight line plotted from the origin to the nominal maximum size of aggregate (NMSA), which reportedly leads to a maximum aggregate density. Cook et al. (2016) concluded that the Power 45 Chart provides the best insight into the effect of gradation on the workability of the concrete but tends to produce mixtures with decreased workability.

- The Individual Percent Retained (IPR) Chart (Richardson 2005, ACI 302 2004), also known as the Haystack Chart, is another commonly used technique in pavement concrete mixture design. For a given gradation, this chart graphically shows the amounts retained on each sieve size and suggests a maximum boundary of 18% and a minimum boundary of 8% for each sieve (Cook et al. 2016). Only a limited amount of research has been published to demonstrate the validity of the limits (Richardson 2005). Cook et al. (2016) stated that the IPR Chart is easier to use than the Power 45 Chart and is an important step in effectively proportioning aggregate in slip-form paving mixtures to improve workability and reduce the required paste content.
- The Tarantula Curve is based on the IPR Chart. The Tarantula Curve describes an envelope that reports the desirable amount of materials retained on each sieve, as shown in Figure 5 (Ley and Cook 2014). The aim is to combine the individual aggregates available so that the combined system is within the envelope and as close to the center of the envelope as possible.

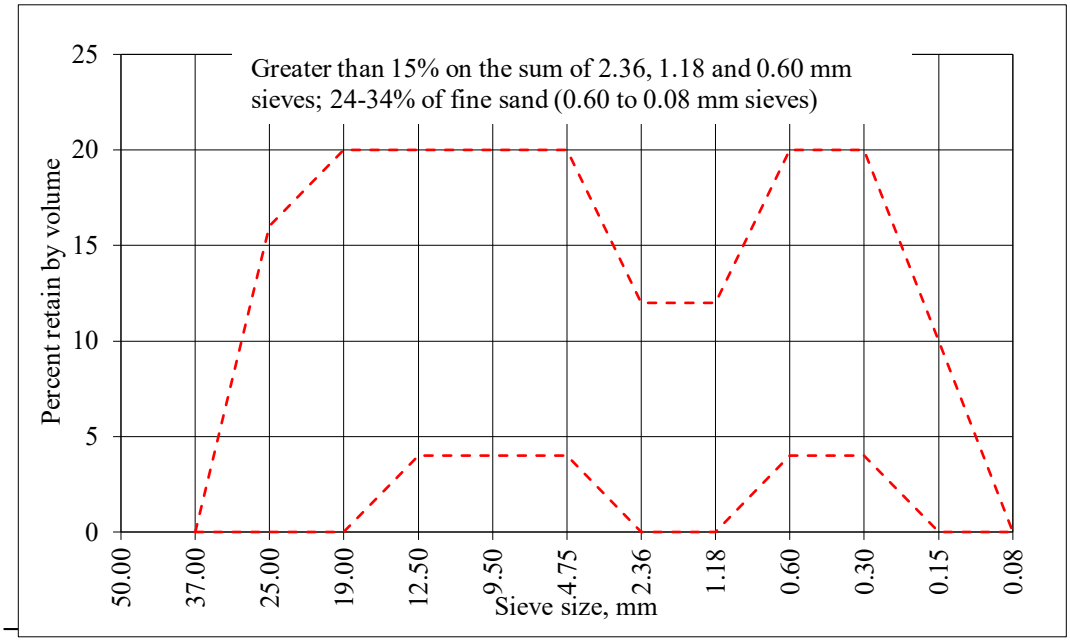

Figure 5. Tarantula curve

Additional requirements of this method include the following:

- The total volume of coarse sand (#8 to #30) must be a minimum of 15%.
- The total volume of fine sand (#30 to #200) must be within 24% and 34%.
- The flat or elongated coarse aggregate must be limited to 15% or less at a ratio of 1:3, according to ASTM D4791.

The premise of the Voids Content method (Wang et al. 2014, Goltermann et al. 1997, de Larrard 1999, Dewar 1999, Powers 1948) is to minimize the void content of the aggregate component to reduce the amount of paste required to fill the spaces (Cook et al. 2016). Multiple packing models have been developed, but their complexity and a lack of material parameters has limited the use of some models (Day 2006).

The Specific Surface Area method (Neville 2012, Day 2006, Powers 1948), similar to the Voids Content method, suggests that for a fixed paste content and aggregate volume, gradations with higher surface areas can require more paste to achieve a given workability. The method is quantitatively presented as the surface area divided by the volume of the aggregate. An unrealistic assumption of this method is that aggregate particles are considered to be spherical in shape and to have a diameter halfway between the passing and retained sieve sizes (Cook et al. 2016).

The Gradation Specification method (ASTM C33) requires individual size boundaries for aggregates (Cook et al. 2016).

Regardless of the methodology for optimizing the combined aggregate system, several aggregate characteristics are important contributors to workability performance and voids (Cook et al. 2016, National Stone, Sand, and Gravel Association 2013, Rached et al. 2010):

- Shape and angularity: Aggregates with an angular shape can create poor packing, resulting in increased paste volume and an increased demand for WRAs. However, the variation in packing density and workability caused by aggregate shape and angularity is not as significant as that caused by changes in the gradation.
- Nominal maximum coarse aggregate size: A larger aggregate size typically results in a lower surface area and, therefore, a mixture that requires less paste content.
- Dust-of-fracture aggregate micro-fines: This characteristic allows a reduction in cementitious material if a given fines content is required.

2.3 EFFECT OF CEMENTITIOUS MATERIALS QUANTITY ON CONCRETE PERFORMANCE

2.3.1 Workability

Workability can be described using three main parameters (Kosmatka and Wilson 2016):

- Cohesiveness: the resistance to segregation
- Consistency: the ease of flow
- Plasticity: the ease of molding

Workability can be affected by a number of factors. In general, increasing the water content in concrete increases workability, while excessive water content may lead to segregation and bleeding (Kosmatka and Wilson 2016, Mindess et al. 2003). Decreasing the binder content increases the stiffness of the paste for a given water content. Concrete with high binder content exhibits high cohesiveness and therefore can become sticky (Kosmatka and Wilson 2016).

In a comprehensive study by Rudy (2009), it was found that the optimum air-free paste contents for a binary cementitious system with fly ash and slag cement should be higher than 22% (about 480 lb/yd^3 of total cementitious materials) and 23% (about 500 lb/yd^3), respectively. Lower amounts can result in problems with concrete workability and necessitate an extremely high dosage of WRAs. Overdosed WRAs may cause an increase in paste shrinkage due to changes in the pore structure and surface

tension (Wassermann et al. 2009). Rudy (2009) found that ternary cementitious systems (i.e., cement + fly ash + slag cement) follow similar trends in workability and requirements for WRAs. A slag cement ternary system exhibited improved resistance to bleeding and cohesiveness when compared to a binary system (Rudy 2009).

A study by Wang et al. (2017) summarized over 150 concrete mixtures with different w/cms to investigate the minimum amount of paste required in a system to achieve a workable mix, as shown in Figure 6.

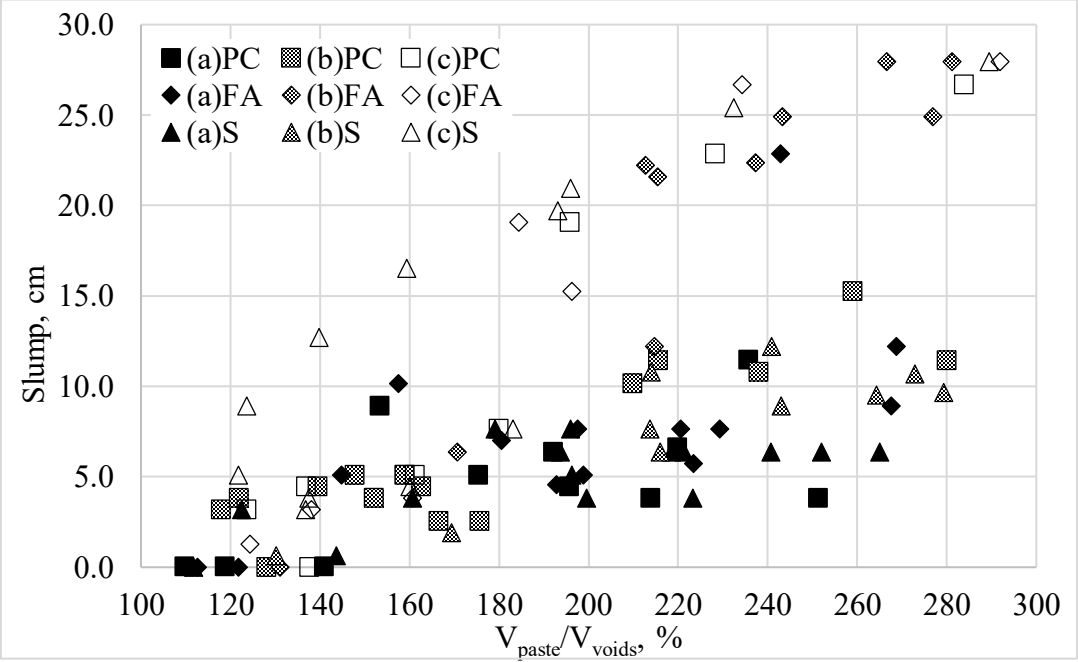

Wang et al. 2017

Figure 6. Relationship between V_{paste}/V_{voids} and workability, with (a) representing 0.35 ≤ w/cm ≤ 0.40, (b) representing 0.40 < w/cm ≤ 0.45, and (c) representing 0.45 < w/cm < 0.55 (1.0 cm = 0.4 in.)

The parameter V_{paste}/V_{voids} was applied to generalize the paste volume demand for voids in a given aggregate system. The authors reported that even with the addition of overdosed WRAs and the use of SCMs, a V_{paste}/V_{voids} value of 110% of seems to be a critical point, below which zero slump may result. In addition, it was reported that a V_{paste}/V_{voids} value below 125% may cause the mixture to exhibit honeycombing and present challenges for mixing, consolidation, and finishing (Yurdakul et al. 2013). A V_{paste}/V_{voids} value within the range of 140% and 250% seems to be sufficient to provide the desired slump for slip-form paving concrete for the aggregate systems tested. In the plain cement mixtures (PC in Figure 6), the ratio of 140% appears to be appropriate regardless of w/cm. For the mixtures containing fly ash (FA in Figure 6), the critical point can be reduced to about 125%, likely because of the spherical morphology of fly ash particles. Mixtures with slag cement (S in Figure 6) may require a slightly higher V_{paste}/V_{voids} value, likely due to the higher fineness of the slag cement (Hale et al. 2008).

2.3.2 Hydration, Setting, and Hardening

The binding quality of cement paste is due to the chemical reaction between the cement and water, which forms two types of calcium hydrates (up to 75% of the weight of portland cement): calcium hydroxide (CH) and calcium silica hydrate (C-S-H). The latter primarily controls concrete setting and hardening, strength, and dimensional stability (Kosmatka and Wilson 2016).

The setting time of concrete, determined in accordance with ASTM C403, is affected by the type and amount of portland cement used, the type and replacement level of SCMs (see Table 6), the w/cm, the concrete temperature, and the use of set-modifying admixtures (Bullard et al. 2006). Gypsum, added at the cement mill when the clinker is ground, acts as a regulator of the initial rate of setting of portland cement. Higher concrete temperatures can generally accelerate the hydration process and yield shortened set times due to the effects of higher temperatures on hydration reaction kinetics. A similar rate of heat release irrespective of w/cm can be found within the first 24 hours, after which a difference begins to be noticed among mixtures with w/cms from 0.30 to 0.51 (Lura et al. 2007). Addis and Alexander (1990) suggested that about 0.4 times as much water (by mass) as cement is needed to completely hydrate cement. In general, the quality of the paste plays the dominant role in controlling the hydration, setting, and hardening behavior of a concrete mixture.

2.3.3 Shrinkage Behavior

Concrete shrinkage can be separated into different mechanisms. These include plastic shrinkage, chemical shrinkage (autogenous shrinkage), and drying shrinkage (Tia et al. 2005). Drying shrinkage, caused by moisture loss, is considered to be the main contributor to total shrinkage strain for normal-strength concrete (ACI 209 2005). Water in small capillary voids (5 to 50 nm) plays an important role in drying shrinkage. The size and volume of the capillary voids are controlled by the initial w/cm and the degree of cement hydration. At a constant w/cm, increasing the degree of hydration decreases the size and volume of the capillary voids. Subsequent drying will result in reduced shrinkage strain (Taylor and Wang 2014, Malhotra and Mehta 1996).

At a given w/cm, drying shrinkage almost linearly increases with paste content/volume in a concrete mixture (Taylor and Wang 2014, Wang et al. 2012, Wang 2011, Hale et al. 2008, Hooton 2000, Pickett 1947). Figure 7 presents shrinkage data from Obla (2012) reorganized by Wang et al. (2017) to express the relationship between V_{paste}/V_{voids} and 56-day drying shrinkage for mixtures with varied w/cms and SCM replacement rates in a fixed aggregate system.

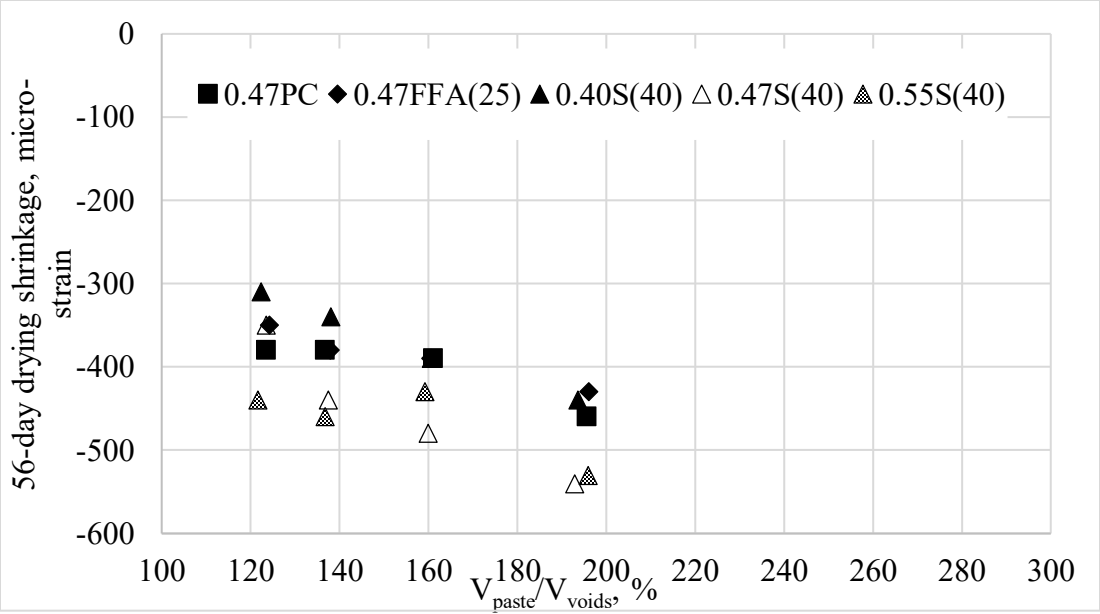

Wang et al. 2017; reorganized from Obla 2012

Figure 7. Correlation between V_{paste}/V_{voids} and drying shrinkage

It is clear in this case that drying shrinkage increases with increasing paste volume. However, factors that influence drying shrinkage are normally interrelated. Compared to paste quantity, factors related to paste quality, such as cement characteristics, SCMs (see Table 6), and chemical admixtures, and other factors, such as aggregate characteristics, curing, environmental conditions, and construction technique, can have a significant effect on shrinkage behavior (Wang 2011).

2.3.4 Transport Properties

Transport properties describe the ion, water, and gas permeability of a concrete mixture. A general conclusion can be drawn that permeability is proportional to the paste content for a given w/cm ratio (Wang et al. 2017, Wassermann et al. 2009). Figure 8, which shows the relationship between V_{paste}/V_{voids} and chloride penetration tested in accordance with ASTM C1202 at 28 and 90 days, respectively, indicates that concrete mixtures with higher V_{paste}/V_{voids} values have higher chloride penetrability (Wang et al. 2017, Arachchige 2008). This is believed to be due to the fact that aggregate is less permeable than paste, especially at early ages (Mindess et al. 2003). However, this effect is diminished in the long term due to ongoing hydration and pozzolanic reactions (see Table 6).

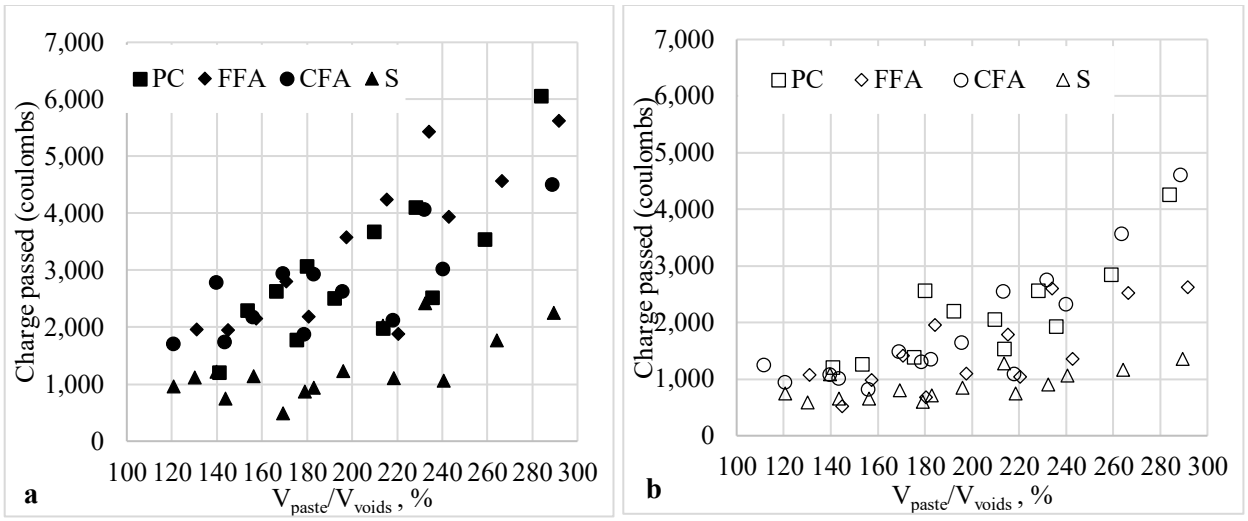

Reorganized from Yurdakul et al. 2013

Figure 8. Relationship between V_{paste}/V_{voids} and chloride permeability at (a) 28 days and (b) 90 days

2.3.5 Strength

Concrete strength is considered to be a function of w/cm and independent of cement content for a given w/cm (Wassermann et al. 2009, Dhir et al. 2004). Therefore, paste content does not affect strength for a given binder system, while paste quality in terms of w/cm and SCMs (see Table 6), aggregate characteristics, and chemical admixtures can be major contributors.

When considering strength in terms of V_{paste}/V_{voids}, Wang et al. (2017) and Yurdakul et al. (2013) concluded that after the paste volume that is required for the mixture to reach a plateau is achieved, further increasing paste content does not provide any benefits to the strength and may even have an adverse effect. Figure 9 shows the correlation between V_{paste}/V_{voids} and 28-day compressive strength for over 200 mixtures. Three sets of mixtures with w/cm ratios of 0.35, 0.45, and 0.50 are highlighted (Wang et al. 2017).

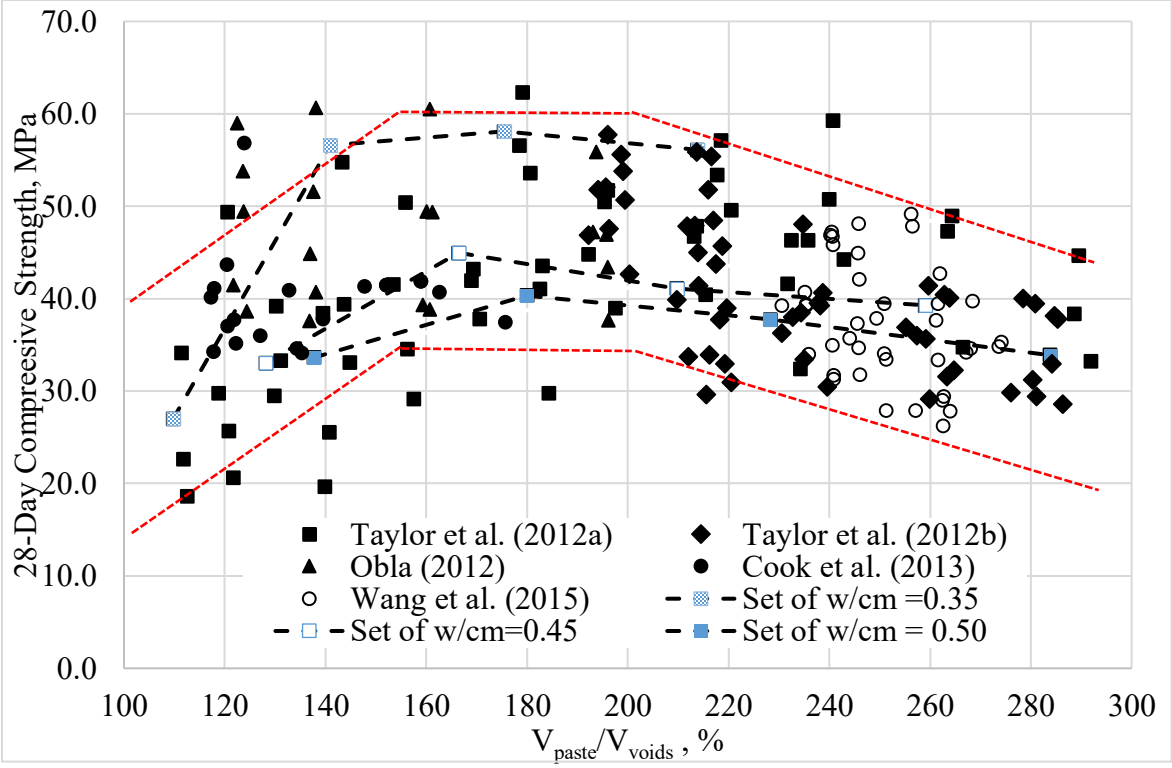

Wang et al. 2017

Figure 9. Correlation between V_{paste}/V_{voids} and 28-day compressive strength (1 MPa = 145 psi)

2.3.6 Freeze-Thaw Durability

Deterioration due to freezing and thawing is a result of the expansive forces that are generated when water in saturated concrete freezes and expands upon freezing (Kosmatka and Wilson 2016). When the osmotic and hydraulic pressures in the capillaries and pores of the cement paste and aggregate exceed the tensile strength of the surrounding paste or aggregate, the cavities dilate and rupture. The cumulative effect of successive freeze-thaw cycles is eventually deterioration of the concrete in the form of cracking, scaling, and disintegration. This effect may be exacerbated in the presence of de-icing salts.

The ability of a concrete to resist damage due to freezing and thawing depends on the characteristics of both the cement paste and the aggregate. The outcome is actually controlled by the interaction of several factors in each case, such as the location of escape boundaries (the distance water has to travel for pressure relief), the pore structure of the system (size, number, and continuity of pores), the degree of saturation (amount of freezable water present), the rate of cooling, and the tensile strength of the material that must be exceeded to cause rupture (Mehta and Monteiro 2006). Two main actions are critical to improve freeze-thaw resistance: (1) providing escape boundaries in the cement paste matrix, which can be controlled using proper air entrainment, and (2) modifying the cement's pore structure, which can be altered using proper mix proportions and curing. Thus, the mechanisms of freezing and thawing resistance for a concrete mixture are ultimately attributed to paste quality rather than paste quantity.

2.3.7 Aggregate Stability

In general, D-cracking or durability cracking occurs when frost-susceptible aggregates are used in concrete subjected to freezing and thawing conditions. In such cases, the expansion of water in the aggregates results in concrete cracking. Alkali-silica reaction describes the reaction between the water, alkali hydroxides in cement paste, and certain siliceous rocks or minerals to form alkali-silica gel, which has the capacity to absorb water and swell (Kosmatka and Wilson 2016). Paste quantity has a marginal effect on either of these aggregate stability issues.

2.4 SUMMARY

Table 7 summarizes the effects of decisions regarding the aggregate system, paste quality, and paste quantity on some of the critical performance characteristics discussed above.

Table 7. Mix proportion parameters that control mixture performance characteristics

		Workability	Shrinkage Behavior	Transport Properties	Strength	Freeze-Thaw Durability	Aggregate Stability
Aggregate System	Type, gradation	√√	-	-	-	-	√√
Paste Quality	Air, w/cm, SCM type and dose	√	√	√√	√√	√√	√
Paste Quantity	V_P/V_V	√	√√	√	-	-	-

In Table 7, the relevance of each of the three components to each of the performance characteristics is indicated by the number of check marks. As the table shows, the aggregate and paste systems have the greatest effects on the concrete performance properties. An excess of paste content, especially binder content, may adversely affect the shrinkage and permeability of concrete mixtures and result in durability issues. However, sufficient paste content is needed to provide a level of workability that is suitable for pavement concrete mixtures. The minimum paste content should be determined based on the voids in the combined aggregate system used in the mixture.

2.5 FUTURE GUIDANCE

The procedure for concrete mixture proportioning can generally be considered in terms of three components: the combined aggregate system, paste quality, and paste quantity. In order to minimize binder content, it is recommended that the quantitative parameter V_{paste}/V_{voids}, developed by Wang et

al. (2017), be used to correlate a mixture's performance with its paste volume for a given aggregate system. The suggested minimum V_{paste}/V_{voids} values for different SCMs and performance properties are provided in Table 8. These values can serve as a starting point for optimizing cementitious materials content in pavement mix design applications.

Table 8. Suggested minimum V_{paste}/V_{voids} for different SCMs

Performance properties	Suggested minimum V_{paste}/V_{voids}, %			
	PC	FFA	CFA	S
Workability	140	125	125	160
Compressive strength	150	175	150	175
Chloride ion penetrability	Practically low when achieving workability and compressive strength requirements			
Drying shrinkage				

Source: Wang et al. 2017

CHAPTER 3: EXPERIMENTAL PROGRAM

3.1 MATERIALS

3.1.1 Cementitious Materials

Type I/II Portland cement (ASTM C150) and Class F fly ash (ASTM C618) were used as the cementitious mixtures for all mixtures. A binary system with 25% (by mass) fly ash replacement was designed.

3.1.2 Aggregate

A single source of coarse aggregate, two types of intermediate aggregates, and a natural river sand were used. Table 9 summarizes the physical properties of aggregates.

Table 9. Aggregate properties

Aggregate Type	Specific Gravity (SSD)	Water Absorption (%)
Coarse	2.73	0.90
Intermediate #1	2.69	1.30
Intermediate #2	2.67	1.50
River Sand	2.63	0.90

Both concrete mixtures were proportioned with an optimized aggregate system, with a weight fraction of 18% coarse aggregate, 33% intermediate #1, 10% intermediate #2, and 39% fine aggregate. The combined aggregate gradations were plotted in a Tarantula curve (Ley et al. 2012), power 45 curve (Kennedy et al. 1994), and Shilstone workability factor chart (Shilstone 1990), as shown in Figure 10.

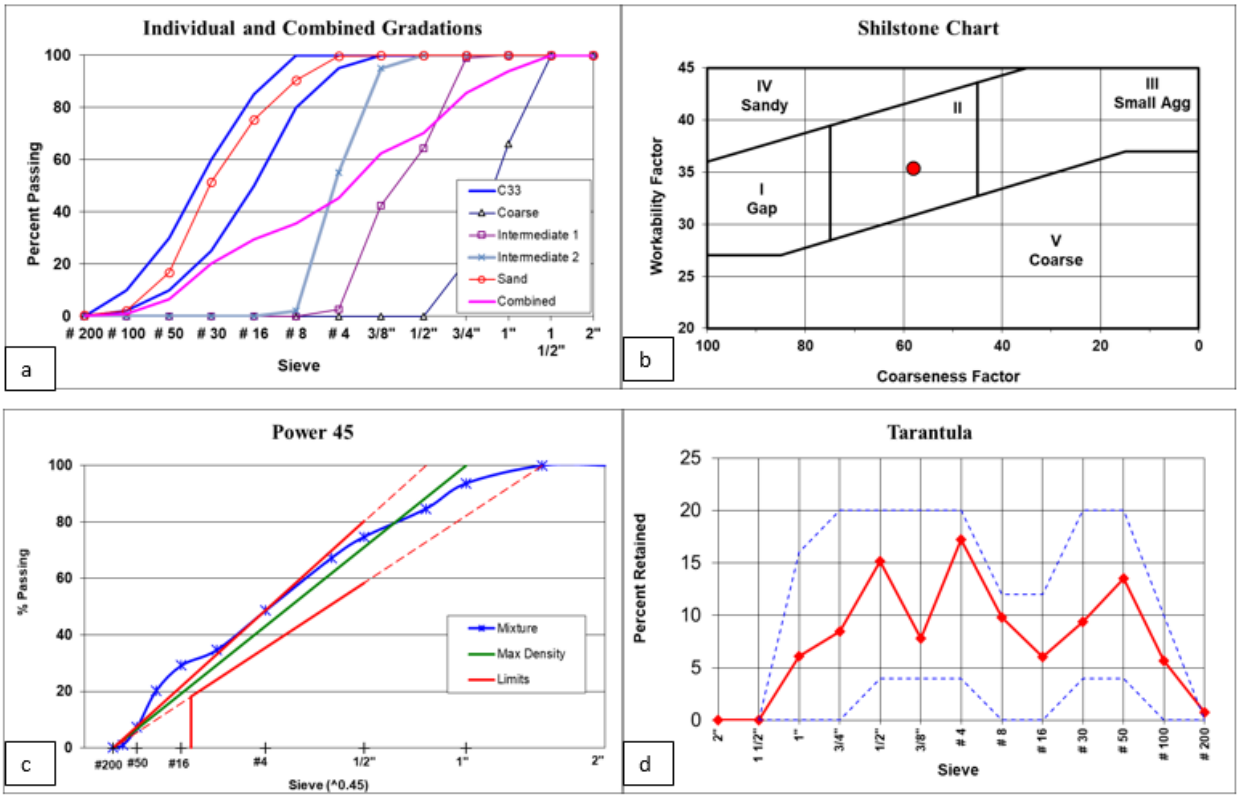

Figure 10. (a) Individual and combined gradations, (b) workability factor chart, (c) power 45 chart, and (d) Tarantula curve

In the workability factor chart, the workability and coarseness factors of the aggregate system fall within Zone II. The combined aggregate system also met the recommendations of the Tarantula plot.

3.1.3 Mixture Proportions

Table 10 offers a summary of the mixture proportions used for casting the pavement at Cells 138 and 238, as well as the concrete mixture used for casting the reference pavement at Cell 524. The mixtures used for building Cells 138 and 238 were proportioned with fixed w/cm of 0.42, while a w/cm of 0.40 was used for the reference concrete used in construction of Cell 524. A binary cement with 25% Class F replacement was used for mixtures with Low and Lower cementitious materials content, compared to 30% fly ash replacement in reference mixture. Air entraining admixture (AEA) and high range water reducing admixture (HRWRA) were used to secure required fresh properties. The percentage voids in aggregate was 27.3% determined based on modified ASTM C 29. Results were incorporated in determining the paste to combined aggregate voids volume ratio (V_{paste}/V_{voids}) using the approach described by Taylor et al. (2015). This approach suggests that V_{paste}/V_{voids} should range between 125 and 175 percent.

Table 10. Concrete mixture proportions

Mix ID	Unit	Type	Low Cementitious (Cell 138)	Lower Cementitious (Cell 238)	Reference (Cell 524)
Cement	lb/yd^3	Type I/II	375	353	400
Fly Ash	lb/yd^3	Class F	125	117	170
Water	lb/yd^3		210	197	228
w/cm			0.42	0.42	0.40
Coarse Agg.	lb/yd^3		322	328	562
Intermediate #1	lb/yd^3		1,071	1,091	1,015
Intermediate #2	lb/yd^3		589	600	305
Fine Agg.	lb/yd^3		1,235	1,258	1,173
Air Entraining Admixture	oz/cwt		1.0	2.0	
Water Reducing Admixture	oz/cwt	High Range	1.0	1.0	
SCM Dosage	% mass		25	25	30
V_{paste}/V_{voids}	%		146	137	
Unit Weight	lb/ft^3		145.4	146.1	

3.2 TEST METHODS

The test program considered for investigating the properties of incorporated concrete mixtures and performance of the investigated cells can be divided into three stages:

- Field tests aimed at assessing the robustness and consistency of the concrete mixtures used for building the cells
- Laboratory tests aimed at investigating the strength development, durability in terms of transport properties, and joint deterioration potential of the concrete mixtures used for building the cells. Samples for lab tests were fabricated in the field.
- Use of instrumentation and in-situ tests aimed at exploring the performance of the pavements over time.

The following field tests were conducted:

- VKelly (AASHTO TP 129) (Figure 11)
- Box test (Cook et al. 2014) (Figure 12)
- Super air meter (SAM) (Ley 2013)
- Air content (ASTM C 231 2014)
- Unit weight (ASTM C 29 2009)
- Microwave water/cementitious ratio
- Semi-adiabatic calorimetry (ASTM C 1753 2015) (Figure 13)
- Maturity, using embedded sensors

The following laboratory tests were conducted:

- Compressive strength measurement (ASTM C 39)
- Modulus of elasticity and Poisson's ratio (ASTM C 469)
- Flexural strength (ASTM C 78)
- Air-void system in hardened state (ASTM C 457)
- Coefficient of thermal expansion (AASHTO T 336)
- Drying shrinkage (ASTM C 157)
- Surface resistivity (AASHTO TP 95 2011) up to 91 days (cylinders)
- Formation factor (AASHTO PP 84-17) up to 91 days (cylinders)
- Low-temperature differential scanning calorimetry

The following instrumentations and in-situ tests were conducted:

- Falling weight deflectometer (MnDOT's FWD Tester, ASTM E2583 07-2015)
- Ride quality (MnDOT's Light Weight Profiler, ASTM E-950)
- Dynamic load test (MnROAD Semi Tractor Trailer)
- Deformations due to environmental conditions (Vibrating Wire Strain Gages)
- Temperature gradient through the depth of pavement structure (Thermocouples)
- Moisture gradient through the depth of pavement structure (Decagon conductivity sensors)
- Evaluating the joint activation using MIRA
- Distress survey (In-situ inspection)
- MIRA Inspection

Figure 11. VKelly test setup

Figure 12. Box test showing voids on concrete surface

Figure 13. Calorimetry test setup for measuring the heat of hydration

3.3 RESULTS

3.3.1 Concrete Mixture Properties

This section summarizes the data obtained from testing the fresh and hardened concrete specimens. Specific tests are discussed below.

The ambient temperature during field testing were in the range of 61.3 to 68.0°F, relative humidity varied from 67 to 87 percent, and wind speed was 3.0 mph.

3.3.1.1 VKelly Test

The VKelly tests indicated that the slump of the mixtures used for Cells 138 and 238 were 2.50 and 1.50 in., respectively. The VKelly index of 0.50 in./$s^{0.5}$ obtained for mixture with lower cementitious content was slightly lower than the recommended minimum of 0.60 in./$S^{0.5}$. However, the mixture with low cementitious content used for Cell 138 exhibited a VKelly index of 0.88 in./$s^{0.5}$, which was within the recommended range (Taylor et al. 2015). Slight adjustments in WRA dosage were necessary to achieve desirable workability during paving with concrete containing lower cementitious materials content.

3.3.1.2 Box Test

The box test indicated better workability for mixture with low cementitious content. An average visual rating of 1.0 was reported for this mixture, corresponding to less than 10 percent overall surface voids.

The visual rating was between 2 and 3 for the concrete with lower cementitious content, indicating 30-50 percent overall surface voids (Cook et al. 2014). No edge slump was observed for the mixtures.

3.3.1.3 Super Air Meter (SAM) Test

The SAM test was conducted to measure the air content in fresh state, as well as the quality of the air void system. Two measurements were performed for each concrete type. The average air content in fresh state was 8.5% and 6.5% for the mixtures with "low" and "lower" cementitious materials contents, respectively, with average SAM numbers of 0.26 and 0.22. Ley (2013) recommends a SAM value below 0.2, which is associated with a spacing factor below 0.008 in for acceptable freeze-thaw durability. The fresh air-void system data obtained for the mixtures used in construction of Cells 138 and 238 suggest proper durability against freeze and thaw cycles.

3.3.1.4 Unit Weight

The average unit weight was 143.0 and 148.1 lb/ft^3 for the mixtures with "low" and "lower" cementitious materials contents, respectively. The theoretical unit weight was 145.4 and 146.1 lb/ft^3 for these mixtures, respectively.

3.3.1.5 Microwave Water Content

The microwave test indicated average w/cm of 0.41 and 0.44 for the mixtures prepared with low and lower contents of cementitious materials, respectively. It is worth mentioning that the design w/cm was 0.42 for both mixtures. The higher w/cm of 0.44 obtained for concrete used in building the Cell 238 can raise concerns regarding the long-term durability of this cell. Increase in shrinkage and lower transport properties could be expected for this mixture.

3.3.1.6 Semi-Adiabatic Calorimetry

The calorimetry curves are presented in Figure 14, and temperature rise data are plotted in Figure 15. No significant difference in temperature rise was observed for the first 10 hours, while slightly higher values were observed for the concrete proportioned with low cementitious materials content afterwards.

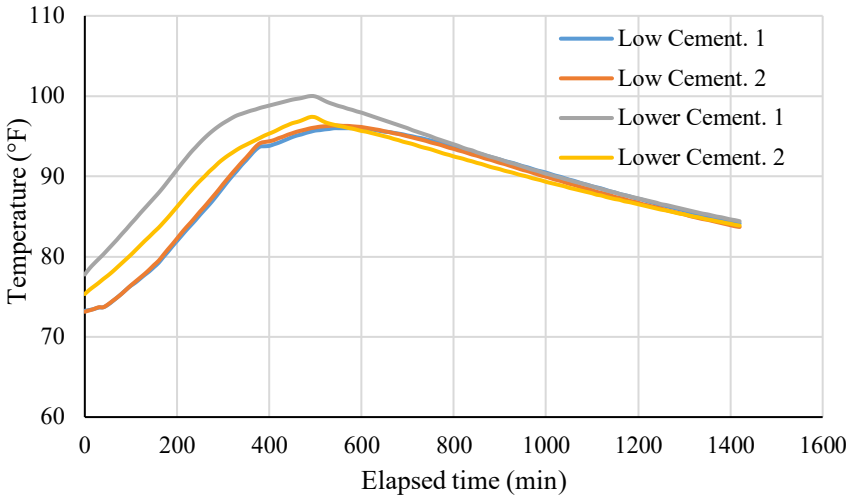

Figure 14. Semi-adiabatic calorimetry results

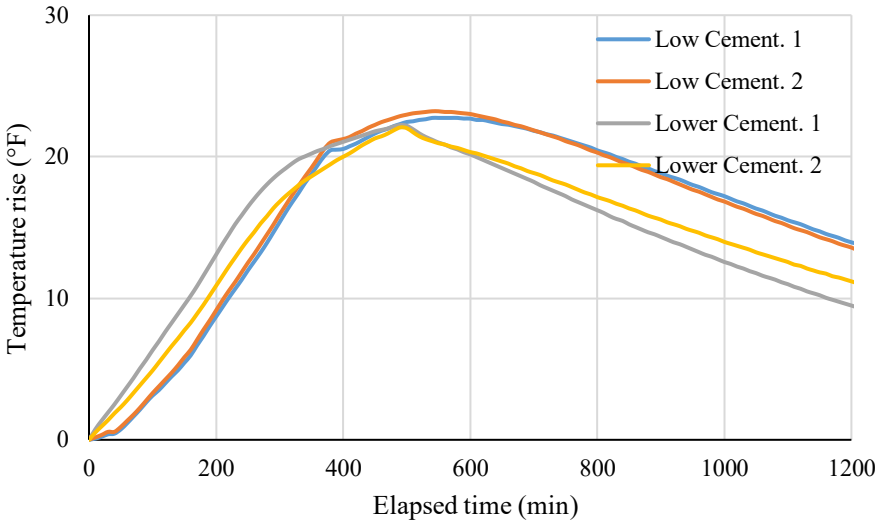

Figure 15. Semi-adiabatic calorimetry temperature rise

The minor variations in temperature raise for the investigated mixtures presented in Figure 15 is believed to be due to the lower cementitious materials content used in construction of Cell 238. However, no abnormalities were observed in terms of delayed setting time or strength development of either of the mixtures and no issues were observed later on during saw cutting the joints.

3.3.1.7 Maturity

Figure 16 presents the average maturity data recorded for the mixtures. Similar performance was observed, regardless of the binder content. This was expected given the same binder composition used in both mixtures. Observations were in agreement with the calorimetry results and early age compressive strength data obtained through laboratory testing (discussed in following sections).

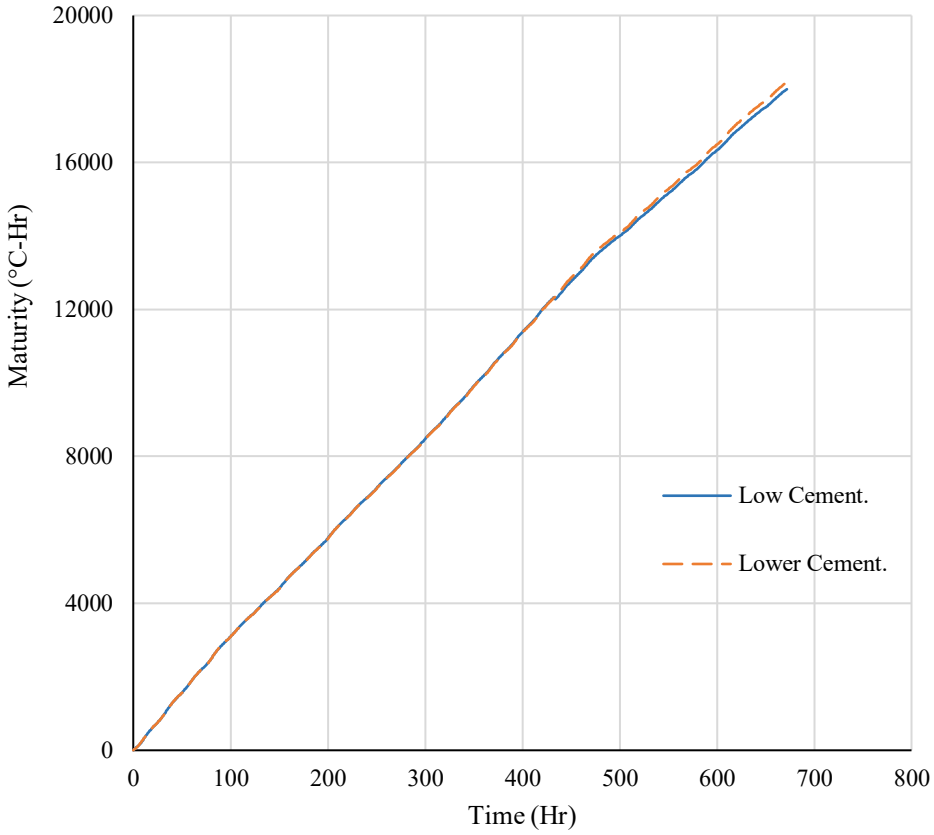

Figure 16. Average maturity data

3.3.1.8 Compressive Strength

The average compressive strength of the mixtures is presented in Figure 17 for up to 28 days. Both mixtures developed comparable compressive strength regardless of the binder content. Both mixtures exhibited a 48-hour strength of approximately 1,750 psi and 28-day strength of higher than 3,500 psi as required by AASHTO PP 84. Both mixtures exhibited the compressive strength of 3,000 psi, required for opening to traffic (MnDOT2016), before 14 days. The slightly higher 28-day compressive strength of the concrete with lower cementitious materials content may be attributed to the lower air content observed for this concrete (6.5% vs. 8.5%).

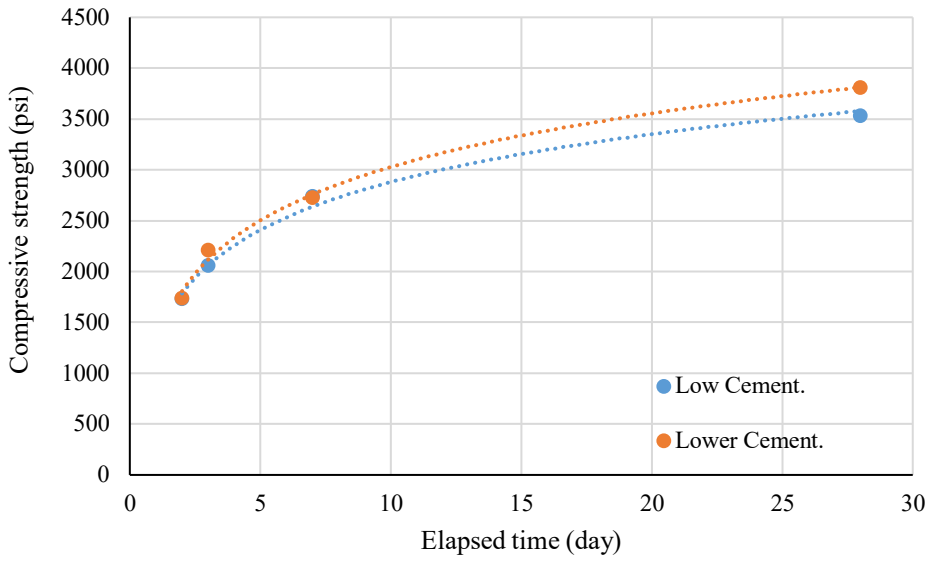

Figure 17. Compressive strength results

3.3.1.9 Modulus of Elasticity and Poisson's Ratio

Static modulus of elasticity (MOE) and Poisson's ratio measurements were conducted at 28 days. The mixture prepared with lower binder content exhibited 28-day MOE of 5.43×10^6 psi, in comparison to 5.26×10^6 psi, for the concrete with low cementitious materials. This can be due to the slightly higher aggregate content in concrete prepared with lower binder content. The 28-day Poisson's ratio values were 0.21 and 0.17 for the mixtures made with lower and low cementitious materials content, respectively. Assuming similar base conditions, and considering the same thickness of the pavements, comparable MOE values obtained for the two mixtures suggest similar response to traffic loading for the investigated cells.

3.3.1.10 Flexural Strength

Flexural strength measurements were conducted at 3, 7, and 28 days. Results are presented in Figure 18. The mixture prepared with low cementitious materials content exhibited a linear trend in flexural strength development, with a 28-day value of 615 psi. The concrete with lower cementitious materials content developed a relatively low 3-day flexural strength of 170 psi. However, the 7- and 28-day flexural strength values for this mixture were comparable to those of the concrete with low cementitious materials content. The 7- and 28-day flexural strength values for concrete made with lower cementitious materials content were 475 and 625 psi, respectively.

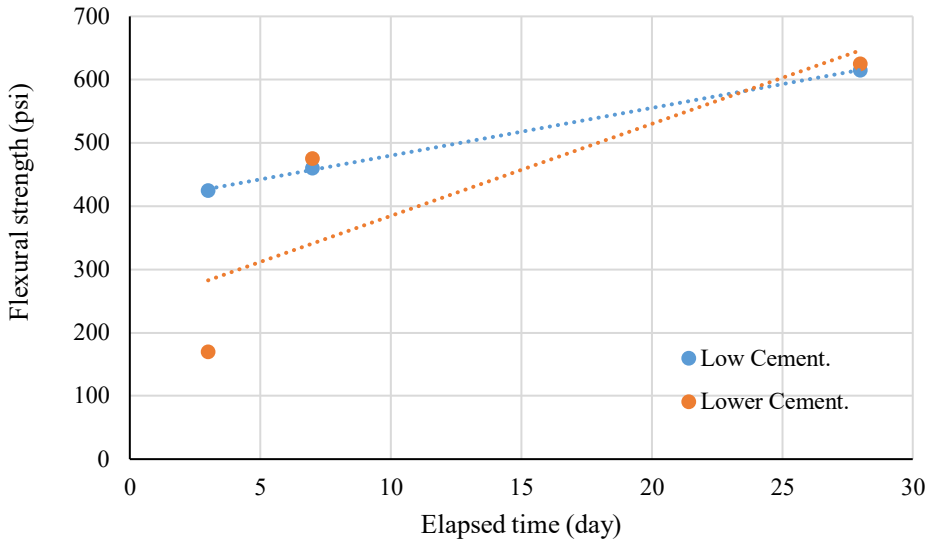

Figure 18. Flexural strength measurements

In general, it was observed that the mixtures prepared with Low and Lower cementitious materials content, used for building the cells 138 and 238, respectively, exhibited comparable mechanical properties. This is in line with the comparable in-situ performance data obtained from testing the Cells 138 and 238.

3.3.1.11 Hardened Air-Void Analysis

An approximate reduction of 1.0% in air content of hardened samples was observed in comparison with the results in the fresh state. Analysis of the hardened specimens indicated an air content of 7.5% for the concrete with low cementitious content (Cell 138) and air content of 5.3% for mixture made with lower binder content (Cell 238). Both these mixtures exhibited spacing factor of 0.002 in. and specific surface area within the range of 1500±100 $in.^2/in.^3$. A spacing factor of no more than 0.008 in. is generally recommended in order to secure a desirable air-void system in moderate exposures (ASTM C 457). The air-void system data obtained in fresh and hardened states suggests potential for desired durability against freezing and thawing cycles. Data obtained during the first year certifies the acceptable performance of the investigated cells. The research team will continue monitoring the cells for signs of any freeze-thaw related distress for the next two years.

3.3.1.12 Coefficient of Thermal Expansion (CTE)

CTE measurement was conducted at 28 days. Both mixtures exhibited a CTE of 5.0×10^{-6} in./in./°F. Lower CTE values can reduce the thermal deformation of rigid pavements. The obtained values were reasonably low compared to the typical values expected for pavement concrete. These were in line with the comparable response of the pavement sections to environmental effects, where both cells exhibited similar strain values and deformation patterns (discussed in following sections).

3.3.1.13 Drying Shrinkage

Shrinkage measurements were conducted at 56 days, including 28 days of moist curing followed by 28 days of drying. The concrete with low cementitious content exhibited a slightly lower shrinkage of 370 με compared to 410 με for the mixture with lower binder content. Even though both numbers can be considered as adequately low drying shrinkage values, this observation can be attributed to the slightly higher w/cm measured for the concrete with lower cementitious content determined through microwave test (w/cm of 0.44 vs. 0.41).

3.3.1.14 Surface Resistivity Test

The criteria for assessing surface resistivity, as proposed by AASHTO PP 84, are summarized in Table 11

Table 11. The average surface resistivity measurements are presented in Figure 19. The investigated mixtures exhibited comparable resistivity, with 91-day values of about 25.0 kohm-cm, corresponding to "Very Low" risk of chloride ion penetration at 91 days. The increasing surface resistivity over time indicates potentially improved performance in the long-term.

Table 11. Chloride ion penetrability classification (Adapted from AASHTO PP 84)

Chloride Ion Penetrability	Greatest Resistivity (kohm-cm)	Lowest Resistivity (kohm-cm)
High	5	~
Moderate	10	5
Low	20	10
Very Low	200	20
Negligible	~	200

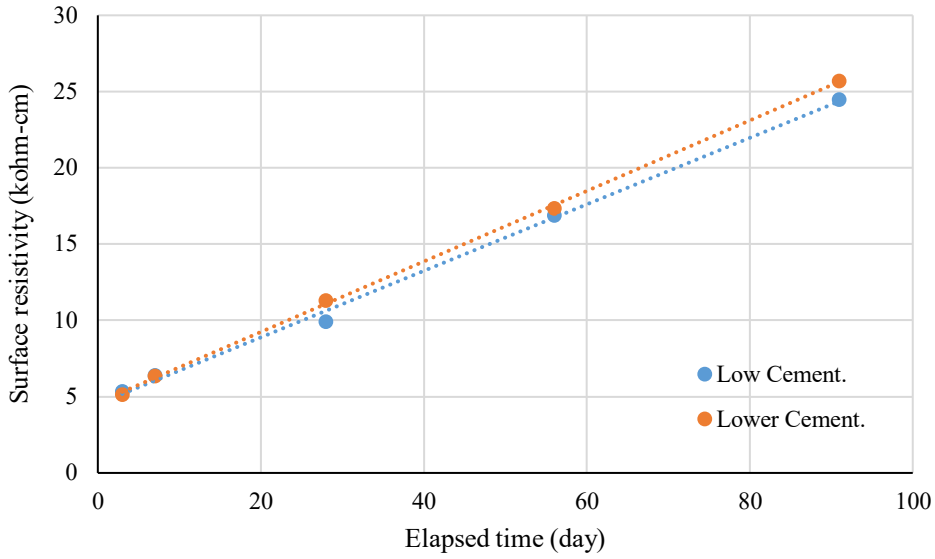

Figure 19. Surface resistivity measurements

3.3.1.15 Formation Factor

Formation factor (FF) development is presented in Figure 20. Measurements are based on assuming a pore solution resistivity of 0.10 Kohm-cm as suggested by Barrett et al. (2016). Reported data are based on moist cured samples rather than vacuum saturated specimens. The investigated mixtures exhibited similar FF values, with 91-day measurements of about 2500, corresponding to "Very Low" chloride ion penetrability as proposed by AASHTO PP 84 (2017).

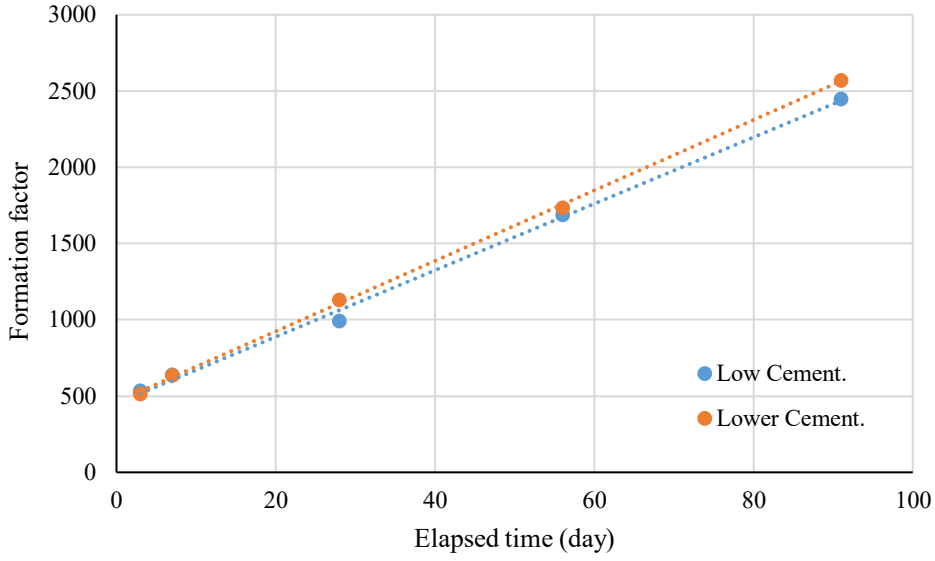

Figure 20. Formation factor results

3.3.1.16 Low-Temperature Differential Scanning Calorimetry

Monical et al. (2016) have proposed a method using low-temperature differential scanning calorimetry (LT-DSC) to quantify the potential for calcium oxychloride formation for cementitious materials in the presence of calcium chloride.

Samples from both mixtures were prepared by grinding hardened paste to a powder that passed through a 75-µm sieve (No. 200). A calcium chloride solution was prepared at a concentration of 20 percent $CaCl_2$ by mass. Then, 10 ±1 mg of powder specimen was mixed with the solution in a powder-to-solution mass ratio of 1 to 1 and tested in accordance with the following procedure (Monical et al. 2016):

8. Store the sample at room temperature for approximately 1 hour after combining the cementitious powder and salt solution to permit any heat associated with the hydration of exposed unreacted surfaces of cementitious materials to dissipate
9. Reduce the temperature to -90˚C at a rate of 3˚C/min and start logging data
10. After reaching -90˚C, expose the sample to a low-temperature loop (cycling the temperature from -90˚C to -70˚C back to -90˚C at a rate of ±3˚C/min) until the solution has frozen
11. Heat the sample at a rate of 0.25˚C/min until the sample reaches a temperature of 50˚C; then, allow the sample to return to room temperature

The heat absorbed during the calcium oxychloride melting phase is evaluated by integrating the heat flow versus time curve. The energy associated with the calcium oxychloride formation can be estimated by measuring the magnitude of the shift in cumulative heat slopes before and after the phase transformation (i.e., the drop in the cumulative heat curve between points A and C, as shown in Figure 21).

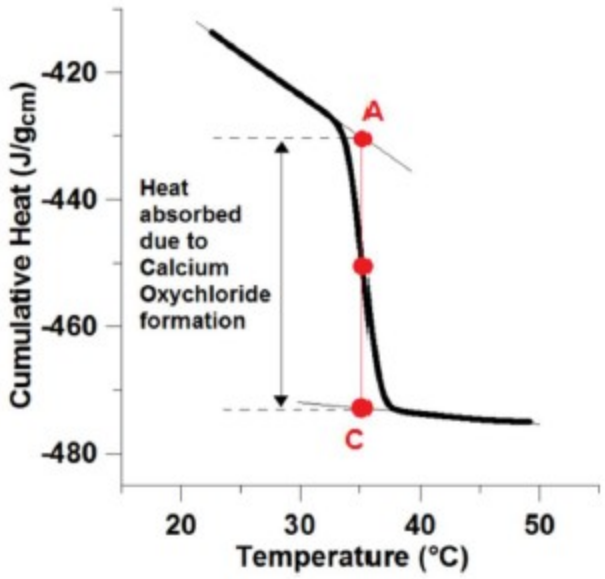

Figure 21. The drop associated with calcium oxychloride formation in cumulative heat curve (Monical et al. 2016)

The specific latent heat can be used to quantify the amount calcium oxychloride through Equation 1:

$$m_{oxy} = \frac{\Delta H_{oxy}}{L_{oxy}} \quad (1)$$

Where, m_{oxy} is the gram of calcium oxychloride per gram of cementitious binder, ΔH_{oxy} (joule per gram of cementitious material) is the latent heat absorbed during the calcium oxychloride phase transformation calculated for samples with different cementitious materials, and L_{oxy} (joule per gram of oxychloride) is the specific latent heat associated with calcium oxychloride phase transformation, which is 186 J/g.

The cumulative heat flow based on LT-DSC results was 6.36 for both investigated mixtures. A typical DSC curve is presented in Figure 22. This resulted in 0.186 and 0.205 gram of calcium oxychloride per gram of paste for the mixtures with low and lower cementitious materials content, respectively. A value of less than 0.15 gram of calcium oxychloride per gram of paste is recommended by AASHTO PP 84 to ensure low risk of oxychloride formation. This indicates that the investigated cells (138 and 238) can be prone to the risk of oxychloride formation if subjected to de-icing salts.

One should note that the electrical resistivity measurement is a function of system porosity and transport properties. However, the oxychloride formation risk is a function of binder chemistry. Therefore, the observations from these two test will not necessarily follow the same trend.

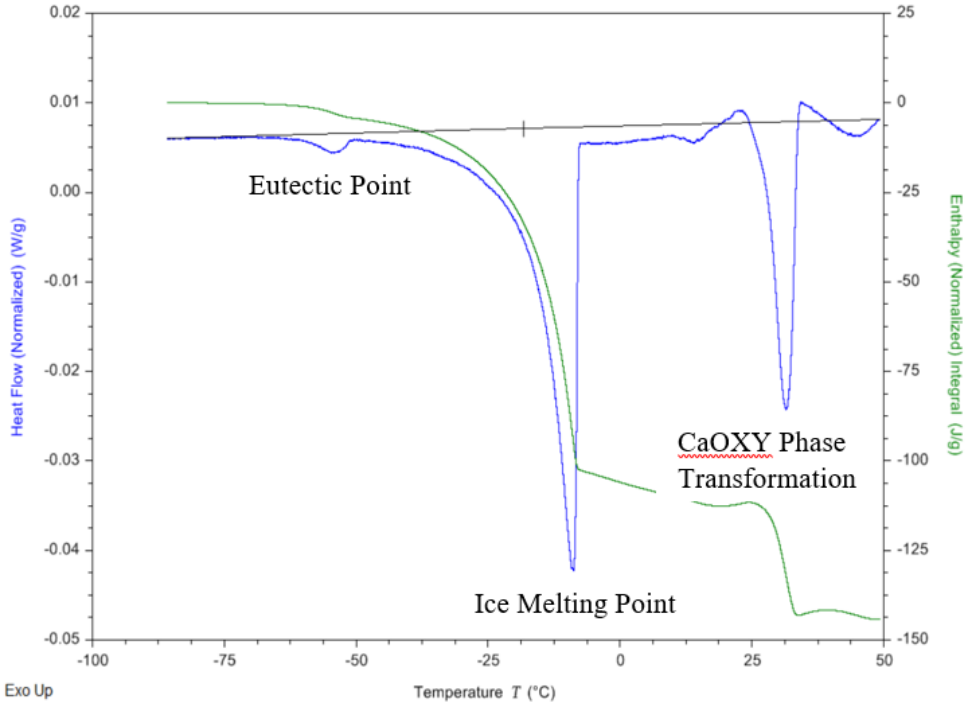

Figure 22. A typical LT-DSC curve

3.3.2 Pavement Performance – In-Situ Measurements

3.3.2.1 Falling Weight Deflectometer

Falling weight deflectometer (FWD) test was conducted on pavement cast with reduced cement content and reference mixture according to the following matrix. Note that the reference cell (cell 524) is 6.0 in. thick, while the 138 and 238 cells were 8.0 in. thick. MnDOT's FWD tester, conforming to requirements of the ASTM E2583 was used for testing the cells. The test setup is shown in Figure 23 .

Figure 23. MnDOT's FWD tester

Test dates:

Reference pavement (cell 524): 09/14/2017, 10/23/2017, 03/15/2018, 05/04/2018, 03/29,2019, and 05/07/2019.

Pavement with low (cell 138) and lower cementitious materials (cell 238): 09/06/2017, 10/24/2017, 03/27/2018, 05/03/2018, and 04/02/2019.

Investigated lanes:

Inside lane and outside lane for all cells

Investigated slabs:

Reference pavement (cell 524): slab #0 and #2

Low cement pavement (cell 138): slab #4, #7, #11, and #14

Lower cement pavement (cell 238): slab #2, #6, #9, and #13

Test positions:

Slab center, corner, mid-edge, joint before, and joint after for all concrete types

Load amounts:

Deflections were collected for one drop at each load level of 6000, 9000, and 12000 lbs, corresponding to approximate stress level of 390, 570, and 750 KPa.

Sensor offsets:

Ten sensors were incorporated to collect the deformation at various distances with respect to the center of the load plate. Table 12 summarizes the sensor spacing.

Table 12. FWD sensor spacing from center of the load plate

Sensor #	1	2	3	4	5	6	7	8	9	10
Distance (in.)	0	8	12	18	24	36	48	60	72	-12

Test data obtained from FWD testing conducted before and after the transverse joints, corresponding to approaching and departure traffics, respectively, were used to calculate the load transfer efficiency (LTE) according to Equation 2.

$$LTE = \frac{\delta_U}{\delta_L} \times 100\% \quad (2)$$

where δ_U is the deflection of the unloaded side of the joint (mm), δ_L is the deflection of the loaded side of the joint (mm), and LTE is the load transfer efficiency (%).

Results are summarized in Figure 24 through Figure 26 for the pavement cast with low cement, lower cement, and reference concrete mixtures, respectively. The values reported in these figures summarize the data obtained for both inside and outside lanes exposed to approach and departure traffic, also known as “Before Joint” and “After Joint” measurements, respectively. Scatter in data makes it difficult to draw trend lines. However, a general trend of slight reduction in LTE values can be observed over time.

Results obtained for inside lane of cell 138 cast with low cementitious materials content indicated LTE values ranging from 79% to 96%, and from 80% to 97% for the approach and departure traffics, respectively. LTE values obtained for the outside lane ranged from 82% to 93% and from 83% to 97% for the approach and departure traffics, respectively.

Similar data were obtained from cell 238, indicating comparable LTE for the departure and approaching traffics for both lanes. For the inside lane, the LTE ranged from 78% to 95% for the approaching and from 81% to 97% for the departure traffic, respectively. LTE results were between 83% and 94% for the outside lanes, regardless of the traffic direction.

Slight reduction in LTE was observed for the reference pavement with average data between 85% and 91%. This can be due to the lower thickness of the reference cell compared to the low cement sections.

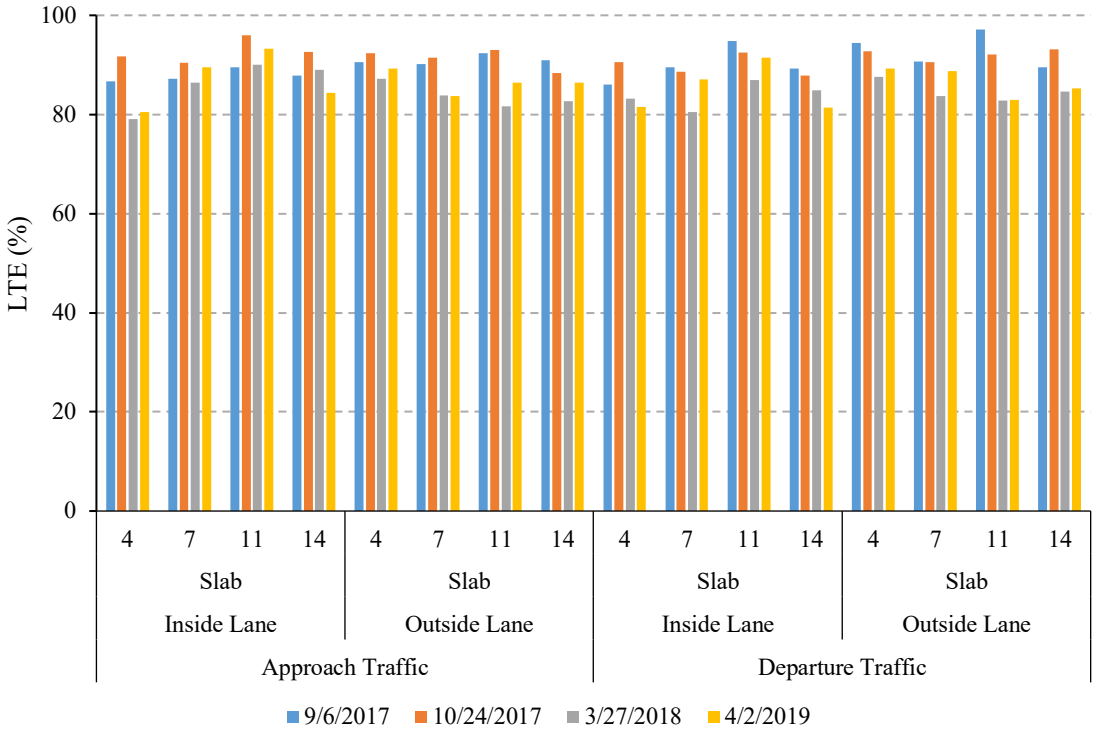

Figure 24. Average LTE data obtained for concrete with low cement content (cell 138)

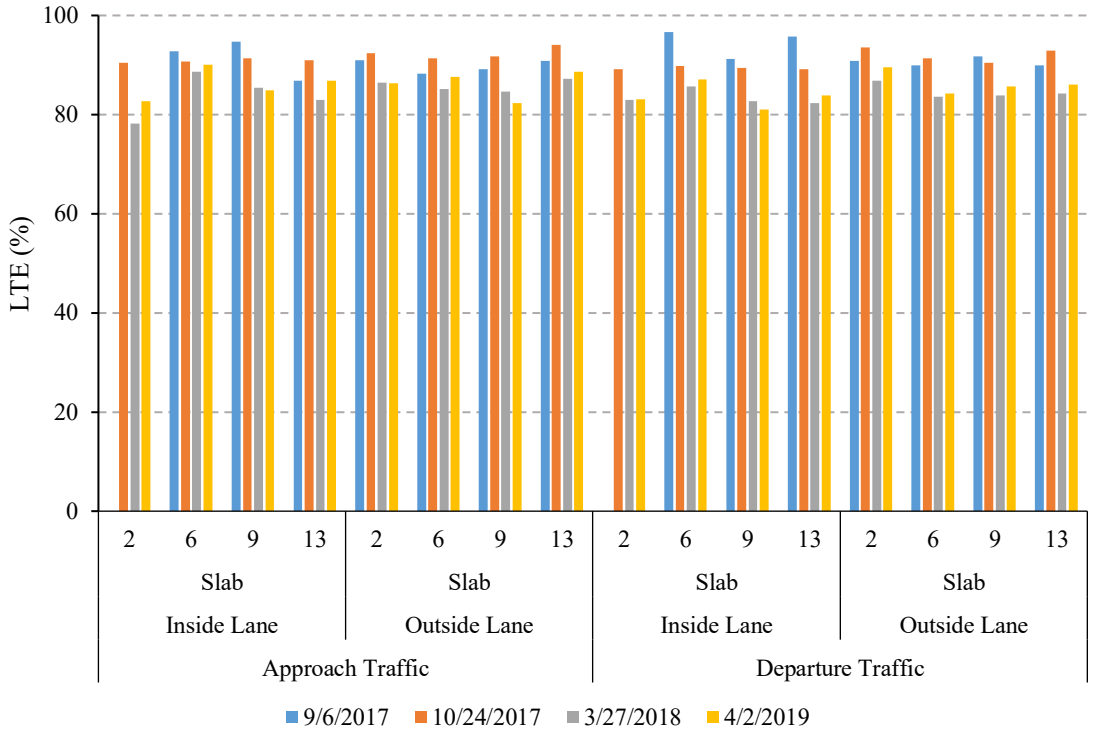

Figure 25. Average LTE data obtained for concrete with lower cement content (cell 238)

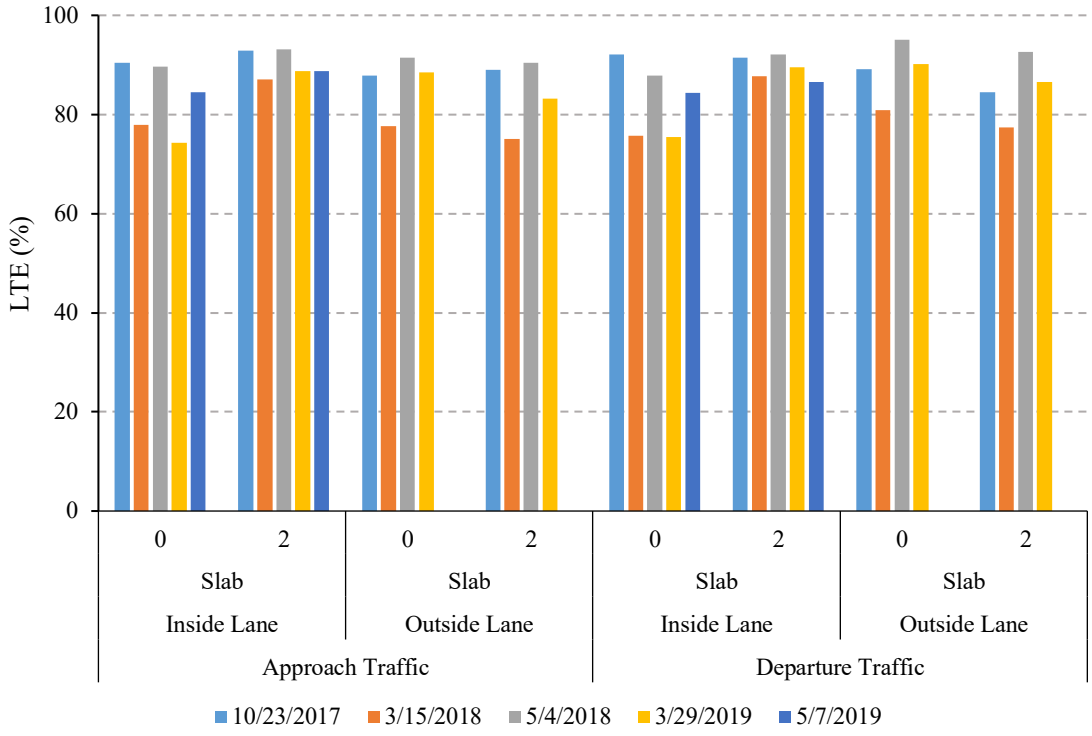

Figure 26. Average LTE data obtained for reference concrete (cell 524)

The LTE data as a function of traffic direction are summarized in Figure 27. In general a linear correlation was observed for the LTE values obtained for the approaching and the departure traffic. In general the LTE values obtained for cells 138 and 238 were comparable, indicating similar load transfer characteristics for these two cells. For both cells, the comparison between the LTE values for departure and approaching traffic indicated higher scatter in LTE values for the inside lane exposed to regular traffic loading. In summary, the LTE values obtained for cells 138 and 238 suggested uniform performance during the first three years.

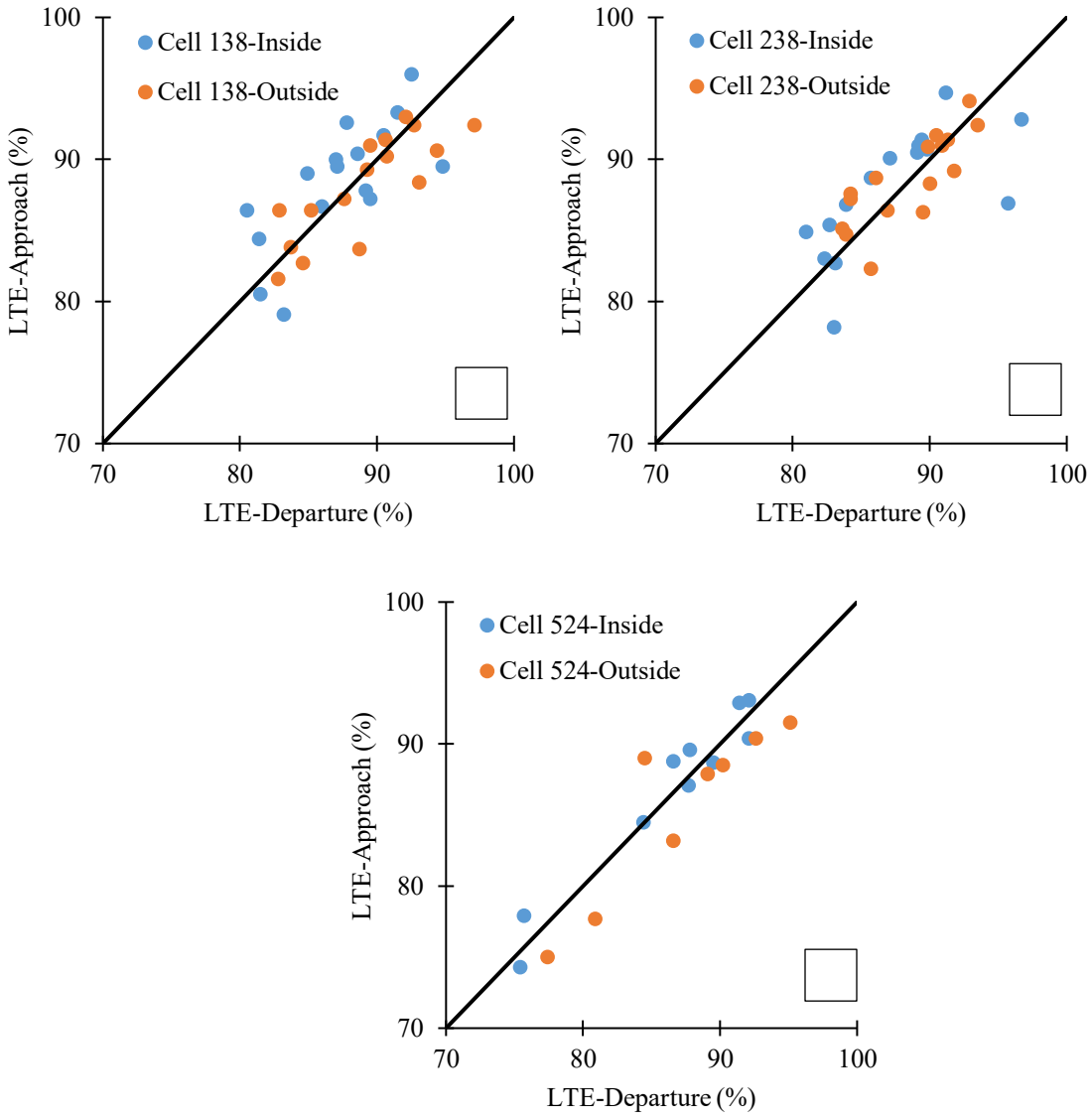

Figure 27. Variation in LTE as a function of traffic direction for low cement concrete (a), concrete with lower cementitious content (b), and reference mixture (c)

A statistical data analysis was conducted to determine the statistically significant differences between the LTE values. Such an analysis enables us to make sure that the conducted comparisons and derived conclusions are robust and not due to experimental errors and noise in data. Analysis of variance (ANOVA) was conducted based on F-test as means of comparing the LTE data obtained for different cells. A statistical analysis software (JMP Pro 15) was used for hypothesis testing at α=0.05 significance level.

Statistical analysis relies on the fact that a calculated P-value less than the significance level means that the factor or the interaction between factors will be statistically significant, while a P-value greater than

the α=0.05 threshold reveals the fact that such a particular factor or interaction will not be statistically significant (Montgomery, 2008). In other words, a P-value less than 0.05 means that there is less than a 5% chance that the observed behavior is due to noise, ensuring that the effect will be statistically significant (Sadati et al. 2016). It should be noted that conducting ANOVA requires the data to follow a normal distribution. Testing the normal distribution of data was performed using the Anderson-Darling method and based on the following null (H0) and alternative (H1) hypotheses at α=0.05 significance level:

- H0: data is following a normal distribution
- H1: the assumption of H0 is not correct

The statistical analysis was performed in two steps. First, the variation of data within a given cell was investigated to see if there is a significant difference in LTE results as a function of traffic direction, lane, test location (slab number), and test date. This was performed for data obtained for cells 138, 238, and 524. The following hypothesis testing scenarios were investigated:

(1) Is there a statistically significant difference in LTE results obtained for a given cell at different times?

- H0: there is no difference in LTE results obtained for a given cell at different times
- H1: the assumption of H0 is not correct

(2) Is there a statistically significant difference in LTE results obtained for different slabs of the same cell?

- H0: there is no difference in LTE results obtained for different slabs of the same cell
- H1: the assumption of H0 is not correct

(3) Is there a statistically significant difference in LTE results obtained for different lanes of a cell?

- H0: there is no difference in LTE results obtained for different lanes of a cell
- H1: the assumption of H0 is not correct

(4) Is there a statistically significant difference in LTE results obtained for different traffic directions?

- H0: there is no difference in LTE results obtained for different traffic directions
- H1: the assumption of H0 is not correct

The distribution of LTE data was initially investigated for all test scenarios to ensure normal distribution of the test data. Anderson-Darling test was performed on the data and the following were observed:

- For cell 138, data did not follow a normal distribution (P-value = 0.025)
- For cell 238, data did not follow a normal distribution (P-value = 0.020)
- For cell 524, data did not follow a normal distribution (P-value = <0.0001)

Knowing the data was not following a normal distribution non-parametric testing was considered for data analysis. A summary of findings is provided below.

Results obtained for investigating overall LTE data for cell 138:

Non-parametric testing was initially considered given the data was not following normal distribution. Based on the Wilcoxon/Kruskal Willis tests, the following P-values were obtained for the aforementioned hypotheses:

- Test date: P-value = <0.0001. In other words, test time had a significant effect on observed LTE data.
- Test slab: P-value = 0.0019. In other words, the variations in LTE results obtained for different slabs were statistically significant.
- Traffic lane: P-value = 0.190. In other words, the variations in LTE results obtained for different traffic lanes were not significant.
- Traffic direction: P-value = 0.754. In other words, the variations in LTE results obtained for different traffic directions were not significant. This is in agreement with the linear correlation previously observed for the approach and departure traffics in Figure 4-a.

Given the fact that over 190 data points were included in these comparisons, which was more than the typically recommended limit of 30 points, it was also considered to assume normal distribution of the LTE data and perform additional parametric testing. Results were in agreement with findings of the non-parametric comparisons, as summarized in Table 13. Test date and slab number were proved to have significant effects on LTE data with P-values lower than 0.05. The least square means plots obtained for different input factors are summarized in Figure 28. Tendency for reduction in LTE over time was observed. Results also exhibited higher LTE values for the outside lane (not exposed to traffic).

Table 13. ANOVA summaries assuming normal distribution of LTE data in cell 138

Source	Nparm	DF	Sum of Squares	F Ratio	Prob > F
Date	3	3	1531.8836	61.6091	<.0001*
Slab	3	3	251.6637	10.1214	<.0001*
Lane	1	1	29.7583	3.5904	0.0597
Traffic Direction	1	1	0.7219	0.0871	0.7682

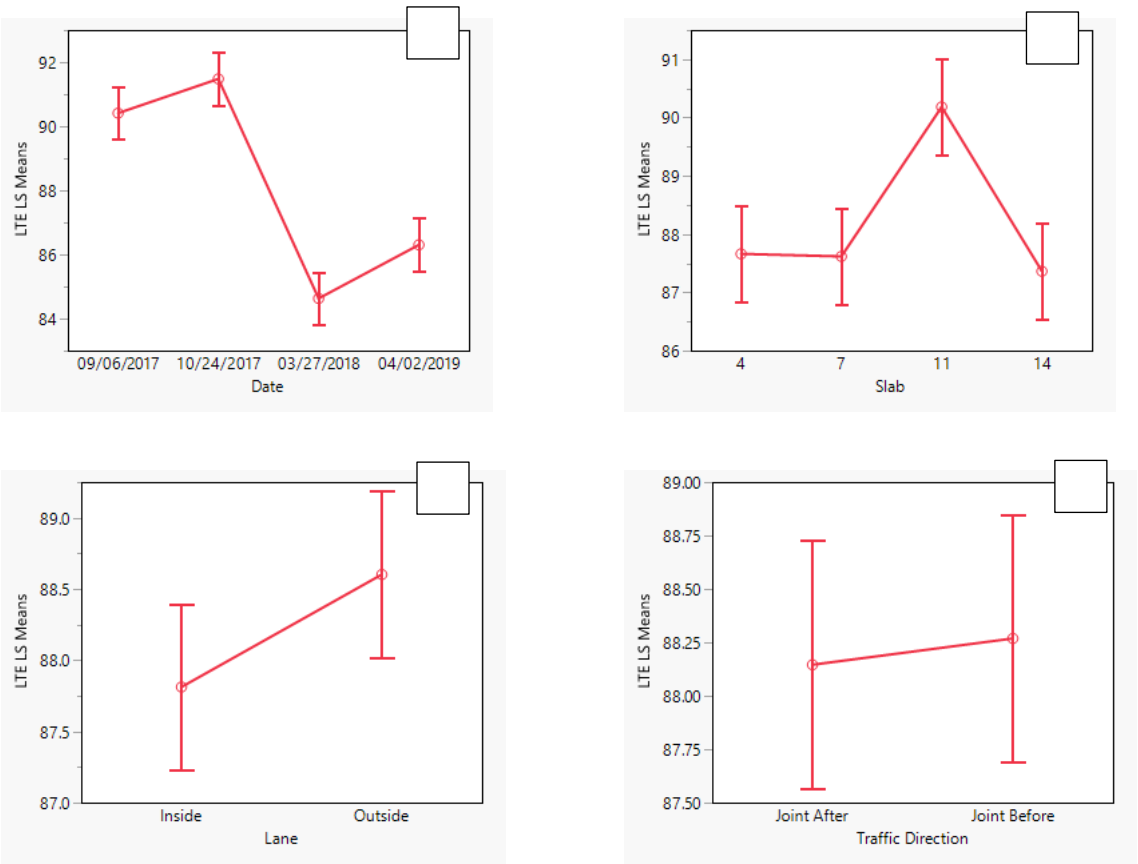

Figure 28. Least square means plots for LTE values of cell 138 as a function of test date (a), slab number (b), lane (c), and traffic direction (d)

Results obtained for investigating overall LTE data for cell 238:

Non-parametric testing was initially considered given the data was not following normal distribution. Based on the Wilcoxon/Kruskal Willis tests, the following P-values were obtained for the aforementioned hypotheses:

- Test date: P-value = <0.0001. In other words, test time had a significant effect on observed LTE data.
- Test slab: P-value = 0.420. In other words, the variations in LTE results obtained for different slabs were not significant.
- Traffic lane: P-value = 0.097. In other words, the variations in LTE results obtained for different traffic lanes were not significant.
- Traffic direction: P-value = 0.332. In other words, the variations in LTE results obtained for different traffic directions were not significant. This is in agreement with the linear correlation observed for the approach and departure traffics in Figure 4-b.

Considering the availability of over 190 data points, parametric testing was also performed with the assumption of normal distribution of LTE data. Results were not in complete agreement with the non-parametric comparisons as summarized in Table 14. Based on the data presented in this table, test date, slab number, and traffic direction had significant effects on LTE results (all with P-values lower than 0.05). Least square means plots obtained for different input factors are summarized in Figure 29. Similar to cell 138, tendency for reduction in LTE over time was observed. Results also exhibited higher LTE values for the outside lane.

Table 14. ANOVA summaries assuming normal distribution of LTE data in cell 238

Source	Nparm	DF	Sum of Squares	F Ratio	Prob > F
Date	3	3	1822.9433	109.4102	<.0001*
Slab	3	3	55.9709	3.3593	0.0201*
Lane	1	1	23.1257	4.1639	0.0428*
Traffic Direction	1	1	5.3009	0.9544	0.3299

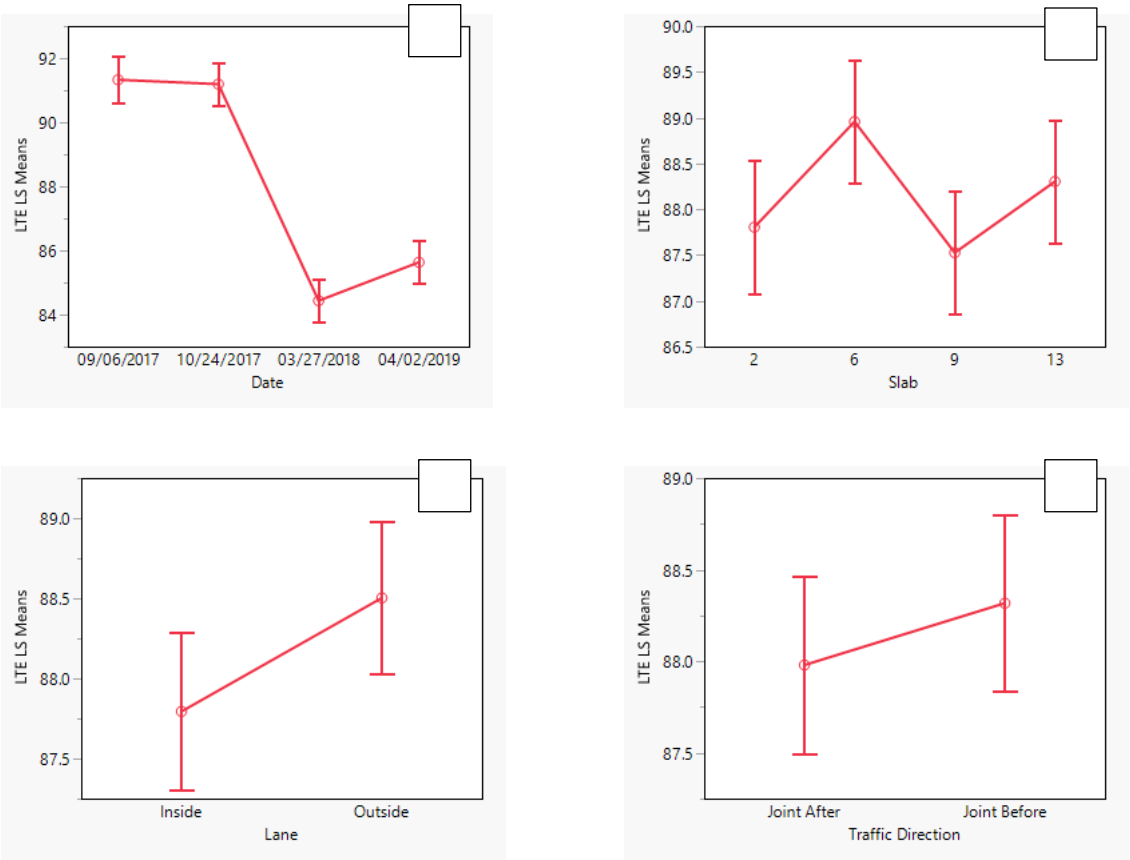

Figure 29. Least square means plots for LTE values of cell 238 as a function of test date (a), slab number (b), lane (c), and traffic direction (d)

Results obtained for investigating overall LTE data for cell 524:

Non-parametric testing was initially considered given the data was not following normal distribution. Based on the Wilcoxon/Kruskal Willis tests, the following P-values were obtained for the aforementioned hypotheses:

- Test date: P-value = <0.0001. In other words, test time had a significant effect on observed LTE data.
- Test slab: P-value = 0.016. In other words, results obtained for different slabs exhibited statistically significant different LTE values.
- Traffic lane: P-value = 0.295. In other words, results obtained for different traffic lanes did not exhibit statistically significant different LTE values.
- Traffic direction: P-value = 0.858. In other words, results obtained for different traffic directions did not exhibit statistically significant different LTE values. This is in agreement with the linear correlation presented for the approach and departure traffics in Figure 4-c.

Considering the availability of over 120 data points, parametric testing was also performed with the assumption of normal distribution of LTE data. Results were in agreement with the non-parametric study as summarized in Table 15. Based on the data presented in this table, test date, slab number, and traffic direction had significant effects on LTE results (all with P-values lower than 0.05). Least square means plots obtained for different input factors are summarized in Figure 30. A scatter in LTE data over time was observed, with a tendency for reduction over time. Results also exhibited higher LTE values for the outside lane.

Table 15. ANOVA summaries assuming normal distribution of LTE data in cell 524

Source	Nparm	DF	Sum of Squares	F Ratio	Prob > F
Date	4	4	2085.6514	35.9184	<.0001*
Slab	1	1	168.9204	11.6364	0.0009*
Lane	1	1	0.2967	0.0204	0.8866
Traffic Direction	1	1	0.8375	0.0577	0.8106

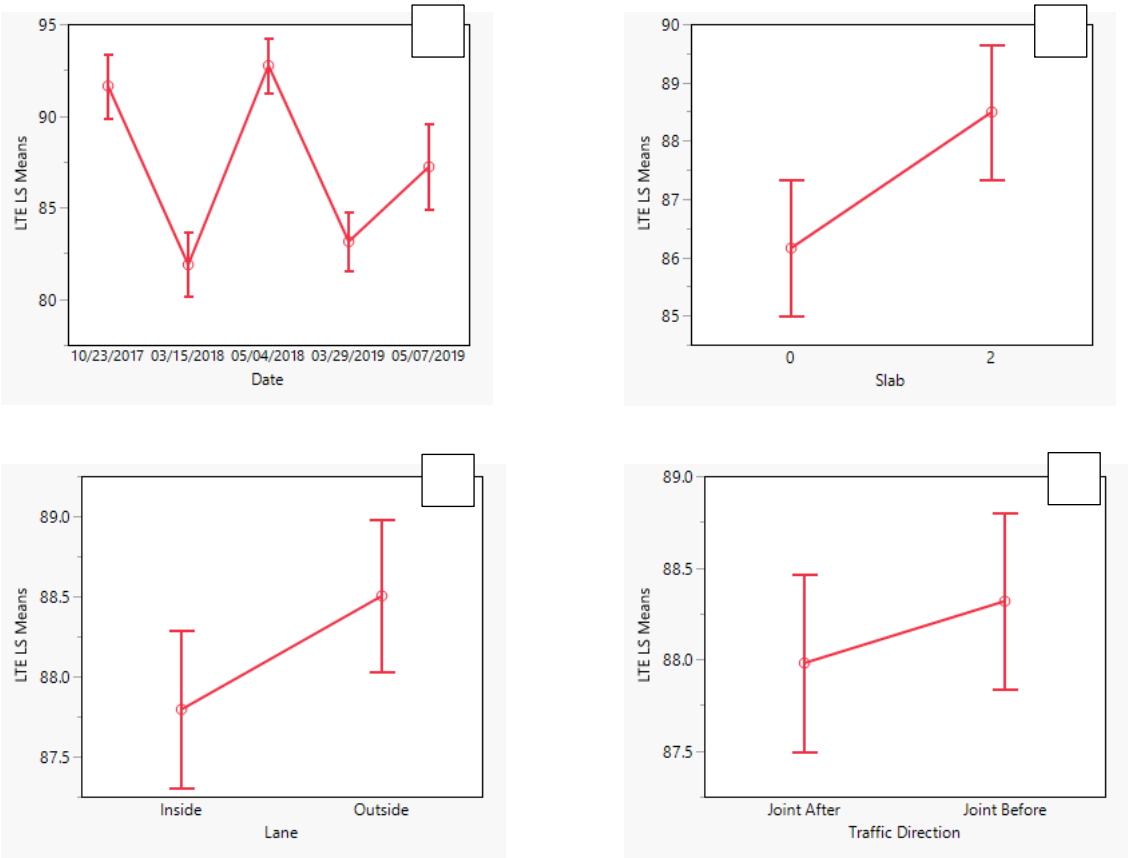

Figure 30. Least square means plots for LTE values of cell 524 as a function of test date (a), slab number (b), lane (c), and traffic direction (d)

Comparing overall LTE data for different cells:

The last step in statistical data analysis was to see if there is a statistically significant difference in LTE results obtained for different cells. Given the lower thickness of cell 524 compared to low cement sections (6.0 in. vs. 8.0 in.), cell 524 was not considered in these LTE comparisons. The following hypotheses were investigated:

- H0: there is no difference in LTE results obtained for cells 138 and 238
- H1: the assumption of H0 is not correct

Non-parametric testing was considered given the data was not following normal distribution. Based on the Wilcoxon/Kruskal Willis tests, a P-value of 0.671 was obtained for the aforementioned hypotheses. In other words, results obtained for different cells (138 vs. 238) did not exhibit statistically significant different LTE values. This means that the concretes prepared with low and lower cementitious materials content had no significant effect on LTE.

Data obtained from testing the slab at interior positions were employed for determining the modulus of subgrade reaction (K) values for the investigated panels according to AASHTO (1993). The area of deflection basin corresponding to 9000 lb. loading was initially calculated based on Equation 3 (AASHTO 1993):

$$AREA = 6 \times \left[1 + 2\left(\frac{\delta_{12}}{\delta_0}\right) + 2\left(\frac{\delta_{24}}{\delta_0}\right) + \left(\frac{\delta_{36}}{\delta_0}\right)\right] \quad (3)$$

where δ_0 is the deflection in the center of loading plate (mm), δ_{12} is the deflection at 12 inches from the plate center (mm), δ_{24} is the deflection at 24 inches from the plate center (mm), and δ_{36} is the deflection at 36 inches from the plate center (mm).

Figure 31 proposed by AASHTO (1993) was then used for calculation of the dynamic K-value based on the calculated AREA and deflection at the center of the loading plate (mils).

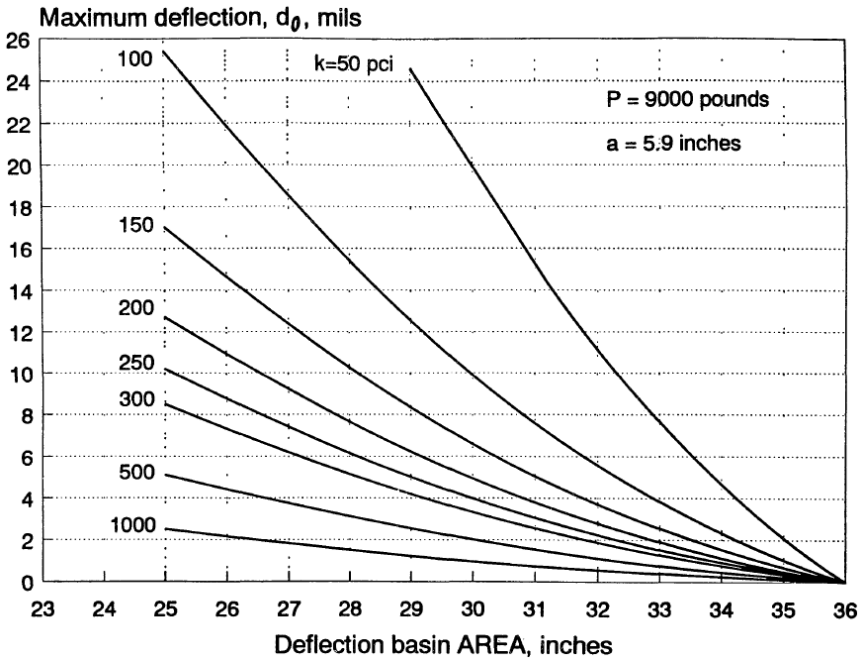

Figure 31. Dynamic k-value as a function of AREA and deflection at the center of the loading plate, borrowed from AASHTO (1993)

Table 16 summarizes the dynamic k-values obtained for the investigated slabs at different testing times obtained for center, corner, and mid-edge of the slabs at inside and outside lanes. The values reported in this table will serve for over-time monitoring the subgrade performance.

In general the k-values were higher for the pavement cast with the reference concrete, indicating better preparation of the subgrade materials. It should be noted that the cell 524 has a sand subgrade versus a clay/loam subgrade for cells 138 and 238. Moreover, test results obtained for the reference cell (cell 524) are affected by the lower slab thickness of 6.0 in. compared to 8.0 in. for cells 138 and 238.

Table 16. Average dynamic k-values (psi)

Cell	Spot	Slab	Test Date										
			2017				2018				2019		
			09/06	09/14	10/23	10/24	03/15	03/27	05/03	05/04	03/29	04/02	05/07
138	Center	4	200	-	-	180	-	350	148	-	-	190	-
		7	168	-	-	195	-	363	150	-	-	210	-
		11	178	-	-	163	-	235	175	-	-	175	-
		14	160	-	-	150	-	285	148	-	-	180	-
238		2	165	-	-	163	-	270	153	-	-	210	-
		6	180	-	-	183	-	370	158	-	-	205	-
		9	168	-	-	175	-	243	158	-	-	170	-
		13	148	-	-	135	-	265	140	-	-	200	-
524		0	-	378	250	-	253	-	-	290	260	-	100
		2	-	315	233	-	250	-	-	265	270	-	140
138	Corner	4	143	-	-	163	-	155	-	-	-	115	-
		7	155	-	-	138	-	150	-	-	-	120	-
		11	135	-	-	130	-	158	-	-	-	135	-

		14	143	-	-	138	-	150	-	-	-	140	-
238		2	138	-	-	166	-	160	-	-	-	140	-
		6	140	-	-	138	-	150	-	-	-	120	-
		9	130	-	-	145	-	160	-	-	-	115	-
		13	140	-	-	158	-	153	-	-	-	130	-
524		0	-	-	-	-	230	-	-	150	250	-	270
		2	-	-	-	-	205	-	-	143	175	-	240
138	Mid-edge	4	100	-	-	83	-	130	-	-	-	75	-
		7	80	-	-	83	-	105	-	-	-	70	-
		11	113	-	-	88	-	108	-	-	-	75	-
		14	93	-	-	83	-	123	-	-	-	95	-
238		2	80	-	-	98	-	108	-	-	-	75	-
		6	83	-	-	75	-	113	-	-	-	65	-
		9	75	-	-	85	-	105	-	-	-	70	-
		13	80	-	-	80	-	75	-	-	-	70	-
524		0	-	-	98	-	190	-	-	120	140	-	150
		2	-	-	88	-	165	-	-	105	140	-	130

3.3.2.2 Ride Quality- Pavement Management Van

MnDOT's Digital Inspection Vehicle (DIV) shown in Figure 32 was used for collection of the ride quality data in terms of International Roughness Index (IRI) and Ride Quality Index (RQI). Lasers are mounted across the front bumper of the test vehicle to measure roughness and faulting of pavement test sections. The lasers measure the pavement's longitudinal profile, and vertical deviations from a flat surface are indicative of roughness. They take a measurement approximately every 1/8-inch as the van travels down the roadway at highway speed. There are additional lasers used for rut (wear) depth measurements mounted at the rear of the vehicle.

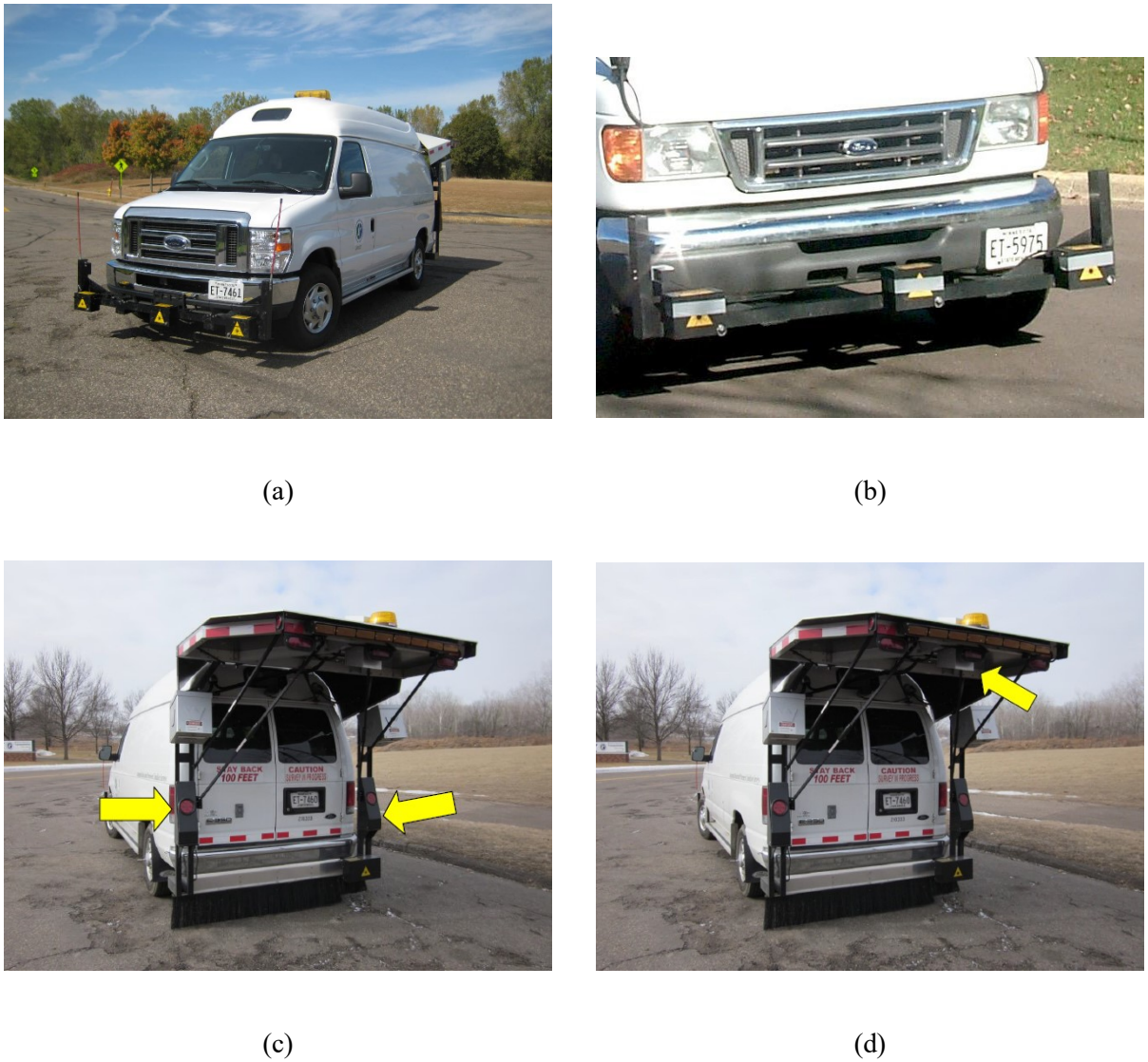

(a) (b)

(c) (d)

Figure 32. MnDOT's Digital Inspection Vehicle (DIV). (a) Pathways Services Inc. Van, (b) lasers used for measuring roughness and faulting, (c) 3-D measurements lasers, and (d) 3-D camera used to record pavement distress

The RQI is determined by first calculating the IRI from the pavement profile measured by the front lasers on the van. This international standard simulates a reference vehicle traveling down the roadway and is equal to the total anticipated vertical movement of this vehicle accumulated over the length of the section (reported in units of m/km or in./mile). The RQI is then calculated using Equations 4 and 5 for IRI values expressed in metric and U.S. customary systems, respectively. The pavement ratings corresponding to RQI values are presented in Table 17,

$$RQI_{Rigid\ Pavement} = 6.634 - 2.813 \times \sqrt{IRI} \quad (4)$$

$$RQI_{Rigid\ Pavement} = 6.634 - 0.353 \times \sqrt{IRI} \quad (5)$$

Testing was performed on 11/03/2017, 11/30/2017, 06/14/2018, 07/09/2018, and 07/14/2018 for the reference (524), low cement (138), and lower cement (238) cells. Results are summarized in Table 18 through Table 20.

. Considerable spread in IRI data and corresponding RQI ratings were observed for the reference cell (524). Results suggest IRI values ranging between 1.1 and 5.9 m/km (70-374 in./mile) and corresponding RQI ratings of “Very Poor” to “Good”. Results were more uniform for the low cement (138) and lower cement (238) cells, with IRI values ranging between 2.5 and 3.3 m/km (158-210 in./mile) and corresponding RQI ratings of “Fair” and “Good”.

Table 17. RQI data and corresponding pavement performance

RQI Value	Verbal Rating
4.1 - 5.0	Very Good
3.1 - 4.0	Good
2.1 - 3.0	Fair
1.1 - 2.0	Poor
0.0 - 1.0	Very Poor

Table 18. Ride quality data measured using DIV and corresponding rating index for cell 524

Concrete Type	Test Date	Lane	Wheel Path	IRI (m/km)	RQI	Avg. RQI	Rating
Reference; Cell 524	11/03/2017	Inside	Left	2.7	2.0	2.1	Fair
			Right	2.6	2.1		
		Outside	Left	1.1	3.7	3.6	Good
			Right	1.1	3.6		
	11/30/2017	Inside	Left	3.0	1.8	1.6	Poor
			Right	3.3	1.5		
		Outside	Left	1.3	3.5	3.5	Good
			Right	1.2	3.5		
	06/14/2018	Inside	Left	3.0	1.8	1.2	Poor
			Right	4.6	0.6		
		Outside	Left	NA	NA	NA	NA
			Right	NA	NA		
	07/09/2018	Inside	Left	3.7	1.2	0.9	Very Poor
			Right	4.8	0.5		
		Outside	Left	1.3	3.4	3.4	Good
			Right	1.3	3.4		

	07/26/2018	Inside	Left	2.4	2.3	1.0	Very Poor
			Right	5.9	-0.2		
		Outside	Left	1.9	2.8	2.6	Fair
			Right	2.2	2.4		

Table 19. Ride quality data measured using DIV and corresponding rating index for cell 138

Concrete Type	Test Date	Lane	Wheel Path	IRI (m/km)	RQI	Avg. RQI	Rating
Low cement; Cell 138	11/03/2017	Inside	Left	2.2	2.5	2.5	Fair
			Right	2.1	2.5		
		Outside	Left	1.4	3.4	3.3	Good
			Right	1.4	3.3		
	11/30/2017	Inside	Left	2.1	2.5	2.5	Fair
			Right	2.2	2.4		
		Outside	Left	1.4	3.3	3.3	Good
			Right	1.5	3.2		
	06/14/2018	Inside	Left	1.9	2.8	2.7	Fair
			Right	2.0	2.6		
		Outside	Left	2.5	2.2	2.5	Fair
			Right	1.9	2.7		
	07/09/2018	Inside	Left	1.8	2.8	3.0	Fair
			Right	1.5	3.2		
		Outside	Left	1.7	2.9	2.9	Fair
			Right	1.7	2.9		

	07/26/2018	Inside	Left	2.2	2.4	2.5	Fair
			Right	2.2	2.5		
		Outside	Left	1.7	3.0	3.1	Good
			Right	1.5	3.2		

Table 20. Ride quality data measured using DIV and corresponding rating index for cell 238

Concrete Type	Test Date	Lane	Wheel Path	IRI (m/km)	RQI	Avg. RQI	Rating
Lower cement; Cell 238	11/03/2017	Inside	Left	1.5	3.2	3.3	Good
			Right	1.3	3.5		
		Outside	Left	2.0	2.7	2.6	Fair
			Right	2.2	2.4		
	11/30/2017	Inside	Left	1.9	2.8	2.9	Fair
			Right	1.6	3.1		
		Outside	Left	2.0	2.7	2.6	Fair
			Right	2.2	2.4		
	06/14/2018	Inside	Left	1.8	2.8	2.9	Fair
			Right	1.6	3.0		
		Outside	Left	1.4	3.3	3.2	Good
			Right	1.6	3.1		
	07/09/2018	Inside	Left	1.5	3.2	3.3	Good
			Right	1.3	3.4		
		Outside	Left	1.8	2.9	2.8	Fair
			Right	1.8	2.8		

	07/26/2018	Inside	Left	1.6	3.0	3.2	Good
			Right	1.3	3.4		
		Outside	Left	2.0	2.6	2.5	Fair
			Right	2.2	2.5		

3.3.2.3 Ride Quality- Lightweight Profiler

MnDOT's Lightweight Internal Surface Analyzer (LISA), conforming to ASTM E-950 requirements (Figure 33) was also used for collection of the ride quality data in terms of the IRI according to the following timeline:

Reference Concrete (cell 524): testing was performed on 10/26/2017, 03/28/2018, 04/25/2018, 06/11/2018, 08/16/2018, 10/02/2018, 03/19/2019, 05/21/2019, 08/29/2019, and 10/24/2019 on both the inside and outside traffic lanes

Low Cement Concrete (cell 138): testing was performed on 07/18/2017, 07/20/2017, 07/25/2017, 11/03/2017, 11/30/2017, 03/28/2018, 04/23/2018, 05/31/2018, 06/14/2018, 07/09/2018, 07/26/2018, 08/16/2018, 10/02/2018, 03/18/2019, 05/21/2019, 08/29/2019, and 10/24/2019 on both the inside and outside traffic lanes

Lower Cement Concrete (cell 238): testing was performed on 07/18/2017, 07/20/2017, 07/25/2017, 11/03/2017, 11/30/2017, 03/28/2018, 04/23/2018, 05/31/2018, 06/14/2018, 07/09/2018, 07/26/2018, 08/16/2018, 10/02/2018, 03/18/2019, 05/21/2019, 08/29/2019, and 10/24/2019 on both the inside and outside traffic lanes.

Figure 33. MnDOT's Lightweight Profiler

Table 21 through Table 23 summarize the IRI data obtained for the investigated pavement. The reported data are the average of three IRI readings from both the right and left wheel tracks, along with the corresponding Mean Roughness Index (MRI) values. Figure 34 also presents the variation in MRI values over time, for both the inside and outside lanes of the investigated cells during the first three years.

The MRI values obtained for the outside lane were generally lower than the ones recorded for the inside lane (exposed to traffic) at cell 138. Trends were reversed for cell 238, with higher MRI values obtained for the outside lane. The minimum MRI values were recorded during the first month from construction with values limited to 108 in./mile for both cells. In general comparable MRI values were obtained for the measurements conducted in 2018 and 2019.

The data obtained for inside lane of the reference cell (cell 524) revealed consistent performance over time, with no significant difference between measurements performed in October 2017 and the ones taken in October 2019. The MRI values obtained for the outside lane of cell 524 were generally higher than those obtained for the inside lane which is exposed to controlled traffic loading.

MRI values observed for cell 524 seem to be slightly lower than those observed in cells 138 and 238. One should also consider the difference in thickness of the investigated pavements, where the reference cell is 6.0 in. thick, compared to 8.0-in. thick pavement at cells 138 and 238.

It should be noted that a MRI of no more than 65 in./mile is typically recommended by MNDOT. Given the short length of the test cells, such low IRI values are hard to achieve during paving. However, the presented data will only serve as the baseline for comparing the performance of the low cement pavement sections over time. Further data will be available for future annual cell performance reports.

Equation 5 was used for calculating the RQI values corresponding to the IRI data for each wheel path at inside and outside lanes. The average RQI values were then calculated and reported in Table 21, Table 22, and Table 23, for cell 524, cell 138, and cell 238 respectively. For all measurements, results suggest ride quality index of Good or Fair.

Results obtained for cell 138 and cell 238 were comparable to those from DIV measurements on same cells. However, the LISA data observed for cell 524 were more uniform while compared to DIV measurements. In summary, measurements performed by LISA suggested ride quality ratings of “Fair” and “Good” for all investigated cells.

Table 21. Ride quality data measured using LISA and corresponding rating index for cell 524

Concrete Type	Test Date	Lane	Wheel Path	IRI (in./mile)	MRI (in./mile)	RQI (Avg.)	Rating
Reference; Cell 524	10/26/2017	Inside	Left	93.2	99.1	3.1	Good
			Right	105.0			
		Outside	Left	101.1	108.1	3.0	Fair
			Right	115.1			
	03/28/2018	Inside	Left	84.4	89.2	3.3	Good
			Right	94.0			
		Outside	Left	93.2	101.2	3.1	Good
			Right	109.2			
	04/25/2018	Inside	Left	81.1	85.0	3.4	Good
			Right	88.8			
		Outside	Left	85.2	90.6	3.3	Good
			Right	96.0			
	06/11/2018	Inside	Left	100.4	110.6	2.9	Fair
			Right	120.8			
		Outside	Left	109.7	115.9	2.8	Fair
			Right	122.1			
	08/16/2018	Inside	Left	85.0	89.1	3.3	Good
			Right	93.3			
		Outside	Left	94.8	99.2	3.1	Good
			Right	103.6			
	10/02/2018	Inside	Left	86.5	95.9	3.2	Good
			Right	105.2			
		Outside	Left	96.3	102.3	3.1	Good
			Right	108.3			
	03/19/2019	Inside	Left	96.3	104.2	3.0	Fair
			Right	112.1			
		Outside	Left	76.3	80.5	3.5	Good
			Right	84.6			
	05/21/2019	Inside	Left	80.8	86.6	3.3	Good
			Right	92.5			
		Outside	Left	86.5	92.7	3.2	Good
			Right	98.8			
	08/29/2019	Inside	Left	76.3	83.9	3.4	Good
			Right	91.6			
		Outside	Left	86.8	93.5	3.2	Good
			Right	100.1			
	10/24/2019	Inside	Left	85.5	93.9	3.2	Good

			Right	102.3			
		Outside	Left	85.8	92.5	3.2	Good
			Right	99.2			

Table 22. Ride quality data measured using LISA and corresponding rating index for cell 138

Concrete Type	Test Date	Lane	Wheel Path	IRI (in./mile)	MRI (in./mile)	RQI (Avg.)	Rating
Low cement; Cell 138	07/18/2017	Inside	Left	112.7	108.1	3.0	Fair
			Right	103.5			
		Outside	Left	116.0	102.6	3.1	Good
			Right	89.1			
	07/20/2017	Inside	Left	112.5	107.8	3.0	Fair
			Right	103.1			
		Outside	Left	115.7	102.2	3.1	Good
			Right	88.6			
	07/25/2017	Inside	Left	114.5	106.9	3.0	Fair
			Right	99.2			
		Outside	Left	114.5	101.1	3.1	Good
			Right	87.8			
	11/03/2017	Inside	Left	136.35	135.40	2.5	Fair
			Right	134.64			
		Outside	Left	86.11	88.70	3.3	Good
			Right	91.49			
	11/30/2017	Inside	Left	134.13	137.49	2.5	Fair
			Right	140.98			
		Outside	Left	87.75	90.60	3.3	Good
			Right	93.65			
	03/28/2018	Inside	Left	143.60	136.47	2.5	Fair
			Right	129.34			
		Outside	Left	126.98	114.52	2.9	Fair
			Right	102.06			
	04/23/2018	Inside	Left	129.22	120.39	2.8	Fair
			Right	111.55			
		Outside	Left	115.65	102.29	3.1	Good
			Right	88.93			
	05/31/2018	Inside	Left	135.35	127.65	2.6	Fair
			Right	119.95			

		Outside	Left	112.82	101.10	3.1	Good
			Right	89.38			
	06/14/2018	Inside	Left	120.45	124.38	2.7	Fair
			Right	128.37			
		Outside	Left	157.77	139.39	2.5	Fair
			Right	121.52			
	07/09/2018	Inside	Left	116.84	106.89	3.0	Fair
			Right	96.75			
		Outside	Left	109.87	110.25	2.9	Fair
			Right	110.56			
	07/26/2018	Inside	Left	141.80	139.39	2.5	Fair
			Right	136.79			
		Outside	Left	107.97	100.93	3.1	Good
			Right	93.96			
	08/16/2018	Inside	Left	128.95	122.91	2.7	Fair
			Right	116.88			
		Outside	Left	118.67	104.13	3.0	Fair
			Right	89.58			
	10/02/2018	Inside	Left	136.94	129.83	2.6	Fair
			Right	122.72			
		Outside	Left	117.09	105.71	3.0	Fair
			Right	94.33			
	03/18/2019	Inside	Left	150.4	144.7	2.4	Fair
			Right	139.0			
		Outside	Left	142.3	130.8	2.6	Fair
			Right	119.3			
	05/21/2019	Inside	Left	135.6	128.5	2.6	Fair
			Right	121.3			
		Outside	Left	120.7	106.9	3.0	Fair
			Right	93.1			
	08/29/2019	Inside	Left	132.1	126.1	2.7	Fair
			Right	120.1			
		Outside	Left	114.0	102.5	3.1	Good
			Right	90.9			
	10/24/2019	Inside	Left	129.6	124.3	2.7	Fair
			Right	119.1			
		Outside	Left	118.2	103.7	3.0	Fair
			Right	89.3			

Table 23. Ride quality data measured using LISA and corresponding rating index for cell 238

Concrete Type	Test Date	Lane	Wheel Path	IRI (in./mile)	MRI (in./mile)	RQI (Avg.)	Rating
Lower cement; Cell 238	07/18/2017	Inside	Left	100.8	89.6	3.3	Good
			Right	78.5			
		Outside	Left	97.7	104.3	3.0	Fair
			Right	111.0			
	07/20/2017	Inside	Left	100.8	89.7	3.3	Good
			Right	78.6			
		Outside	Left	100.8	105.0	3.0	Fair
			Right	109.2			
	07/25/2017	Inside	Left	98.2	87.1	3.3	Good
			Right	75.9			
		Outside	Left	100.8	104.5	3.0	Fair
			Right	108.2			
	11/03/2017	Inside	Left	93.52	86.80	3.3	Good
			Right	80.09			
		Outside	Left	124.63	133.50	2.6	Fair
			Right	142.12			
	11/30/2017	Inside	Left	118.48	110.44	2.9	Fair
			Right	102.45			
		Outside	Left	125.01	132.61	2.6	Fair
			Right	140.47			
	03/28/2018	Inside	Left	109.40	103.06	3.1	Good
			Right	96.72			
		Outside	Left	105.82	111.47	2.9	Fair
			Right	117.11			
	04/23/2018	Inside	Left	99.14	90.00	3.3	Good
			Right	80.85			
		Outside	Left	99.10	104.45	3.0	Fair
			Right	109.80			
	05/31/2018	Inside	Left	100.24	90.93	3.3	Good
			Right	81.61			
		Outside	Left	102.51	105.00	3.0	Fair
			Right	107.49			
	06/14/2018	Inside	Left	116.77	110.25	2.9	Fair
			Right	103.66			
		Outside	Left	90.54	94.41	3.2	Good

			Right	98.71			
	07/09/2018	Inside	Left	93.58	87.88	3.3	Good
			Right	82.37			
		Outside	Left	114.30	115.13	2.8	Fair
			Right	115.57			
	07/26/2018	Inside	Left	104.42	94.85	3.2	Good
			Right	85.22			
		Outside	Left	129.63	133.69	2.6	Fair
			Right	137.55			
	08/16/2018	Inside	Left	104.94	95.63	3.2	Good
			Right	86.32			
		Outside	Left	97.00	103.99	3.0	Fair
			Right	110.99			
	10/02/2018	Inside	Left	101.21	92.96	3.2	Good
			Right	84.71			
		Outside	Left	106.40	111.70	2.9	Fair
			Right	117.01			
	03/18/2019	Inside	Left	134.1	131.4	2.6	Fair
			Right	128.6			
		Outside	Left	117.2	120.4	2.8	Fair
			Right	123.5			
	05/21/2019	Inside	Left	102.3	93.3	3.2	Good
			Right	84.3			
		Outside	Left	103.3	107.7	3.0	Fair
			Right	112.1			
	08/29/2019	Inside	Left	100.7	91.7	3.3	Good
			Right	82.7			
		Outside	Left	103.0	106.0	3.0	Fair
			Right	109.0			
	10/24/2019	Inside	Left	98.8	90.0	3.3	Good
			Right	81.1			
		Outside	Left	100.4	110.2	2.9	Fair
			Right	120.1			

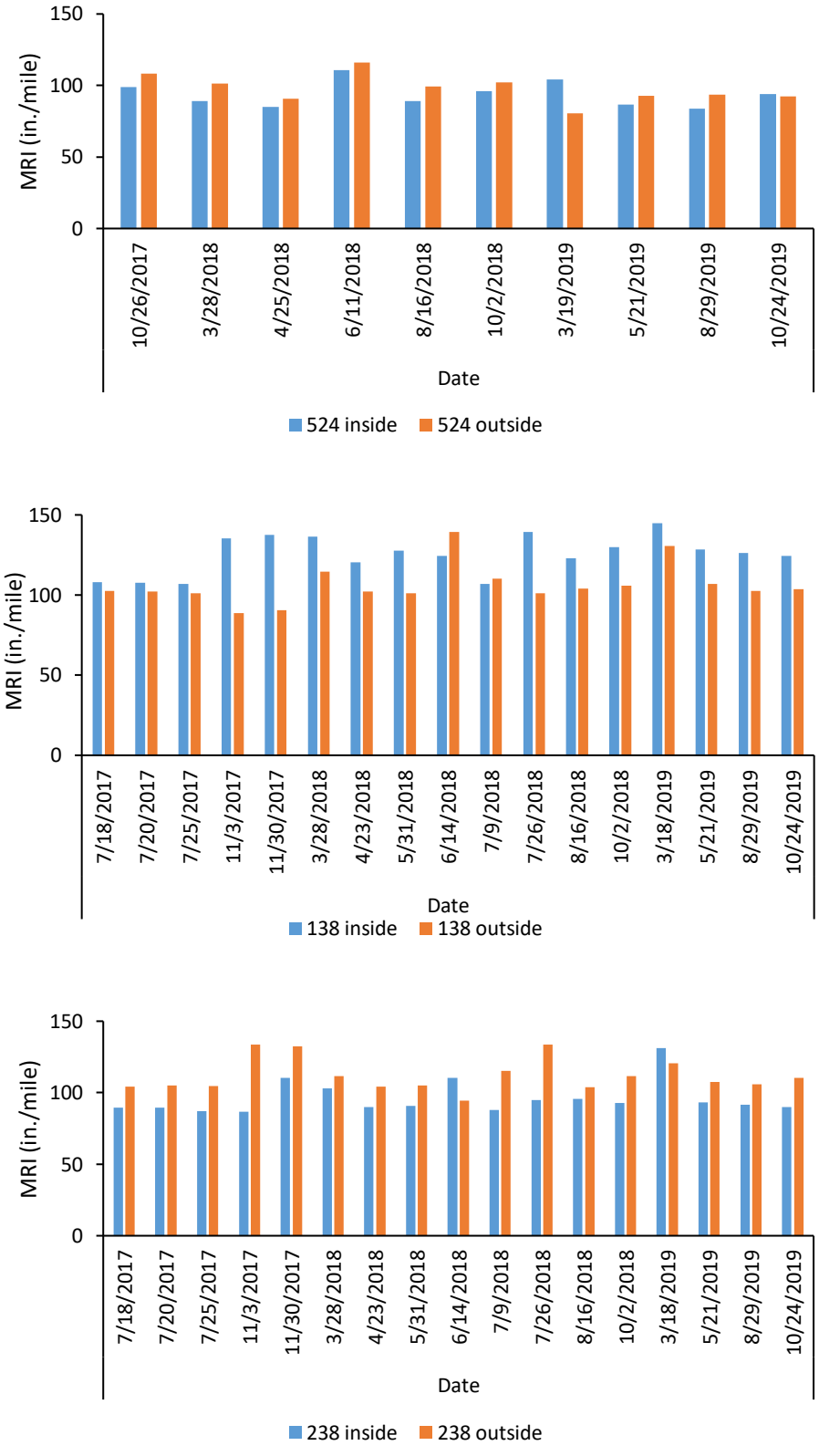

Figure 34. Variation in MRI (in./mile) values as a function of time

Statistical data analysis was conducted to determine the statistically significant variations between the IRI values at α=0.05 significance level. The statistical analysis was performed in two steps. First, the variation of data within each cell was investigated to see if there is a significant difference in IRI results as a function of traffic lane, wheel path, and test date. This was performed for data obtained for cells 138, 238, and 524. The following hypothesis testing scenarios were investigated:

(1) Is there a statistically significant difference in IRI results obtained for a given cell at different times?

- H0: there is no difference in IRI results obtained for a given cell at different times
- H1: the assumption of H0 is not correct

(2) Is there a statistically significant difference in IRI results obtained for different lanes of a cell?

- H0: there is no difference in IRI results obtained for different lanes of a cell
- H1: the assumption of H0 is not correct

(3) Is there a statistically significant difference in IRI results obtained for different wheel paths?

- H0: there is no difference in IRI results obtained for different wheel paths
- H1: the assumption of H0 is not correct

The distribution of IRI data was initially investigated for all test scenarios to ensure normal distribution of the test data. Anderson-Darling test was performed on the data and the following were observed:

- For cell 138, data did not follow a normal distribution (P-value = 0.001)
- For cell 238, data did not follow a normal distribution (P-value = <0.0001)
- For cell 524, data did follow a normal distribution (P-value = <0.078)

Given the normality test results, non-parametric testing was initially considered for cells 138 and 238. A summary of observations is provided below.

Results obtained for investigating overall IRI data for cell 138:

Non-parametric testing was initially considered given the data was not following normal distribution. Based on the Wilcoxon/Kruskal Willis tests, the following P-values were obtained for the aforementioned hypotheses:

- Test date: P-value = <0.0001. In other words, test time had a significant effect on observed IRI data.
- Traffic lane: P-value = <0.0001. In other words, IRI results obtained for different lanes exhibited a statistically significant difference.
- Wheel path: P-value = <0.0001. In other words, IRI results obtained for different wheel paths exhibited a statistically significant difference.

Given the fact that over 120 data points were included in these comparisons, which was more than the typically recommended limit of 30 points, it was also considered to assume normal distribution of the IRI

data and perform additional parametric testing. Results were in agreement with findings of the non-parametric comparisons, as summarized in Table 24. All three factors (date, lane, and wheel path) were proved to have significant effects on IRI data with P-values lower than 0.05. Least square means plots obtained for different input factors are summarized in Figure 35. In general it was observed that the IRI values were lower for the outside lane and for the right wheel path. A tendency for time-dependent increase in IRI values was also observed.

Table 24. ANOVA summaries assuming normal distribution of IRI data in cell 138

Source	Nparm	DF	Sum of Squares	F Ratio	Prob > F
Date	12	12	11866.470	12.2154	<.0001*
Lane	1	1	5961.167	73.6373	<.0001*
Wheel path	1	1	9962.696	123.0674	<.0001*

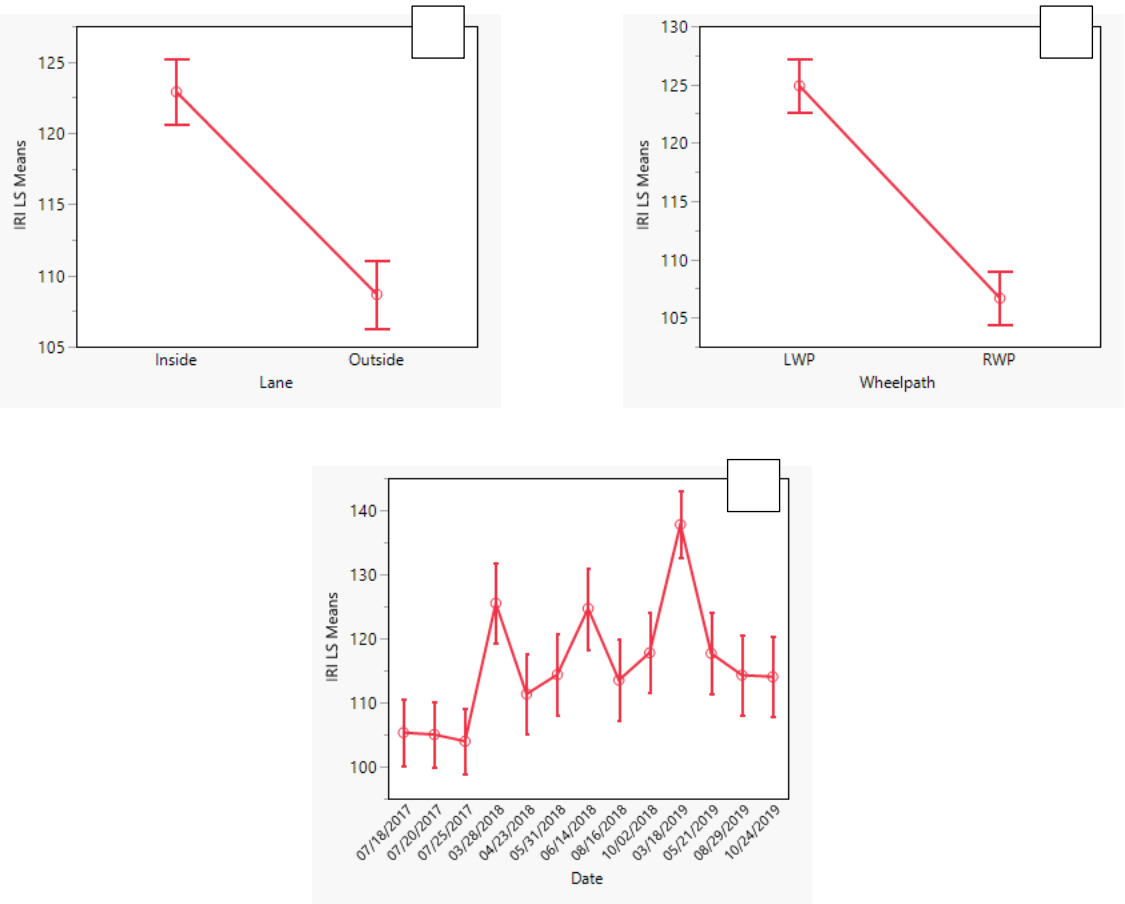

Figure 35. Least square means plots for IRI values of cell 138 as a function of lane (a), wheel path (b), and test date (c)

Results obtained for investigating overall IRI data for cell 238:

Non-parametric testing was initially considered given the data was not following normal distribution. Based on the Wilcoxon/Kruskal Willis tests, the following P-values were obtained for the aforementioned hypotheses:

- Test date: P-value = 0.001. In other words, test time had a significant effect on observed IRI data.
- Traffic lane: P-value = <0.0001. In other words, IRI results obtained for different lanes exhibited a statistically significant difference.
- Wheel path: P-value = 0.675. In other words, IRI results obtained for different wheel paths did not exhibit a statistically significant difference.

Given the fact that over 120 data points were included in these comparisons, which was more than the typically recommended limit of 30 points, it was also considered to assume normal distribution of the IRI data and perform additional parametric testing. Not all the results were in agreement with findings of the non-parametric comparisons, as summarized in Table 25. All three factors (date, lane, and wheel path) were proved to have significant effects on IRI data with P-values lower than 0.05. Least square means plots obtained for different input factors are summarized in Figure 36. A tendency for time-dependent increase in IRI values was also observed. Lower average IRI values were observed for the right wheel path. However, higher IRI data was observed for the outside lane at cell 238.

Table 25. ANOVA summaries assuming normal distribution of IRI data in cell 238

Source	Nparm	DF	Sum of Squares	F Ratio	Prob > F
Date	12	12	8932.7079	6.1471	<.0001*
Lane	1	1	3314.0900	27.3675	<.0001*
Wheel path	1	1	501.4341	4.1408	0.0444*

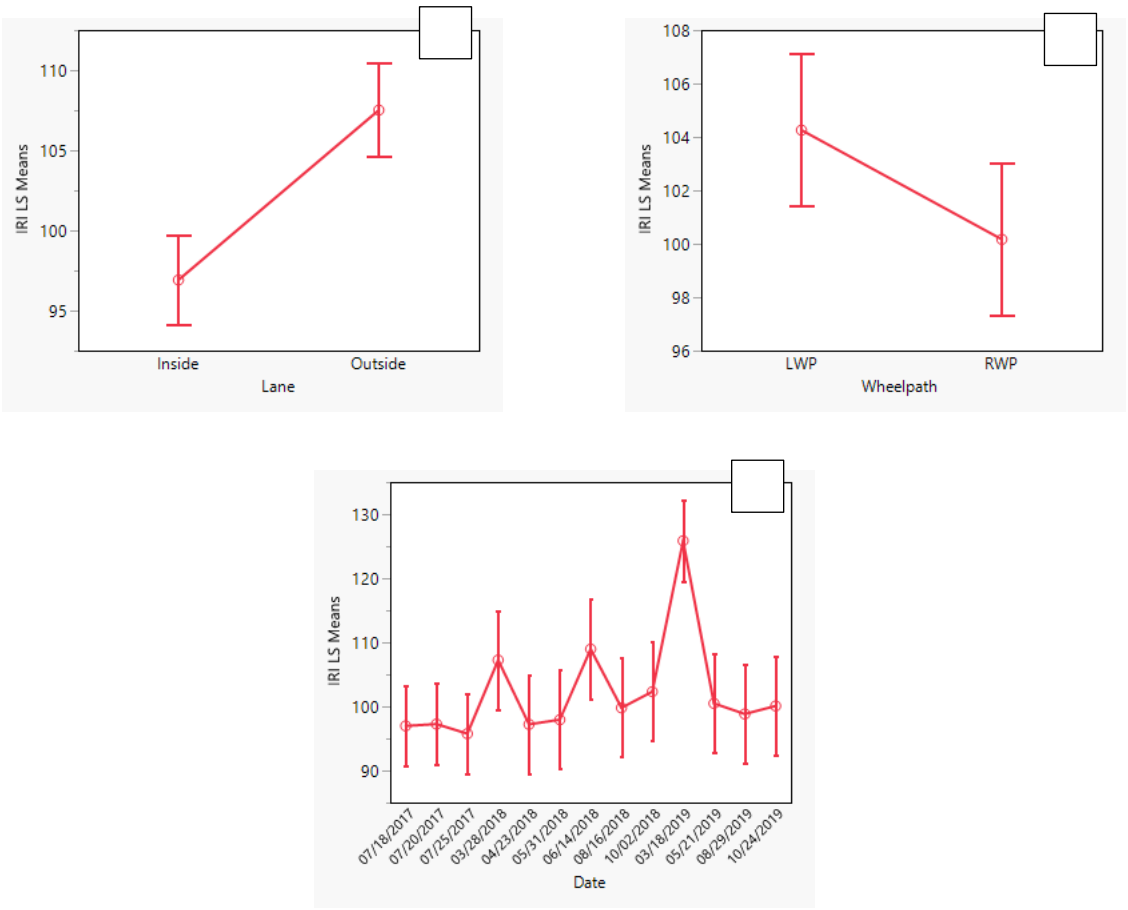

Figure 36. Least square means plots for IRI values of cell 238 as a function of lane (a), wheel path (b), and test date (c)

Results obtained for investigating overall IRI data for cell 524:

Parametric testing was considered given the data was following normal distribution. Hypothesis testing resulted in the following P-values:

- Test date: P-value = <0.0001. In other words, test time had a significant effect on observed IRI data.
- Traffic lane: P-value = 0.013. In other words, IRI results obtained for different lanes exhibited a statistically significant difference.
- Wheel path: P-value = <0.0001. In other words, IRI results obtained for different wheel paths exhibited a statistically significant difference.

All three factors (date, lane, and wheel path) were proved to have significant effects on IRI data with P-values lower than 0.05. Least square means plots obtained for different input factors are summarized in Figure 37.

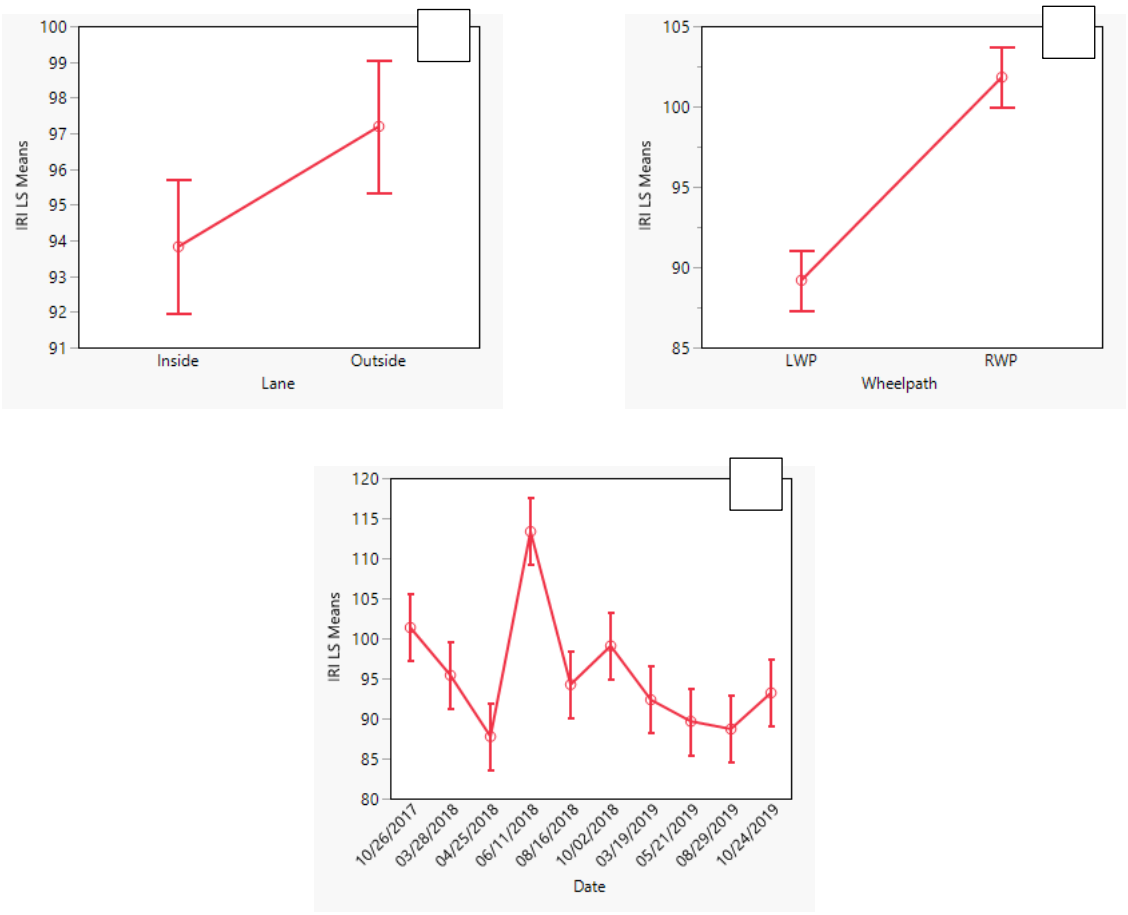

Figure 37. Least square means plots for IRI values of cell 524 as a function of lane (a), wheel path (b), and test date (c)

Comparing the IRI results obtained for different cells:

The last step in statistical data analysis was to see if there is a statistically significant difference in IRI results obtained for different cells. The following hypotheses were investigated:

- H0: there is no difference in IRI results obtained for different cells
- H1: the assumption of H0 is not correct

Non-parametric testing was considered given the data was not following normal distribution. Based on the Wilcoxon/Kruskal Willis tests, a P-value of <0.0001 was obtained for the aforementioned hypotheses. In other words, results obtained for different cells (138 vs. 238 vs. 524) exhibited statistically significant different IRI values.

Even though not following normal distribution, hypothesis testing was performed using parametric testing which resulted in the same conclusion, i.e. significantly different IRI values for various cells. The least square means plot obtained for different cells is presented in Figure 38, suggesting the lowest IRI values for reference cell (cell 524) and the highest IRI numbers for low cement section (cell 138).

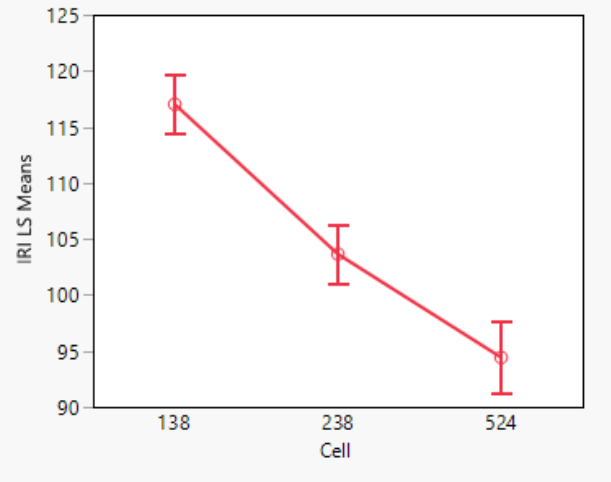

Figure 38. Least square means plots for IRI values of different cells

Considering the time-dependent variations in IRI data observed at different test cells, it was decided in this phase of the study to establish trend lines to determine the increase in IRI as function of time for inside lanes (exposed to traffic). Results are summarized in Figure 39 for both cells 138 and 238. This was also performed for the reference cell 524. However, the results exhibited reduction of IRI over time, i.e. negative slope of the trend line, and therefore the data was not included in this report.

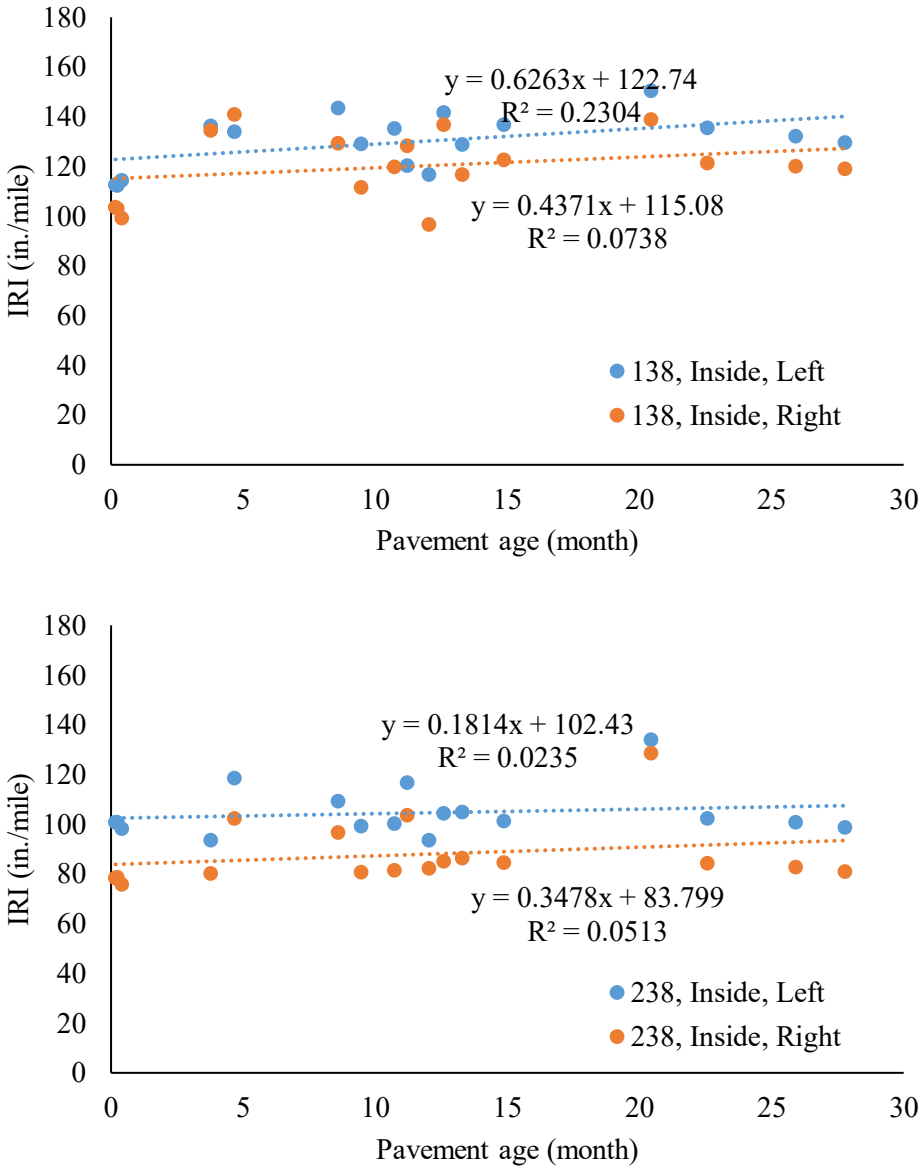

Figure 39. Variation in IRI values as a function of time, cell 138 (top) and cell 238 (bot.)

3.3.2.4 Surface Evaluation- Pavement Management Van

MnDOT's Digital Inspection Vehicle (DIV) shown in Figure 32 was also used for measuring wear depth and surface macro texture. Macro texture measurements were performed on 11/03/2017, 11/30/2017, 07/09/2018, and 07/14/2018 for the reference (524), low cement (138), and lower cement (238) cells. Three measurements were obtained for each test date. The average values and corresponding standard deviations are presented in Figure 40. Data obtained for reference cell (cell 524) seem to be slightly

higher than those obtained for low and lower cement sections. However, one should note that the results are generally close and comparable. A slight increase in macro texture depth was observed over time and regardless of the concrete type. This is specially highlighted for the inside lanes (exposed to traffic).

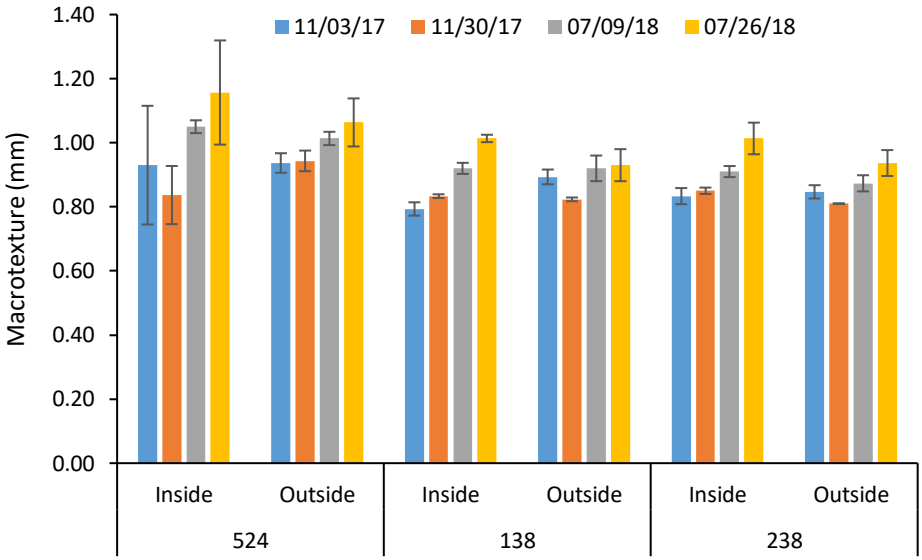

Figure 40. Macro texture measurements (mm) as a function of time

Wear depth measurements were performed on 11/03/2017, 11/30/2017, 06/14/2018, 07/09/2018, and 07/14/2018 for the reference (524), low cement (138), and lower cement (238) cells. Three measurements were obtained for each test date. The average values are presented in Table 26. For each concrete type, the wear depth values were comparable for the inside and outside lanes. The average wear depth data obtained for different concrete types were also comparable.

Table 26. Average wear depth measurements (mm)

Test Date	Lane	Wheel Path	Reference (Cell 524)		Low Cement (Cell 138)		Lower Cement (Cell 238)	
			Wear Depth (mm)	Avg. Wear	Wear Depth (mm)	Avg. Wear	Wear Depth (mm)	Avg. Wear
11/03/2017	Inside	Left	2.5	2.4	1.5	2.7	1.4	2.4
		Right	2.5		3.8		3.4	
	Outside	Left	1.1	2.4	1.7	2.7	1.9	2.4
		Right	3.0		2.8		3.2	
11/30/2017	Inside	Left	2.2	2.1	1.6	2.2	1.3	2.2
		Right	2.0		2.8		3.0	
	Outside	Left	1.3	2.1	1.8	2.2	2.1	2.2
		Right	3.2		2.9		3.1	
06/14/2018	Inside	Left	1.9	2.1	1.3	2.1	1.0	1.6
		Right	2.3		3.0		2.2	
	Outside	Left	NA	NA	3.6	2.1	1.2	1.6
		Right	NA		5		2.7	
07/09/2018	Inside	Left	1.9	2.2	1.3	1.9	1.1	1.7
		Right	2.5		2.6		2.3	

	Outside	Left	1.0	2.2	1.1	1.9	1.5	1.7
		Right	2.9		1.9		2.6	
07/26/2018	Inside	Left	1.5	2.0	0.9	1.3	0.6	1.1
		Right	2.5		1.6		1.6	
	Outside	Left	0.5	2.0	1.0	1.3	1.3	1.1
		Right	2.4		2.2		2.6	

3.3.2.5 Dynamic Load Test

A 5-axle, 18-wheel semi-tractor trailer with total weight of 80 kips was used for loading the pavement sections. Figure 41 offers a schematic view of the vehicle configurations. Table 27 summarizes the axle loads. Testing was conducted on pavement cast with low and lower cement content on 09/13/2017, 03/21/2018, 05/02/2018, 07/31/2018, and 10/31/2018. The loading was conducted at two speed levels of 5 and 35 mph, replicated five times per speed scenario. For each pavement type, response to the dynamic lading was recorded by 8 sensors, installed at different depths and locations as detailed in Figure 42. The CE sensors measure the dynamic strain gages and VWs are the vibrating wire strain gages. The investigated sensors were located at top and bottom of the slabs, at both the corner and mid-edge spots of the instrumented panels, as detailed in Table 28 and Table 29.

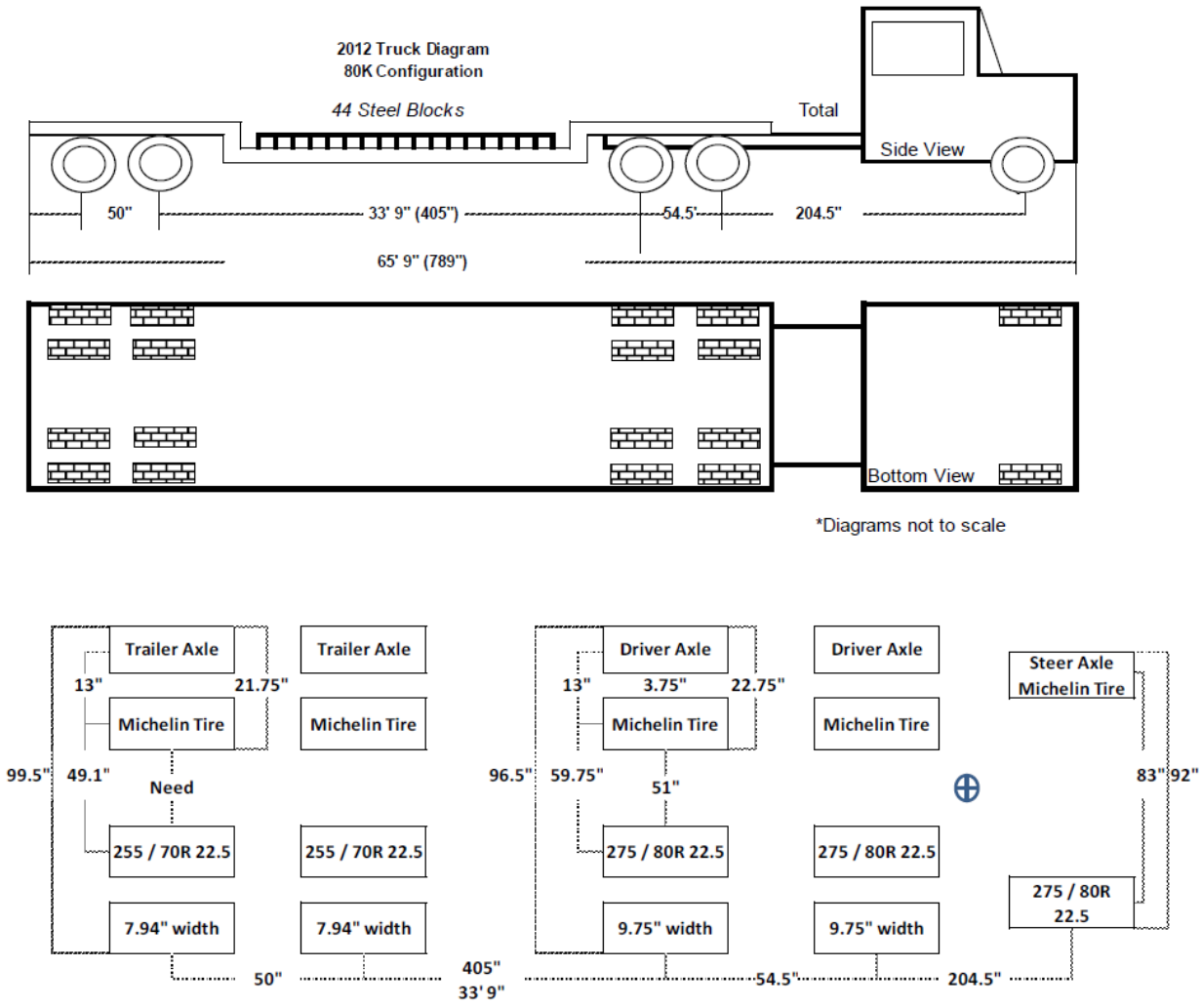

Figure 41. Vehicle dimensions and axle configurations for the Workstar truck and the Towmaster trailer employed for dynamic loading (MnDOT 2013)

Table 27. Axle weight for the Workstar truck and the Towmaster trailer employed for dynamic loading (MnDOT 2013)

	Tractor	Tractor Tandem		Trailer Tandem	
Total Weight	Steering Axle	Front Axle	Back Axle	Front Axle	Back Axle
79,700	11,700	17,650	16,450	16,800	17,100
		34,100		33,900	

Figure 42. Sensor installation plan for Cell 138 (top) and Cell 238 (bottom).

Table 28. As-built location of sensors installed in mixtures prepared with low and lower cementitious materials content

Cell 138				Cell 238			
Sensor #	**Station**	**Offset (ft)**	**Depth (in.)**	**Sensor #**	**Station**	**Offset (ft)**	**Depth (in.)**
CE001	9353.95	11.2	0.8	CE001	9474.07	10.9	0.8
CE002	9353.95	11.2	7.5	CE002	9474.07	10.9	7.5
CE003	9360.01	11.0	0.8	CE003	9480.08	10.9	0.8
CE004	9360.01	11.0	7.5	CE004	9480.08	10.9	7.5
CE005	9368.98	10.8	0.8	CE005	9489.07	10.9	0.8
CE006	9368.98	10.8	7.5	CE006	9489.07	10.9	7.5
CE007	9374.97	10.8	0.8	CE007	9495.02	11.1	0.8
CE008	9374.97	10.8	7.5	CE008	9495.02	11.1	7.5

Table 29. Detailed layout of the sensors embedded in Cell 138 and Cell 238

Cell 138 & 238			
Location in Slab	**Depth**	**Orientation**	**Sensor #**
Corner	Top	Transverse	CE001
		Transverse	CE005
	Bot.	Transverse	CE002

		Transverse	CE006
Mid-Edge	Top	Longitudinal	CE003
		Longitudinal	CE007
	Bot.	Longitudinal	CE004
		Longitudinal	CE008

Data was recorded with a frequency of 1200 Hz. The total test time was about 5 and 20 s for loading at 35 and 5 mph, respectively. The average of readings obtained through first 2 and 0.5 seconds were calculated and employed as the base line for normalizing the data for 5 and 35 mph scenarios, respectively. Figure 43 presents an example of traffic loading data obtained from Sensor # CE008, located at bottom part, mid-edge of Cell 238. Given the high frequency of data recording, trend lines were employed for further clarification of the load-deflection patterns as shown in Figure 43. Note that the scattered blue lines are the normalized raw data and the trend line is shown in yellow, which clearly depicts the local maxima under the front wheel and the rear tandem axels.

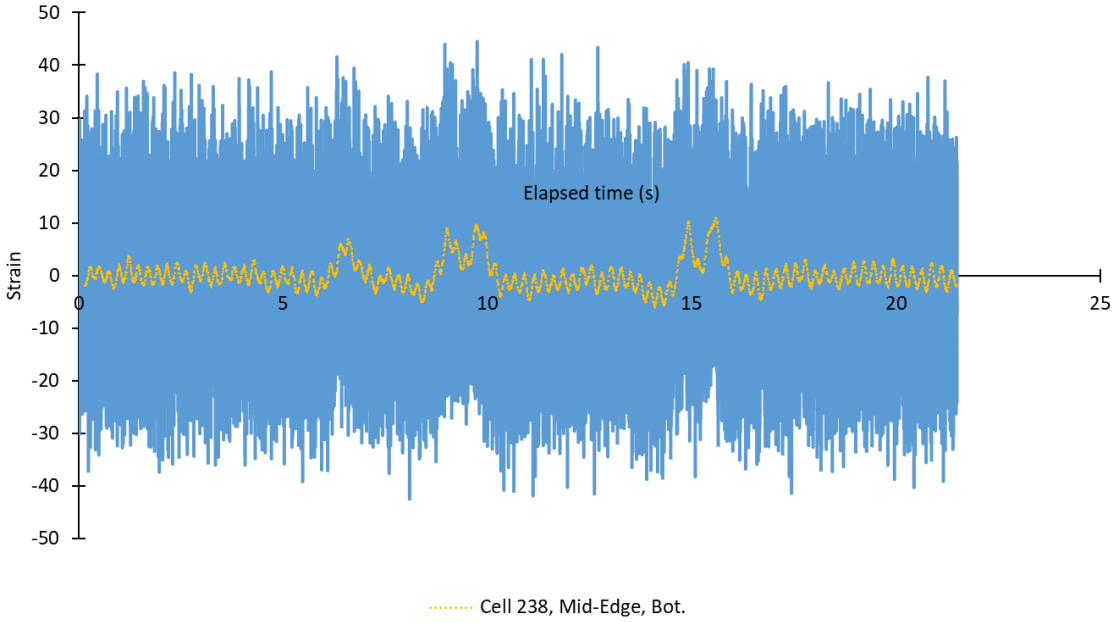

Figure 43. Sample raw data and corresponding trend line obtained from dynamic load test

Figure 44 and Figure 45 present the trend lines observed for sensors embedded at different depths and different spots of pavements made with low and lower cementitious materials content. Change in direction of stress was observed with the load moving on the pavement surfaces. Trends were similar for the data obtained from both cells cast with Low or Lower cementitious materials content. Results indicate similar performance for the two sensors located at the same depth and the same spot of the panels within the same concrete type. Comparable responses were obtained for loading the pavement at 5 and 35 mph, for a given combination of test spot, sensor depth, and concrete type. However, deformations were higher for the sensors located at mid-edge compared to those located at corner of the slabs. Moreover, the sensors embedded at bottom and top of the mid-edge spots exhibited more symmetrical data, corresponding to compressive and tensile strains (and stresses) induced by the moving truck.

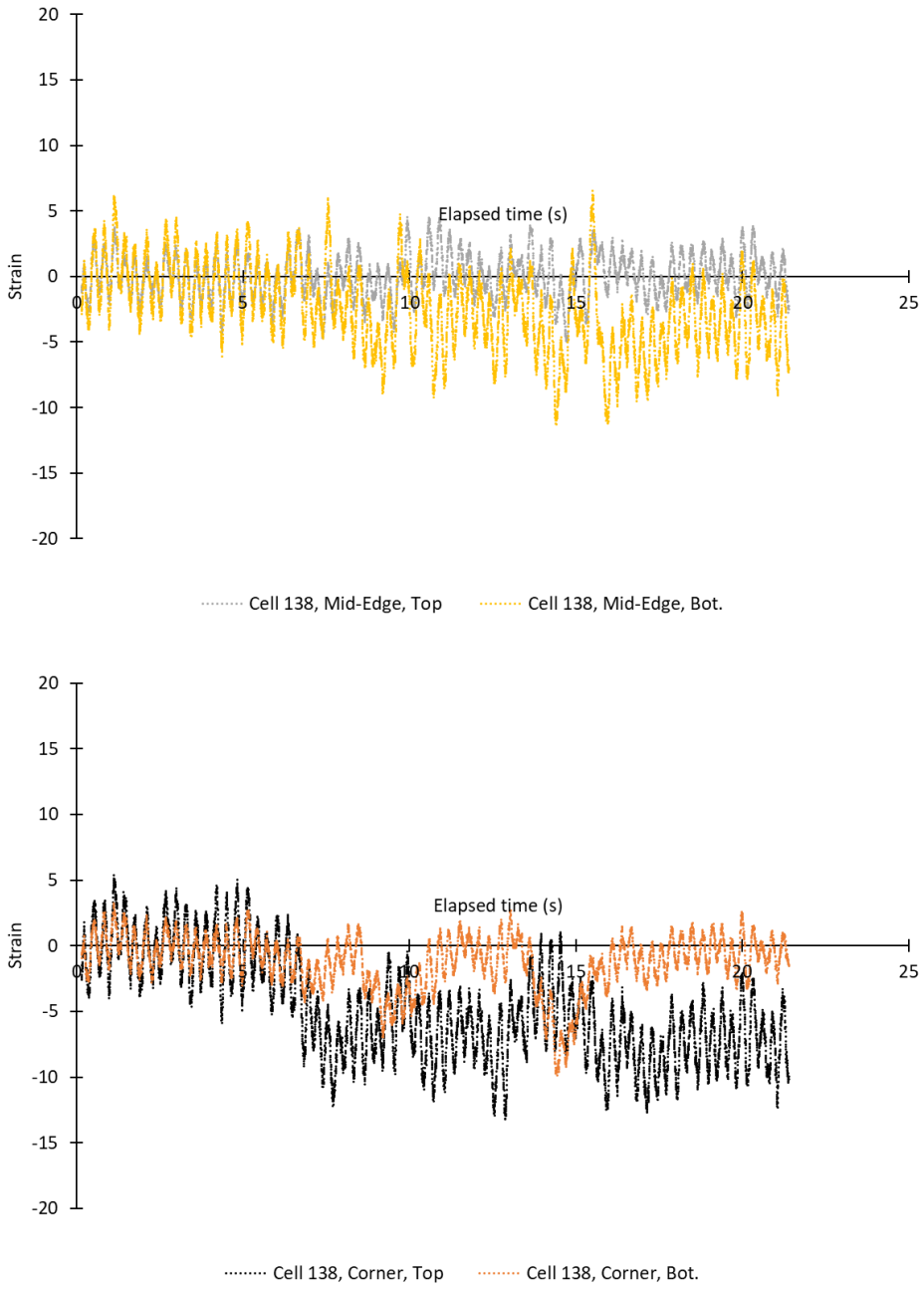

Figure 44. Load-deflection patterns for Cell 138 at corner and mid-edge

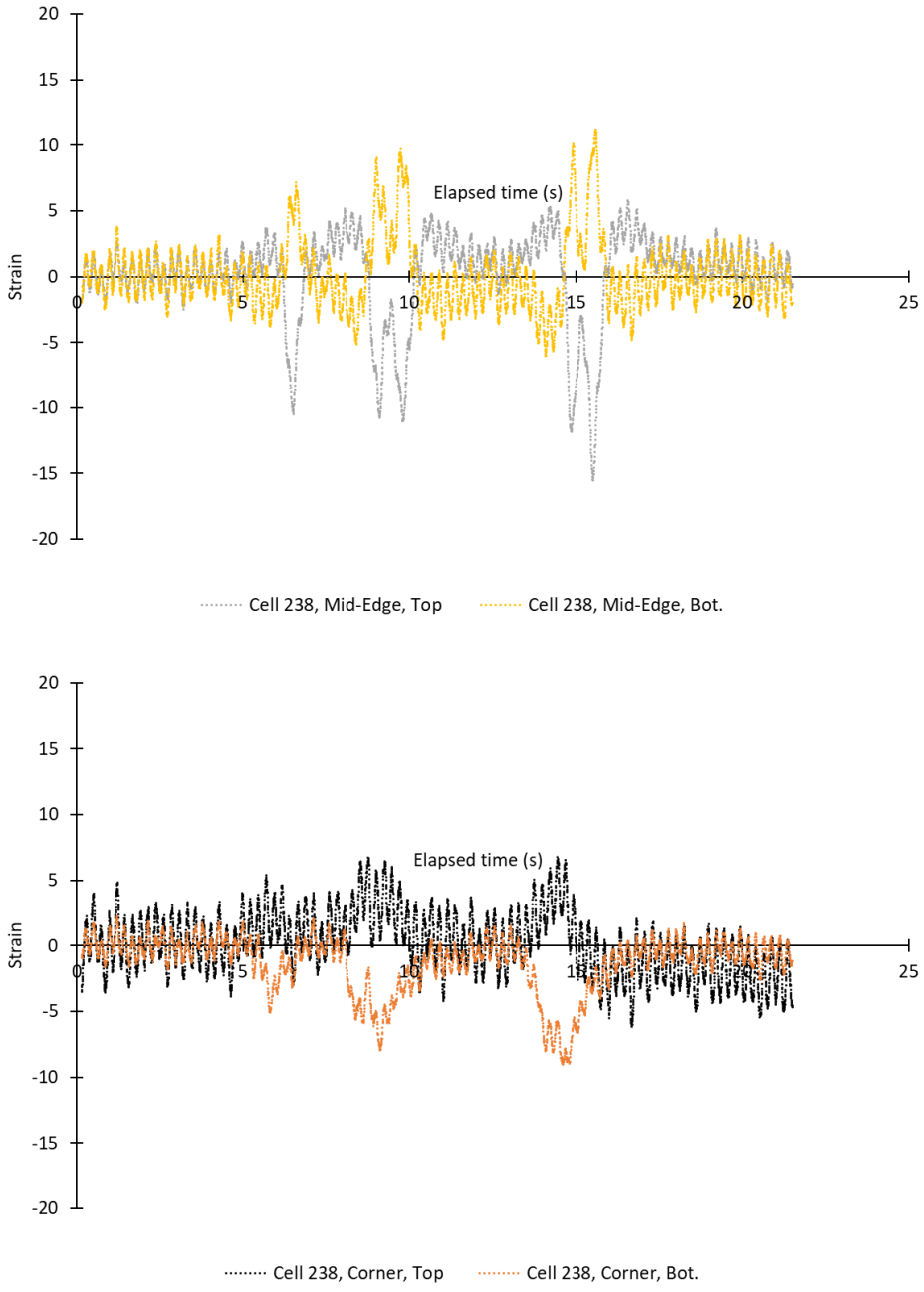

Figure 45. Load-deflection patterns for Cell 238 at corner and mid-edge

Table 30 summarizes the minimum and maximum strain values obtained for sensors located at top and bottom parts of the investigated panels. The values reported in this table are the average of five sets of readings per scenario. It should be noted that even though the loading test was performed five times for each section, the first sets of measurements yielded significantly lower strain values in almost all test scenarios. Therefore, the presented data are the average values for four measurements conducted at 5 and 35 mph. Moreover, the reported values were not corrected for traffic wander.

The values reported in this table are high for an 8.0 in. thick pavement. But this can be in part due to the noise in recording the data. The maximum and minimum strain values were comparable for both concrete types and did not follow a constant pattern favoring a certain mixture. In other words, the variation in cementitious materials content did not have a significant effect on registered maximum and minimum values and the investigated cells exhibited comparable response to traffic loading. This was in line with the comparable load-deflection patterns obtained for the mixtures presented in Figure 44 and Figure 45. It should be noted that some of the CE sensors did not respond to the dynamic loading conducted on 07/31/2018 and 10/31/2018. This was reflected in Table 30.

Table 30. Summary of the Max. and Min. strain values obtained through different testing scenarios for sensors embedded in Cell 138 and Cell 238

Cell #				**138**				**238**			
Location on Slab				**Corner**		**Mid-Edge**		**Corner**		**Mid-Edge**	
Depth				**Top**	**Bot.**	**Top**	**Bot.**	**Top**	**Bot.**	**Top**	**Bot.**
5 mph	09/13/2017	Avg.	Min.	-104	-59	-110	-60	-117	-54	-133	-55
			Max.	46	37	41	49	43	27	34	42
		Std.	Min.	7	6	8	8	17	5	4	10
			Max.	3	3	2	4	3	1	1	1
	03/21/2018	Avg.	Min.	-157	-62	-170	-70	-92	-42	-92	-50
			Max.	61	54	50	66	52	32	37	49
		Std.	Min.	4	8	7	8	29	6	31	6
			Max.	1	1	1	4	1	1	3	4
	05/02/2018	Avg.	Min.	-121	-55	-126	-57	-137	-53	-151	-56

			Max.	32	28	31	36	69	35	42	62
		Std.	Min.	17	7	16	6	12	3	11	1
			Max.	1	0	2	1	4	2	4	7
	07/31/2018	Avg.	Min.	-171	-93	-121	-172	-89	-57	NA	-61
			Max.	124	82	102	121	45	30	NA	41
		Std.	Min.	30	7	27	27	23	15	NA	10
			Max.	16	11	9	18	4	1	NA	3
	10/31/2018	Avg.	Min.	-279	-160	NA	-242	-151	NA	NA	-120
			Max.	279	162	NA	246	113	NA	NA	117
		Std.	Min.	12	9	NA	7	71	NA	NA	7
			Max.	12	4	NA	12	42	NA	NA	5
35 mph	09/13/2017	Avg.	Min.	-104	-56	-109	-61	-129	-59	-132	-67
			Max.	40	33	35	40	35	22	28	33
		Std.	Min.	14	8	11	12	7	6	4	4
			Max.	3	2	3	2	3	2	2	1
	03/21/2018	Avg.	Min.	-155	-65	-168	-76	-102	-52	-109	-54
			Max.	57	51	48	62	50	29	32	42
		Std.	Min.	22	15	19	14	18	11	9	12

			Max.	4	4	2	3	12	2	2	6
	05/02/2018	Avg.	Min.	-142	-73	-149	-84	-152	-58	-159	-67
			Max.	69	52	54	76	61	32	37	51
		Std.	Min.	12	6	9	6	20	13	16	18
			Max.	5	5	1	6	6	2	2	4
	07/31/2018	Avg.	Min.	-115	-74	-148	-95	-118	-55	NA	-69
			Max.	101	64	91	94	36	26	NA	36
		Std.	Min.	17	15	56	5	6	4	NA	11
			Max.	3	3	10	5	0	0	NA	2
	10/31/2018	Avg.	Min.	-253	-142	NA	-219	-131	NA	NA	-103
			Max.	263	149	NA	228	125	NA	NA	105
		Std.	Min.	20	8	NA	20	12	NA	NA	8
			Max.	23	13	NA	19	11	NA	NA	9
*No reliable sensor data were available											

3.3.2.6 In-Situ Static Deformation

Vibrating wire strain gages (VWSG) embedded at corner and mid-panel areas were used to monitor the total in-situ deformations due to environmental loads. Exact loation of these sensors are summarized in Table 31.

Table 31. Location of vibrating wire strain gages embedded in cells 138 and 238

Cell 138				Cell 238			
Sensor #	**Station**	**Offset (ft)**	**Depth (in.)**	**Sensor #**	**Station**	**Offset (ft)**	**Depth (in.)**
VW001	9384.13	11.0	0.8	VW001	9459.00	10.9	0.8
VW002	9384.13	11.0	7.5	VW002	9459.00	10.9	7.5
VW003	9390.16	6.0	0.8	VW003	9464.98	6.0	0.8
VW004	9390.16	6.0	7.5	VW004	9464.98	6.0	7.5

The recorded deformations were caused by a combination of concrete shrinkage, warping due to moisture loss, curling due to temperature gradient within the depth of concrete, and linear deformation of the sensors and the surrounding concrete due to variations in temperature.

The raw frequency data recorded by the VWSGs were converted to iso-thermal strain values as instructed by Equations 6 and 7 (MnDOT 2013).

$$S = FW^2 \times D \tag{6}$$

$$\varepsilon_{iso-thermal} = (S_1 - S_0) + [(T_1 - T_0) \times (\alpha_{st} - \alpha_c)] \tag{7}$$

where S is the value of strain calculated based on vibration frequency (με), FW is the vibration frequency registered by the VWSG (Hz), D is the gage factor equal to 0.003304, $\varepsilon_{iso-thermal}$ is the iso-thermal concrete strain (με), S_1 is the strain (με) at temperature T_1 (°C), S_0 is the strain (με) corresponding to baseline measurement at baseline temperature T_0 (°C), and α_{st} is the coefficient of thermal expansion of steel equal to 12 in./in./°C, and α_c is the coefficient of thermal expansion of concrete equal to 9 in./in./°C as reported in the first year performance report.

Figure 47 presents the strain history and temperature data recorded during the first two years from casting the cells. Time zero readings correspond to the strain values at the time of placing the concrete. For both mixtures, VWSG 1 and VWSG 3 present the deformations close to the surface of the concrete, at corner and mid-panel, respectively, while VWSG 2 and VWSG 4 present the deformations at bottom

part of the concrete, at corner and mid-panel, respectively. VWSG 1 and VWSG 2 had transverse orientation, while VWSG 3 and VWSG 4 were oriented longitudinally.

In general, the investigated sensors exhibited similar deformation pattern, with a tendency towards negative strain values, corresponding to compressive stresses. The sensors located at top parts of the pavement exhibited higher values compared to the ones placed at bottom part of the pavement. The sensors with longitudinal orientation generally exhibited higher strain values compared to the traverse direction at same depth. The strain values obtained for Cell 138 cast with low cementitious materials were higher than the corresponding values at Cell 238 with lower cementitious materials content.

A range of 45˚C was observed for the variations in seasonal temperature as presented in Figure 46 and Figure 47. However, such cyclic variations were not exactly reflected in total strain values. This highlights the fact that other factors, including shrinkage and/or warping in light of moisture gradient in depth governed the deformations.

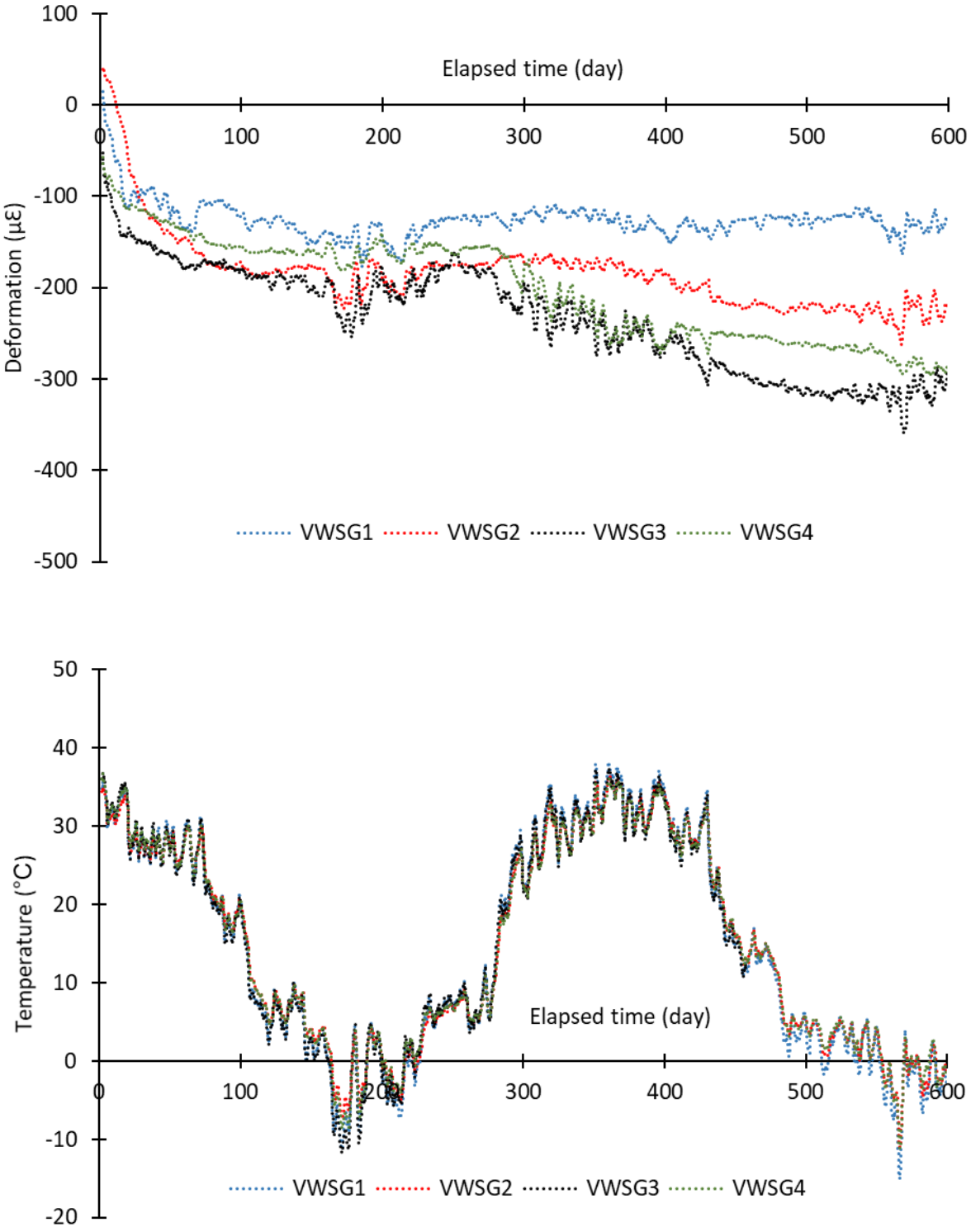

Figure 46. Iso-thermal in-situ deformation (με) for Cell 138 (top) and corresponding temperature readings (bot.)

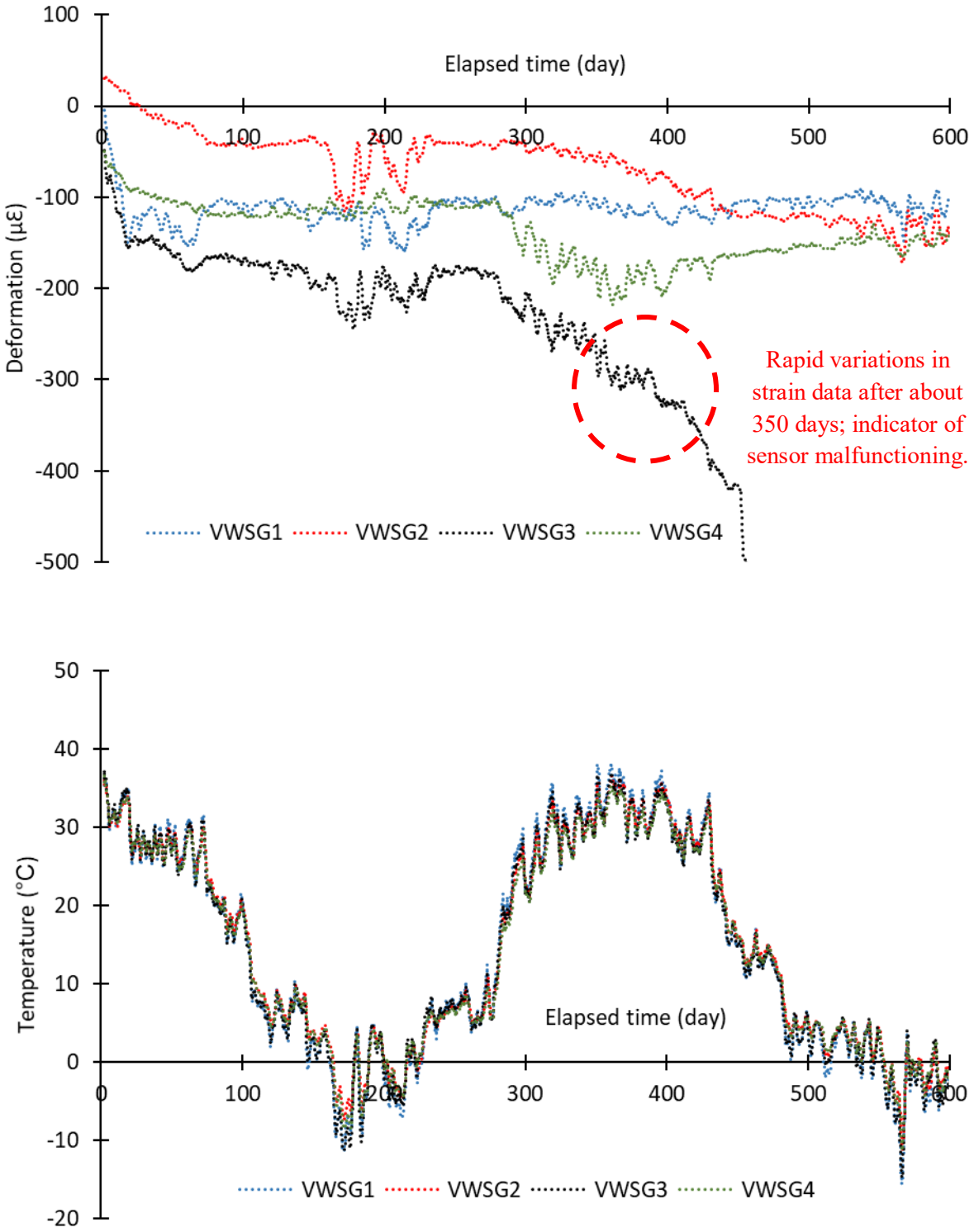

Figure 47. Iso-thermal in-situ deformation (με) for Cell 238 (top) and corresponding temperature readings (bot.)

3.3.2.7 Temperature of pavement structure

Thermocouple trees were employed for monitoring the temperature variations within the depth of pavement structure, including the concrete slab and the base layer Table 32.

offers a summary of placement details for thermocouples incorporated at different spots in Cell 138. Data obtained from sensors embedded in Station 9396.13 (TC#1 to TC#8) are presented in this section. Data obtained from sensors embedded in Station 9390.8 (TC#9 to TC#20) are presented in Appendix A.

Table 32. Placement details for thermocouples in Cell 138

Station	Offset (ft)	TC #	Depth from surface (in.)	Surrounding material
9396.13	-11.44	1	0.5	Concrete
		2	1	Concrete
		3	4	Concrete
		4	7.5	Concrete
		5	8.5	Gravel
		6	10.5	Gravel
		7	12	Gravel
		8	14	Clay
9390.8	-6.17	9	0.5	Concrete
		10	1	Concrete
		11	4	Concrete
		12	7.5	Concrete
		13	8.5	Gravel
		14	12	Gravel
		15	14	Clay
		16	24	Clay
		17	36	Clay
		18	48	Clay
		19	60	Clay
		20	72	Clay

Figure 48 presents the trend lines obtained for variations in temperature at different depths of concrete slab at Cell 138. Trend lines were employed to avoid the wide scatter in data, thus making it easier to follow the trends. Results indicated uniform patterns in temperature fluctuations regardless of the depth. Data obtained for thermocouples were similar to temperature data recorded by the VWSGs shown in Figure 46 and Figure 47.

The actual temperature measurements at top and bottom of pavement are presented in Figure 49. Data indicates a wider range of short- and long-term variations in temperature reading at top part of the pavement while compared to the depth of the slab. Figure 50 presents the extent of variation in temperature between top and bottom part of the concrete slab. The black line is the trend line, exhibiting higher temperatures at surface during the warmer seasons and higher temperatures at bottom of the slab during the cold seasons. The blue line is the actual data, exhibiting up to 15°C temperature difference between top surface and bottom during the cold season. This corresponds to a gradient of over 2°C/in. (3.6 °F/in.) within the depth of the slab.

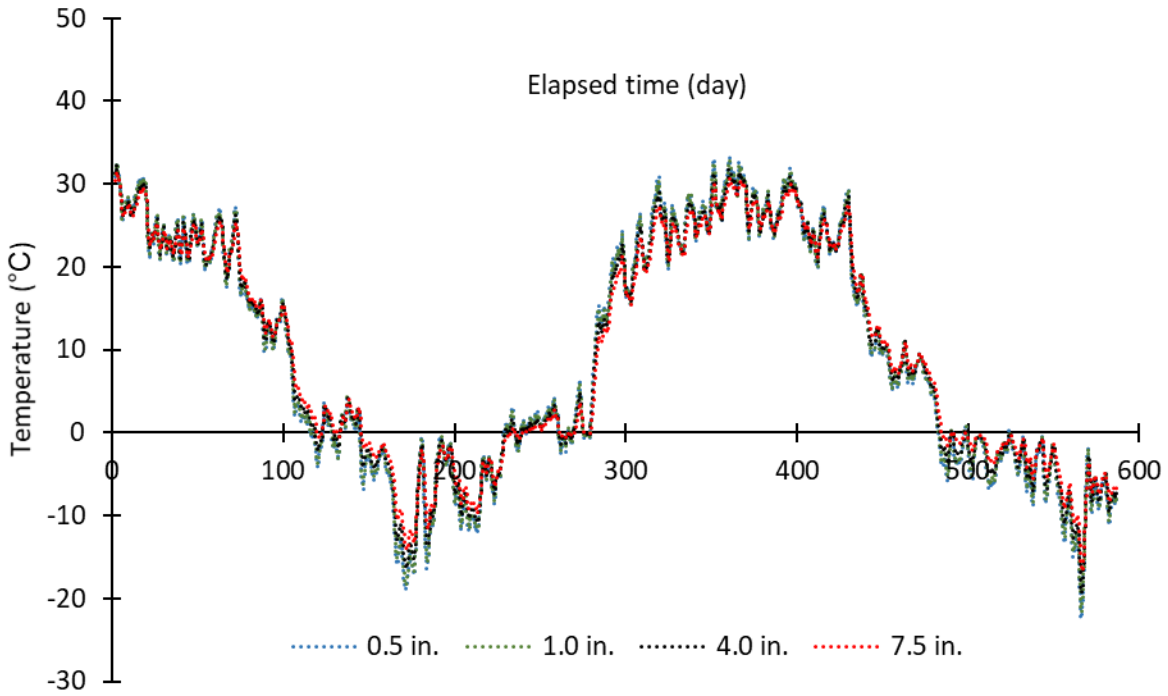

Figure 48. Temperature variations at different depths of concrete slab in Cell 138

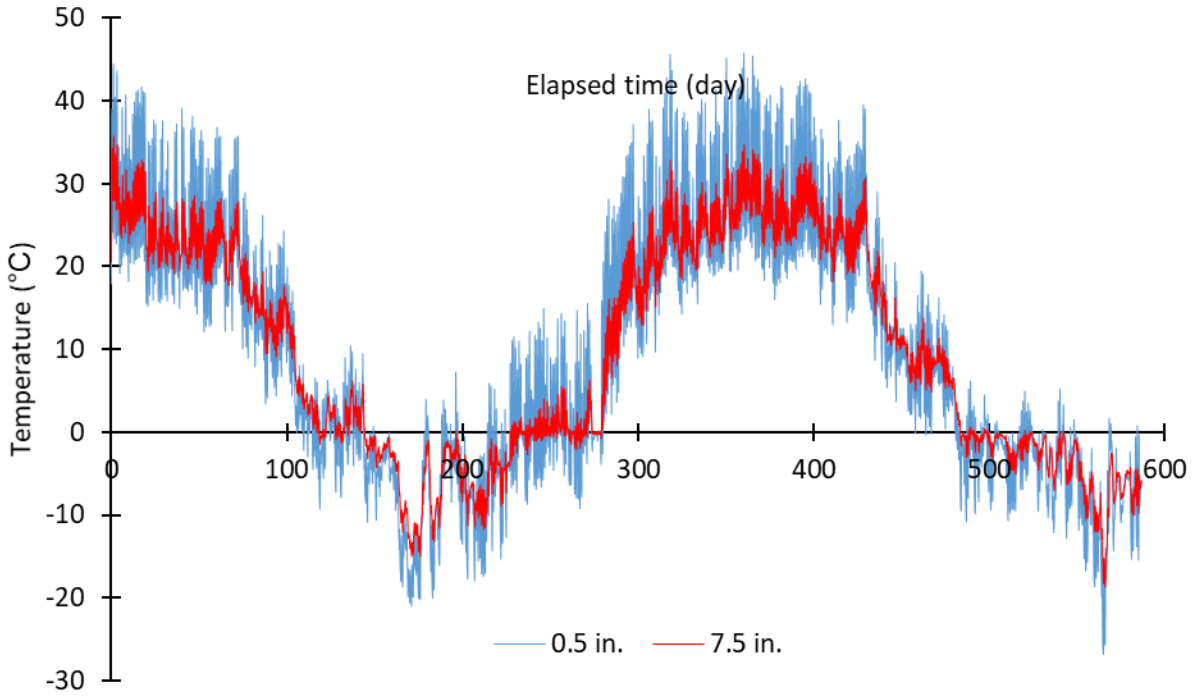

Figure 49. Temperature readings at top (0.5 in.) and bottom (7.5 in.) of concrete slab in Cell 138

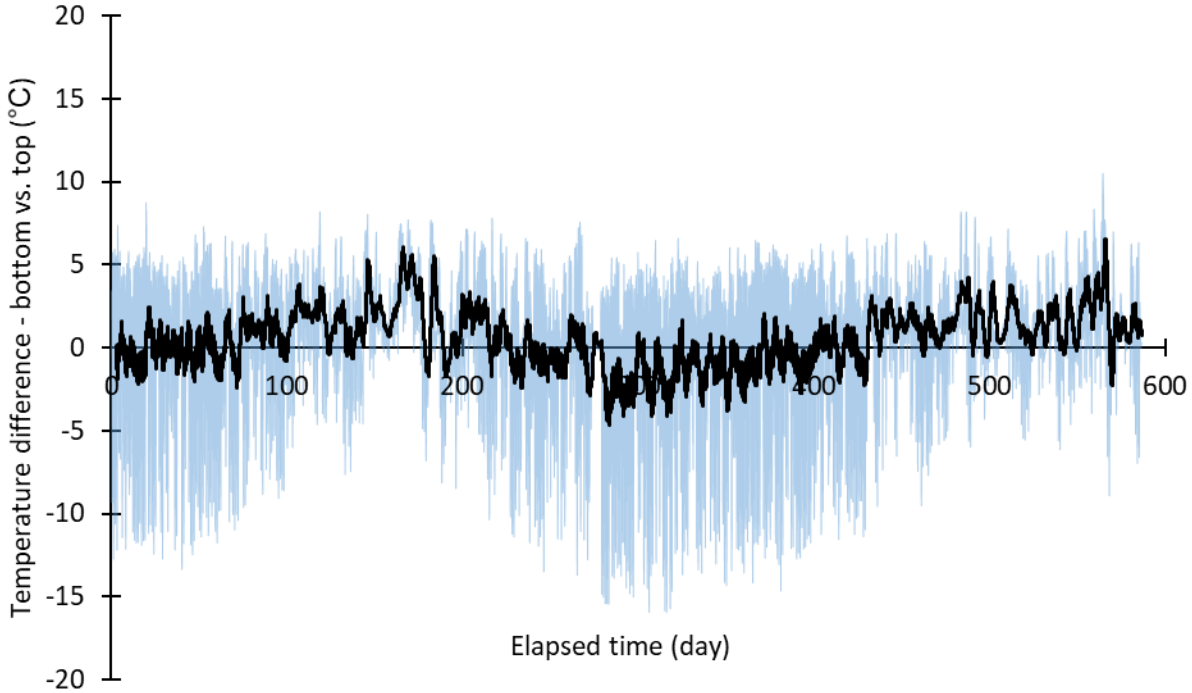

Figure 50. Temperature variations between the top and bottom of concrete slab in Cell 138

Temperature profile underneath the concrete slab is presented in Figure 51. Trends were comparable to those observed for the concrete slab, with lower variations between the maximum and minimum values. It is worth mentioning that the base layer experienced freezing conditions in over 130 days within the first year.

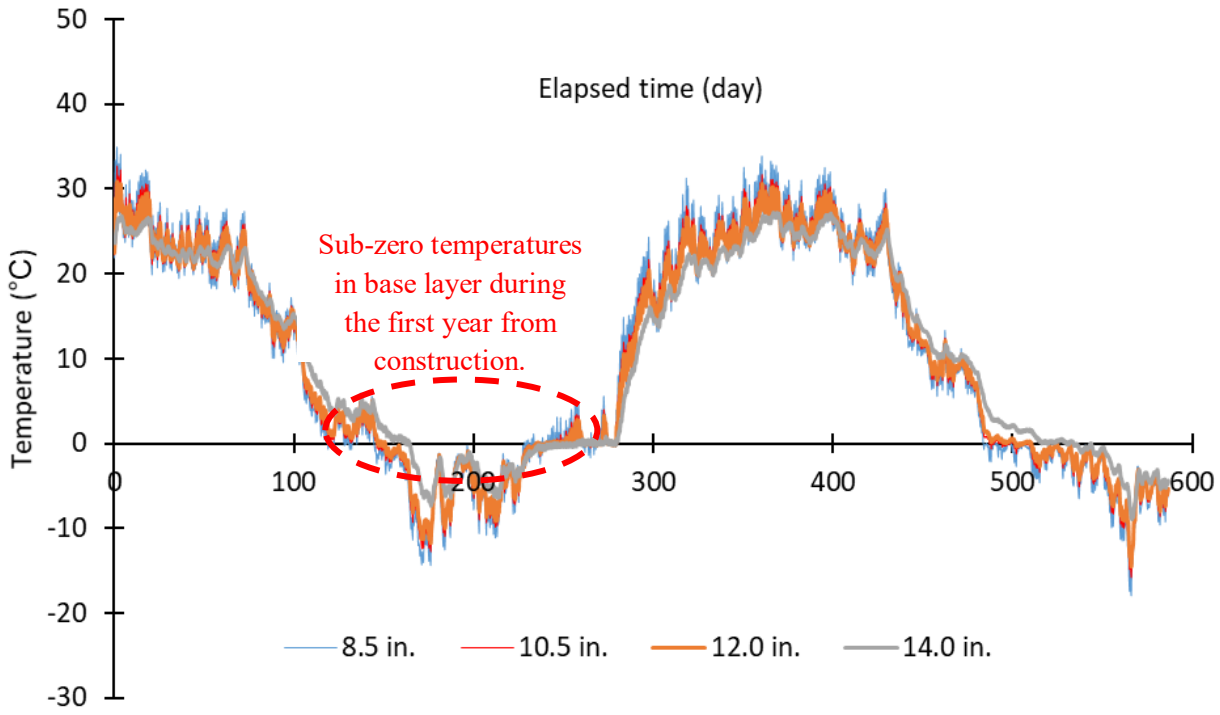

Figure 51. Temperature variations at base layer underneath the concrete slab in Cell 138

3.3.2.8 Moisture in pavement structure

Decagon 5TE sensors were employed for monitoring the variations in moisture content within the depth of pavement structure, including the concrete slab and the base layer. Table 33 offers a summary of placement details for 5TE sensors incorporated at different spots in Cell 138 as presented in the construction report.

Table 33. Placement details for 5TE sensors in Cell 138

Sensor ID	Station	Offset (ft)	Depth (in.)	Surrounding material
EC001	9390.73	-5.69	1.0	Concrete
EC002	9390.73	-5.69	4.0	Concrete
EC003	9389.90	-6.01	12.0	Class 5 aggregate
EC004	9389.90	-6.01	24.0	Clay
EC005	9389.90	-6.01	30.0	Clay

No calibration equation is curently available to convert the raw data to VWC for the sensors embedded in concrete. The EW data obtained for EC001 and EC002 (EW1 and EW2) were not included in this section. Data are available in Appendix. Calibration as presented in Equations 8 and 9 (MnDOT 2013) was considered to determine the volumetric water content (VWC) based on the raw data for sensors embeded in Class 5 aggregate base and clay subgarde, respectively:

$$VWC_{Class\,5} = 0.0003 \times EW - 0.0239 \quad (8)$$

$$VWC_{Clay} = 0.0003 \times EW - 0.0021 \quad (9)$$

Figure 54 presents the variations in VWC (%) for sensors embeded in the 5.0 in. thick layer of Class 5 aggregate base (EW3). This sensor is located at depth of 12.0 in. from pavement surface, which corresponds to 4.0 in. from underneath the concrete slab. Variation in base layer temperature at same depth (obtained from thermocouples) is also presented in Figure 53.

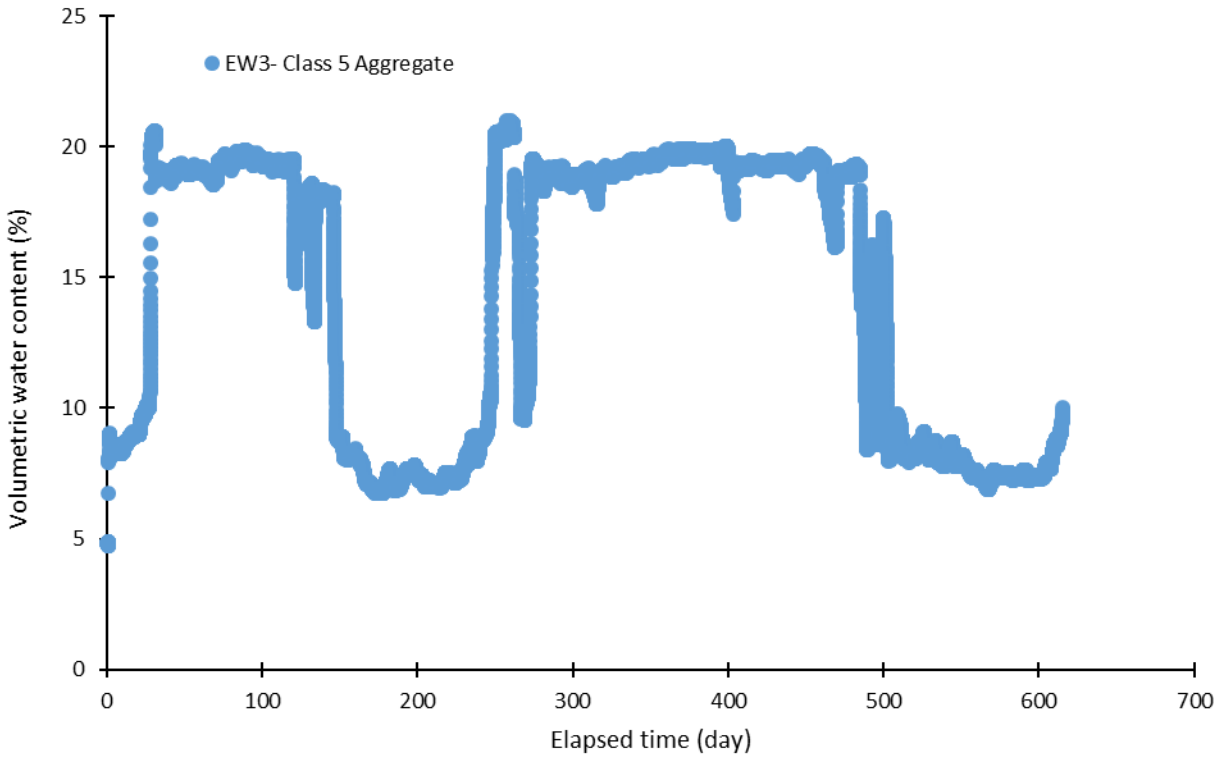

Figure 52. Variations in volumetric water content (%) at base layer underneath the concrete slab in Cell 138

Data presented in Figure 52 indicated VWC of 13% to 21% when the base layer is not frozen. VWC results exhibited a tendency to drop to values as low as 6% to 8% when the base layer is exposed to subzero temperatures. Examples of this condition are observed for recordings between 150 and 250 days, as well as recordings between 500 and 600 days. Such transitions are sudden and can occure in a day or two. These observations are in agreement with temperature fluctuations presented in Figure 53.

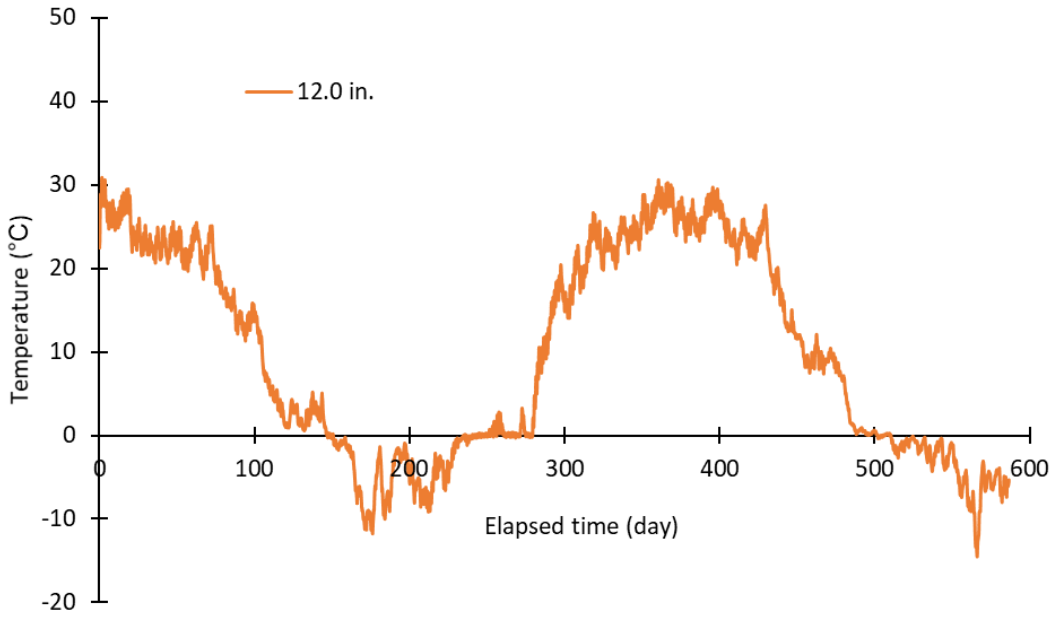

Figure 53. Thermocouple temperature readings at Class 5 aggregate base layer underneath the concrete slab in Cell 138

Trends were similar for the sensors embeded in the clay subgrade underneath Cell 138. However, higher VWC values were observed for the clay layer while compared to Class 5 aggregate. Data obtained for sensor embeded at 24.0 in. from surface, presented in Figure 54, indicated VWC of 30% to 37% when the base layer is not frozen. Again the VWC results exhibted a significant drop to values as low as 12% to 14% when the clay subgrade was exposed to freezing temperatures. For the sensors located in clay subgrade, such transitions occurred during a longer period of time (about 1-3 weeks).

Trends obtained for the 5TE sensor embeded at depth of 36 in. (presented with yellow color in Figure 54) were in general agreement with the data obtained at depth of 24.0 in. Lower VWC of 6-10% was observed at this depth for the freezing temperatures. Moreover, higher VWC of about 42% was observed at this depth during the period of 25 to 150 days. Such a trend was not observed for the period of 300 to 500 days. A sudden drop in VWC was recorded during this period of time. The reason for such an observation is not clear at this time, but sensor malfunctioning can be a reason for this observation.

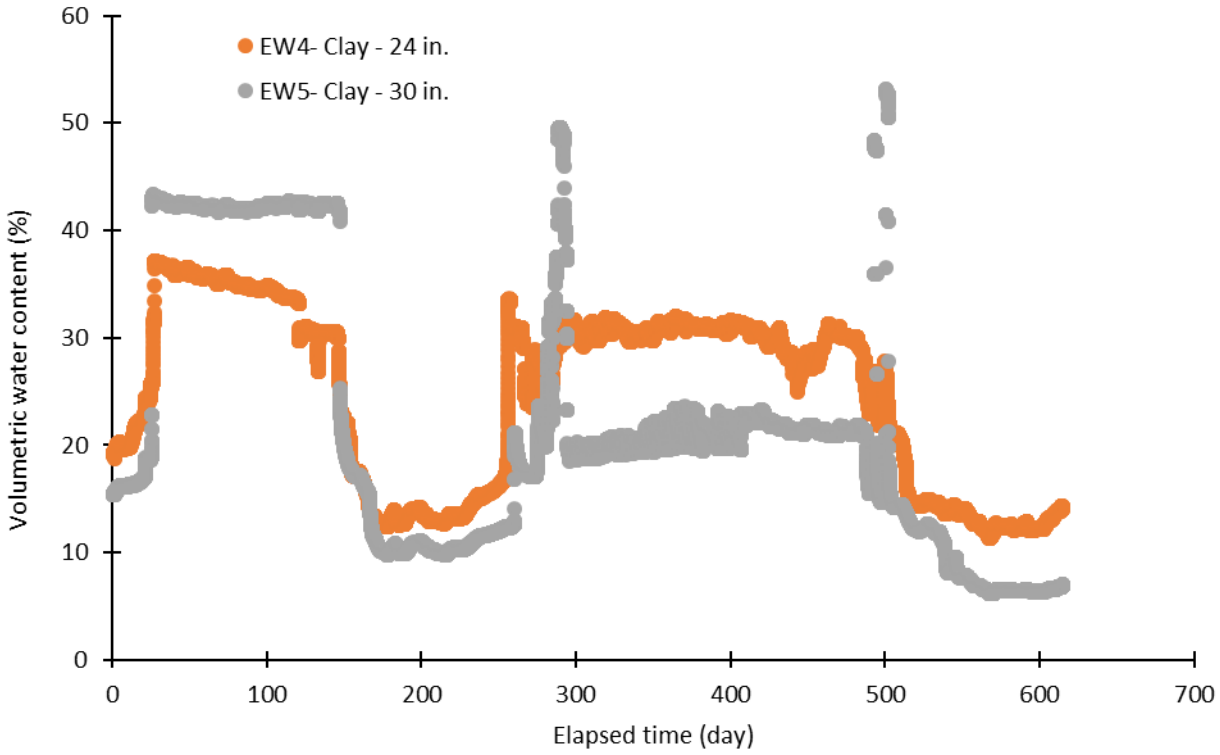

Figure 54. Variations in volumetric water content (%) in depth of clay subgrade underneath the concrete slab in Cell 138

3.3.2.9 Evaluating Joint Activation using MIRA test

On September 21st, 2017, a non-destructive test method based on ultrasonic shear-wave tomography was employed to explore the joint activation. The MIRA device (Figure 55) contains 40 dry point contact (DPC) transducers that send and receive low-frequency (55 kHz) shear-wave ultrasonic pulses (Vosoughi and Taylor 2017). The test was repeated 10 times at each joint, and the average results were reported. Figure 56 presents sample processed data obtained from MIRA test. The left figure is the filter signal and the right figures are obtained by normalizing the transmitted energy across each transducer to transmitted energy of transducer number 6 for determining whether or not cracking occurred at the joint. Normalized values lower than the threshold suggest crack development at examined joints.

Figure 55. Mira test setup

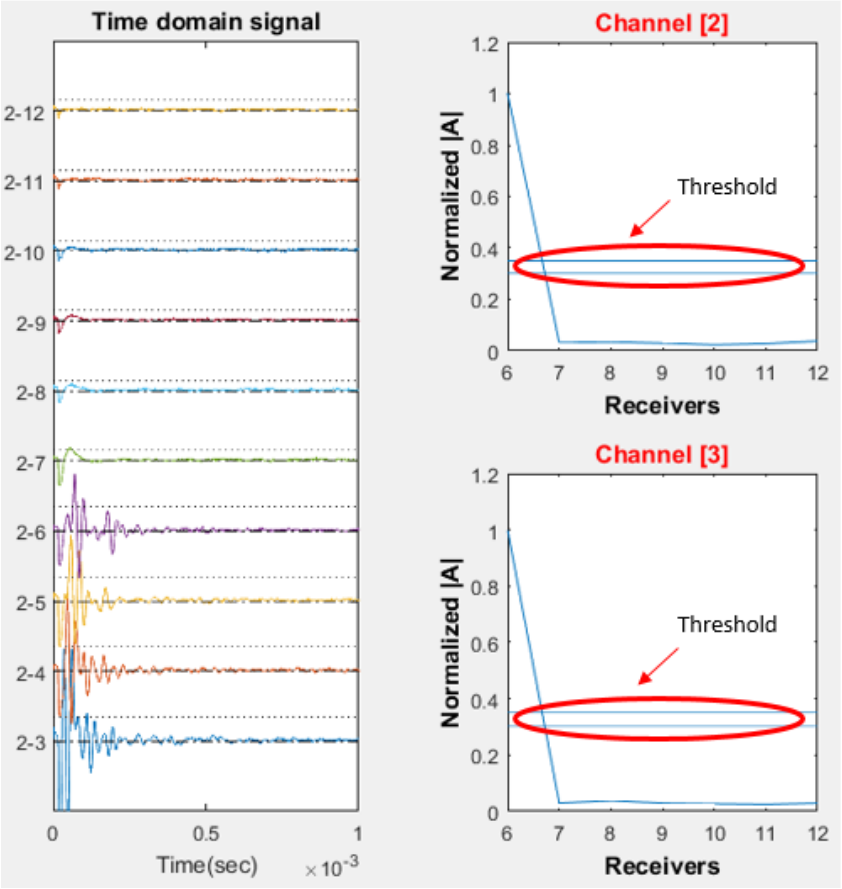

Figure 56. Processed Mira test data

Figure 57 summarizes the MIRA test results. The obtained data indicated cracking in all joints within Cells 138 and 238. No cracking was observed at the joints at the ends of the section, i.e. joints A and C shown in Figure 57. The outside lane only experiences the environmental loads, while the inside lane is loaded by MnROAD 80k truck.

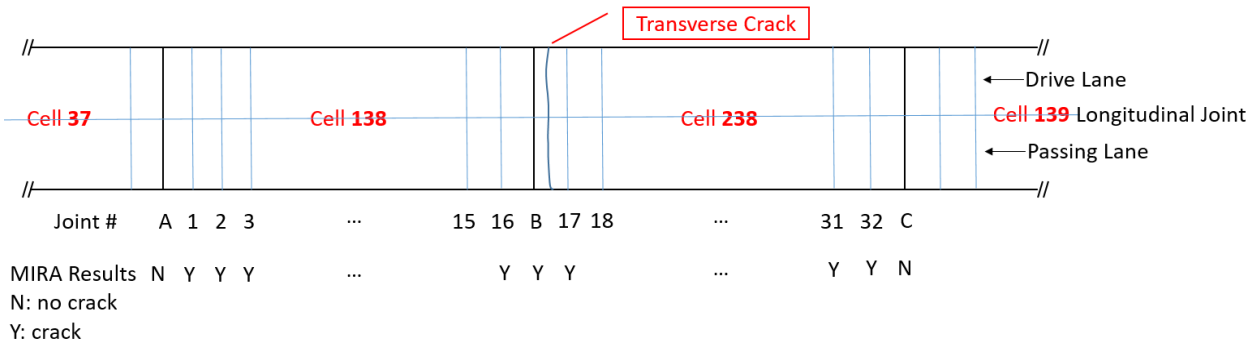

Figure 57. Joint cracking map – All joints deployed by the measurement event on 09/21/2017

3.3.2.10 Distress Survey

During the distress survey conducted in November 2018, a diagonal crack was observed in the traffic lane of Cell 138. The crack starts about 1.0 ft. from the intersection of the transverse and longitudinal joints and continues with an almost 45 degrees angle towards the shoulder of the inside lane as presented in Figure 58. Potential problems with base and/or subgrade may have contributed to formation of the cracks. Stresses caused by traffic loading can be another reason for cracking in this panel. The research team will monitor the crack and further investigate the potential cause for distress.

Figure 58. Cracking occurred on inside lane at Cell 138

It was reported by MnDOT staff that a transverse crack was observed on February 27, 2018, on the first panel transition from Cell 138 to 238 across both inside and outside lanes. The crack is about 5 feet from the downstream joint and angling slightly away from mid-panel as shown in Figure 59. Further cracking (Figure 60Figure 69) was also observed in July 2018 near the wheel path at Cell 238.

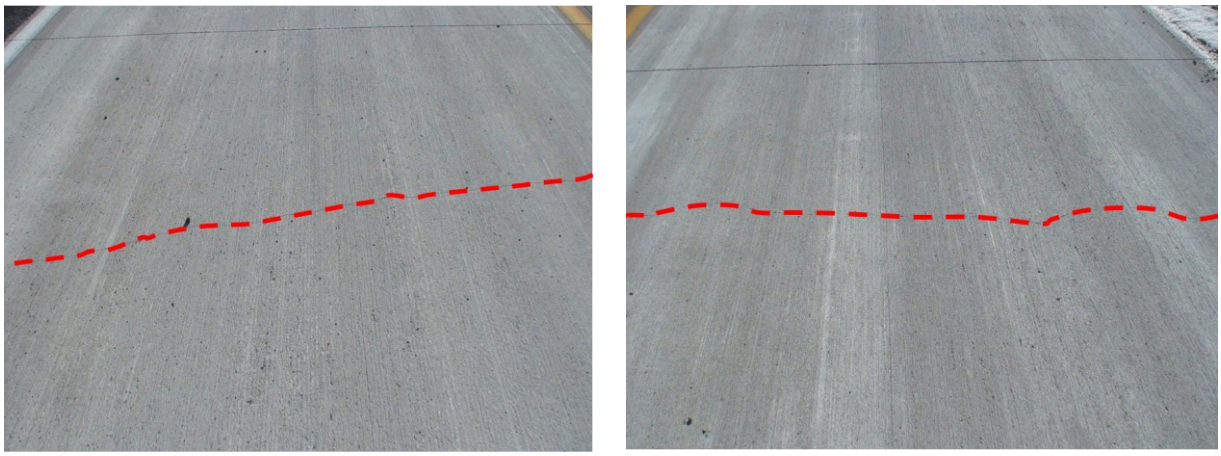

Figure 59. Transverse crack occurred on outside lane (left) and inside lane (right) at Cell 238

Site visit and coring was conducted on November 6, 2018 to further elucidate the reason for progressive cracking at Cell 238. In-situ investigations suggested that the main transverse cracking at this location was induced by the utility line underneath the pavement (Figure 61).

In collaboration with staff at MnROAD, the research team obtained four cores from Cell 238 to further investigate the reason for the observed distress. Two of these cores (C-1 and T-1) were extracted from the concrete adjacent to the transverse crack as shown in Figure 61. Core C-1 was obtained from the outside lane and core T-1 was obtained from the inside lane (exposed to traffic). Moreover, two cores were extracted (C-2 and T-2) from a panel with no cracking to serve as the reference (Figure 62). It should be noted that in each location, cores were obtained from both the inside and outside lanes to understand the potential effect of traffic loading (if any) on the observed distress. The pavement thickness at the distress area was about 8.0 in. compared to 9.0 in. for the panel with no sign of distress.

Figure 60. Further distress in form of cracking near the wheel path at Cell 238

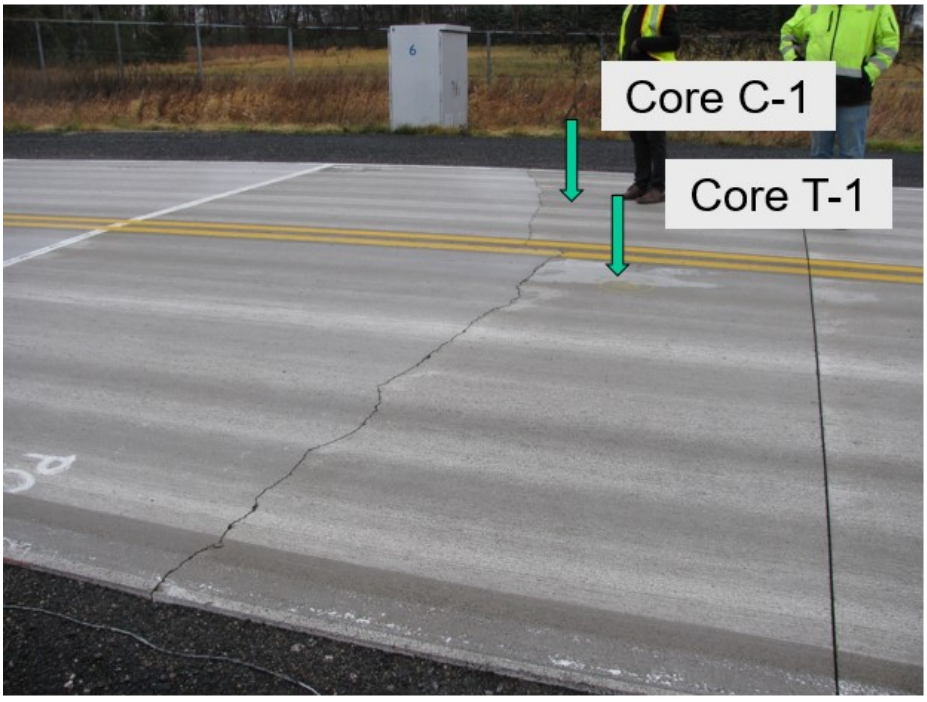

Figure 61. Distress in form of cracking near the wheel path at Cell 238

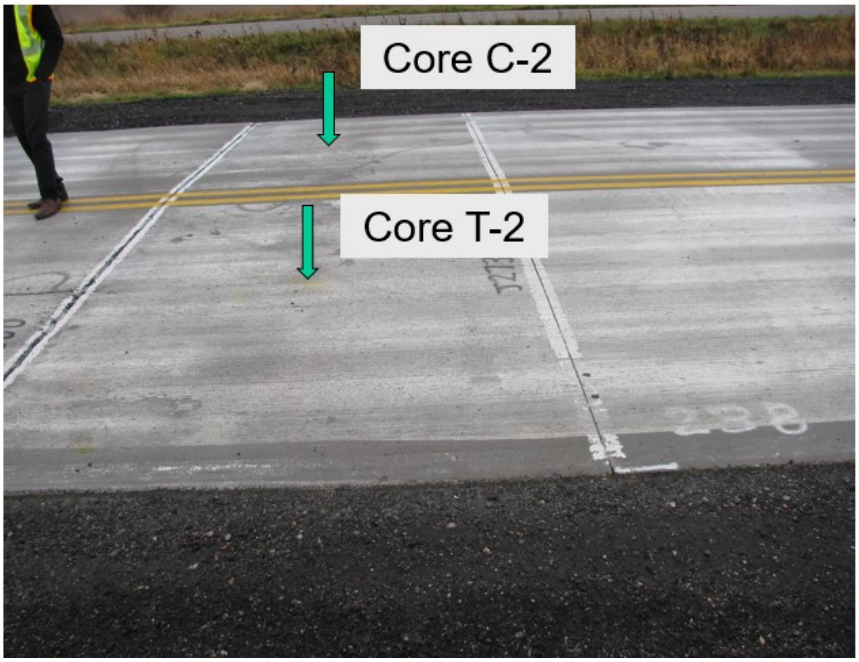

Figure 62. Panel with no cracking at the beginning of Cell 238 to serve as reference

Borehole permeability test was also conducted to compare the permeability of the base layer at the coring spots (ASTM D6391). This test involves monitoring the rate of water infiltration trough the base layer using a standpipe with a falling head. The test setup is presented in Figure 63.

Figure 63. Borehole permeability test setup

Drop in water level was monitored over time and the average rate of flow during periods of stable measurements was reported for each coring spot. Stable readings were obtained for core holes number T-1, T-2, and C-2. However, the run off through concrete cracks made it impossible to obtain stable readings for the C-1 location. Higher base permeability was observed for the area with no distress as presented in Table 34.

Table 34. Data obtained from testing core samples and core holes

Core ID	Pavement Thickness (in.)	Location	Surface Resistivity (kohm-cm)	Base Permeability (ft/day)
T-1	7.75	Distressed area, Cell 238	95.0	1.78
C-1	8.0		90.5	N/A
T-2	8.875	Area with no distress, Cell 238	81.0	5.20
C-2	9.0		90.0	4.93

The visual inspection of the Core T-1, extracted from the main distressed area revealed segregation of coarse aggregates from mortar as presented in Figure 64. No such problem was observed for the rest of the cores. Such a segregation can lead to limited contribution of coarse aggregates in restraining the mortar during shrinkage. Moreover, reduced local modulus of elasticity, along with the stresses exerted by traffic loading in the area adjacent to the transverse crack can be considered as the other contributors to the distress observed in Cell 238. Potential problems with base and/or subgrade can also contribute to formation of the cracks as a result of punching forces exerted by the traffic load.

Cores were transported back to the laboratory at Iowa State University for further investigation, including electrical resistivity measurement. The samples were cured in water for 7 days to ensure comparable moisture conditions. Resistivity data are summarized in Table 34. Comparable resistivity data was observed for all four cores.

Figure 64. Segregation of coarse aggregate in distress area; Core T-1 (Left) and corresponding core hole (Right)

As of November 2018, the distress in Cells 138 and 238 was limited to the reported cracks. So far the in-situ inspection of the cells exposed to environmental conditions and traffic loading, indicated proper quality of the pavement surfaces at both cells. No issues were observed for the surface texture at Cell 138. Finishing problems were occasionally observed at pavement surfaces in Cell 238. This is believed to be due to the lower workability of the mixtures with lower cementitious materials content as stated in previous reports. Figure 65Figure 71 presents examples of typical surface quality at Cell 138, along with the observed finishing problems at Cell 238.

Figure 65. Typical surface quality at Cell 138 (top), and finishing issues observed at Cell 238 (Bot.)

The most recent distress survey was conducted in fall 2019. No further cracking or materials related distress in cell 138 and 238 occurred during the third year. The only signs of distress were the cracks previously recorded and discussed in the second year performance report.

Only one diagonal crack exists in cell 138 as shown in Figure 66 and schematically presented in Figure 67. The crack starts about 1.0 ft. from the intersection of the transverse and longitudinal joints and continues with an almost 45 degrees angle towards the shoulder of the inside lane as presented in Figure 66. Potential problems with base and/or subgrade may have contributed to formation of the cracks. Stresses caused by traffic loading can be another reason for cracking in this panel.

Figure 66. Cracking occurred on inside lane at cell 138

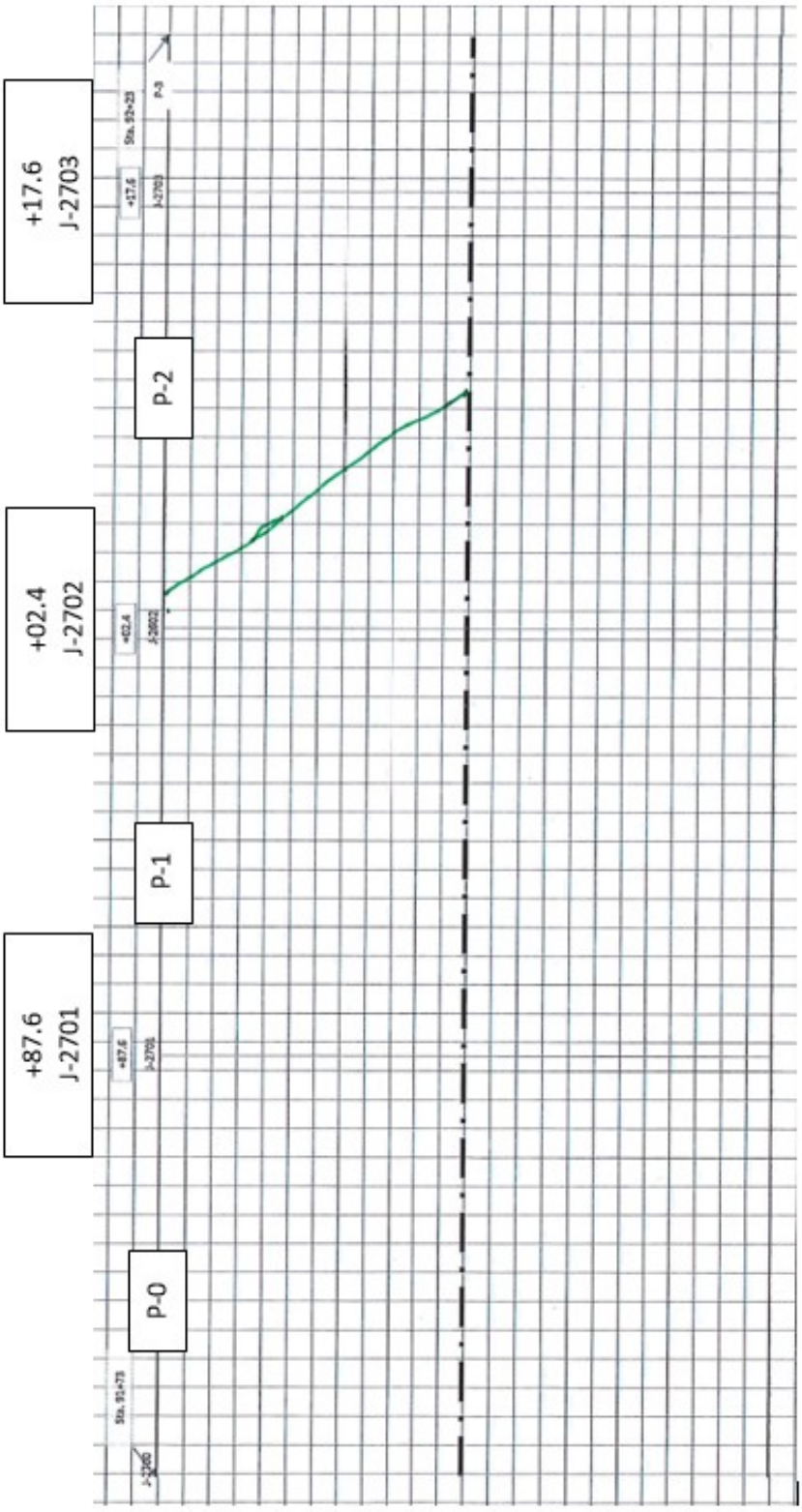

Figure 67. Schematic plan view of the cracking occurred on inside lane at cell 138

Cracking and distress in cell 238 is limited to the first panel transition from cell 138 to 238. The crack is about 5 feet from the downstream joint and angling slightly away from mid-panel as shown in Figure 68. Map cracking is also available in areas adjacent to the crack as shown in Figure 69. Figure 70 presents a schematic plan view of the cracking in cell 238.

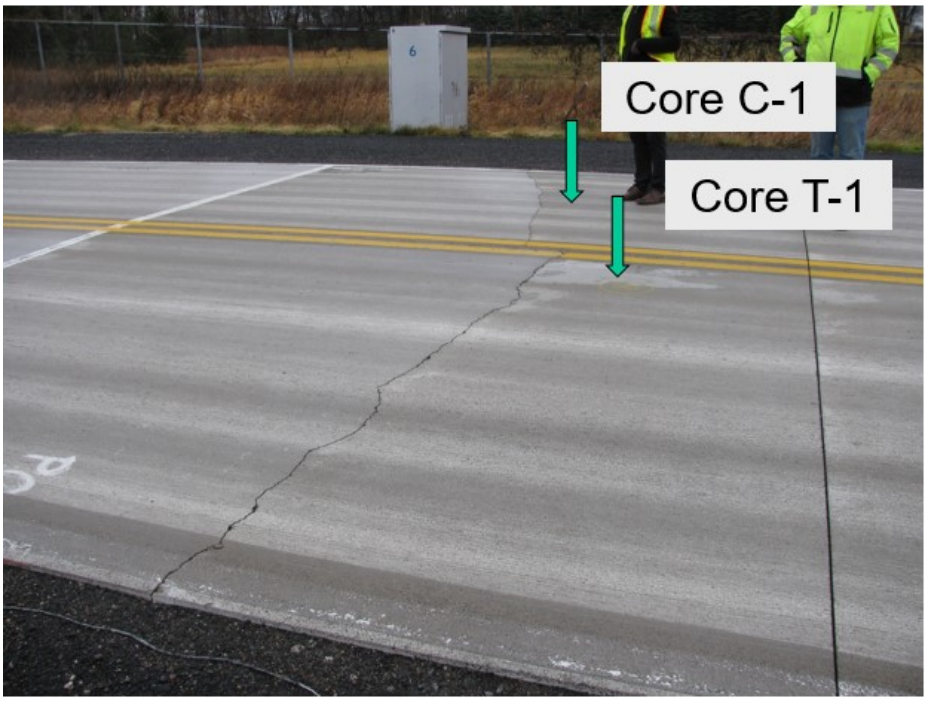

Figure 68. Transverse crack occurred on outside lane (left) and inside lane (right) at cell 238

Figure 69. Further distress in form of map cracking near the wheel path at cell 238

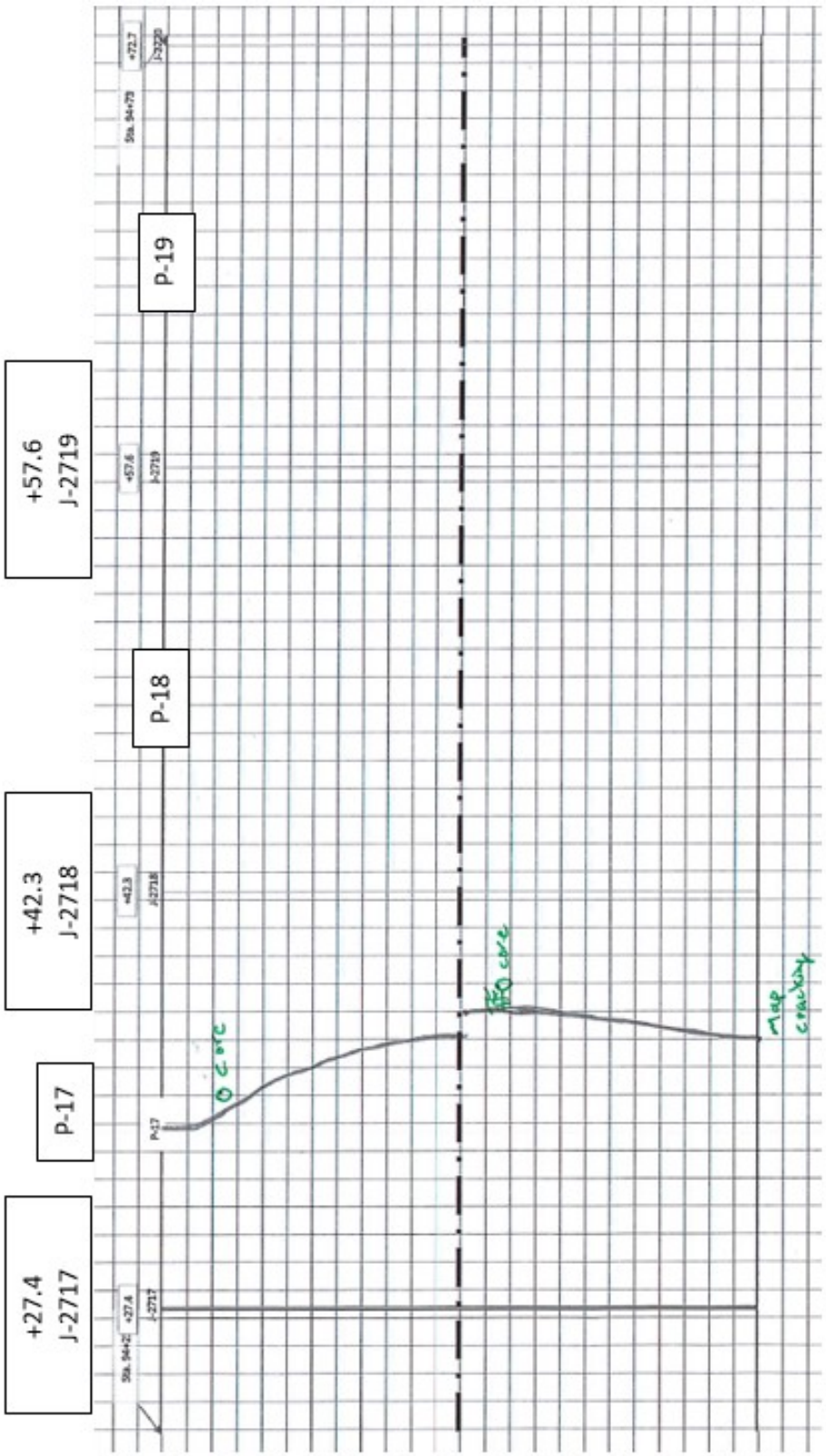

Figure 70. Schematic plan view of the cracking occurred on inside lane at cell 238

So far the in-situ inspection of the cells exposed to environmental conditions and traffic loading, indicated proper quality of the pavement surfaces at both cells. No issues were observed for the surface texture at cell 138. Finishing problems were occasionally observed at pavement surfaces in cell 238. This is believed to be due to the lower workability of the mixtures with lower cementitious materials content as stated in previous reports. Figure 71 presents examples of typical surface quality at cell 138, along with the observed finishing problems at cell 238.

Figure 71. Typical surface quality at cell 138 (top), and finishing issues observed at cell 238 (Bot.)

3.3.2.11 MIRA Investigation

Readings were taken using the MIRA ultrasonic device by MNDOT staff on both test and the control sections in October 2020.

Locations of the readings and the recorded pulse velocities are shown in Table 35 and the data are summarized in Figure 71.

Table 35. MIRA Test locations and data

Section	Panel	Reading	Loading	Pulse Velocity (m/s)
Low Cement	138	1	Environmental	2660
Low Cement	138	2	Traffic	2730
Low Cement	138	3	Environmental	2670
Low Cement	138	4	Traffic	2670
Lower Cement	238	1	Environmental	2730
Lower Cement	238	2	Traffic	2670
Lower Cement	238	3	Environmental	2670
Lower Cement	238	4	Traffic	2610
Control	524	1	Traffic	2890
Control	524	2	Environmental	2710
Control	524	3	Traffic	2730
Control	524	4	Environmental	2800

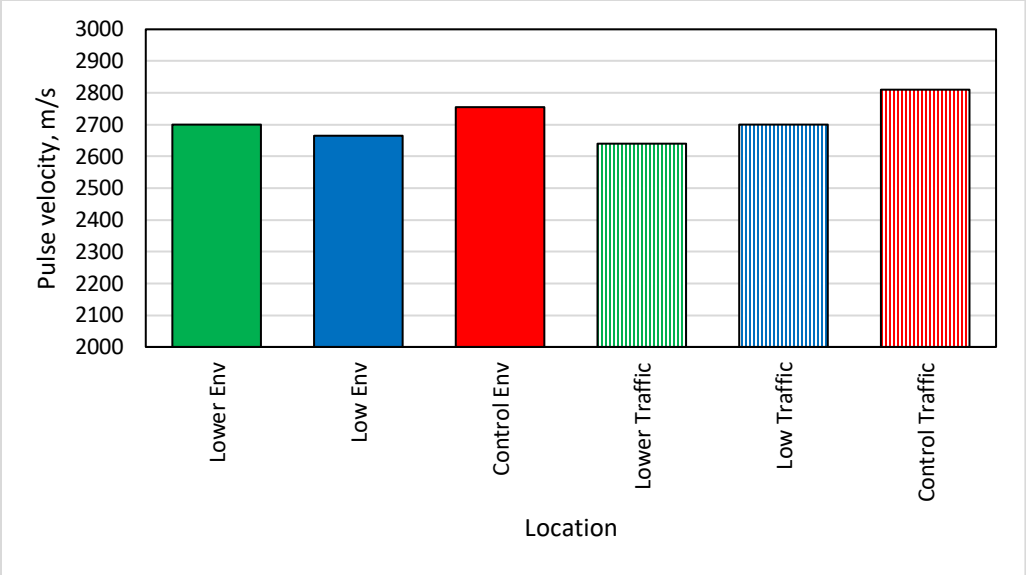

Figure 72. Measured Pulse Velocity Data

All of the readings are in the range 2600 to 2900 m/s. There is a slight increase in pulse velocity with binder content. The increase in pulse velocity with traffic loading is likely more related to variability in construction practices and the test method than an artifact of loading, as any distress or damage would be expected to reduce recorded velocity.

The data were also analyzed to observe defects in the measured zone as shown in Figures 73 to 78.

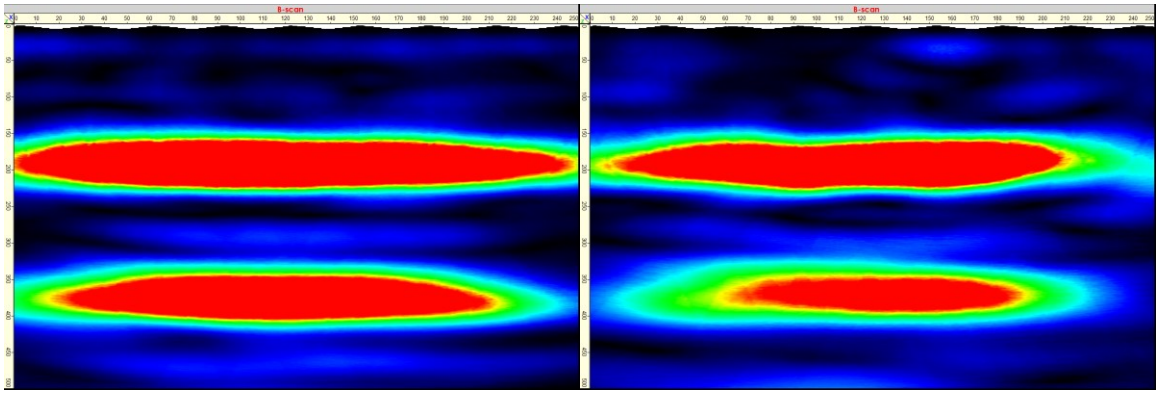

Figure 73. MIRA Plot for readings 138-1 and 3, Low cement, Environmental Exposure

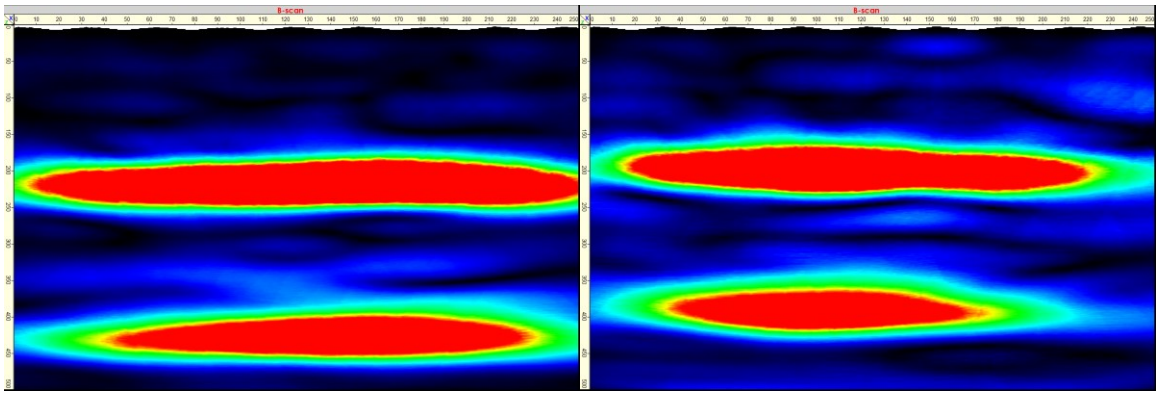

Figure 74. MIRA Plot for readings 138-2 and 4, Low cement, Traffic Exposure

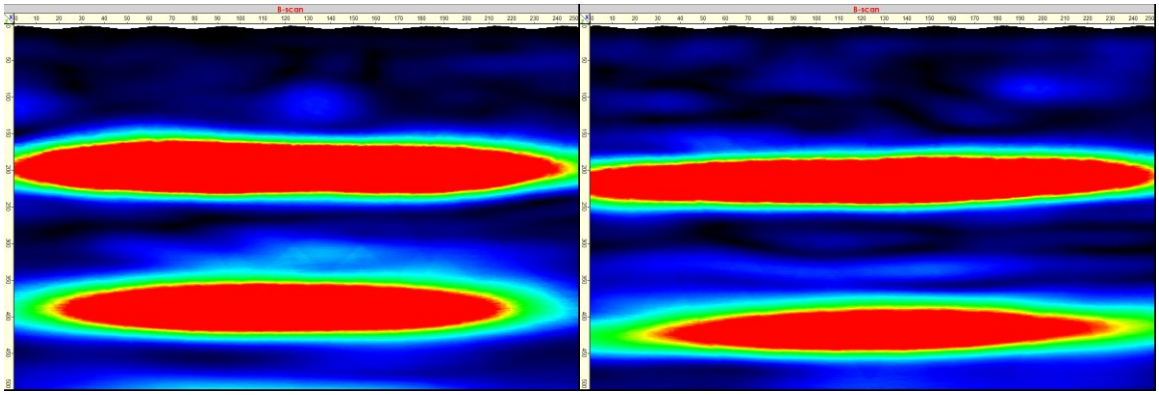

Figure 75. MIRA Plot for readings 238-1 and 3, Lower cement, Environmental Exposure

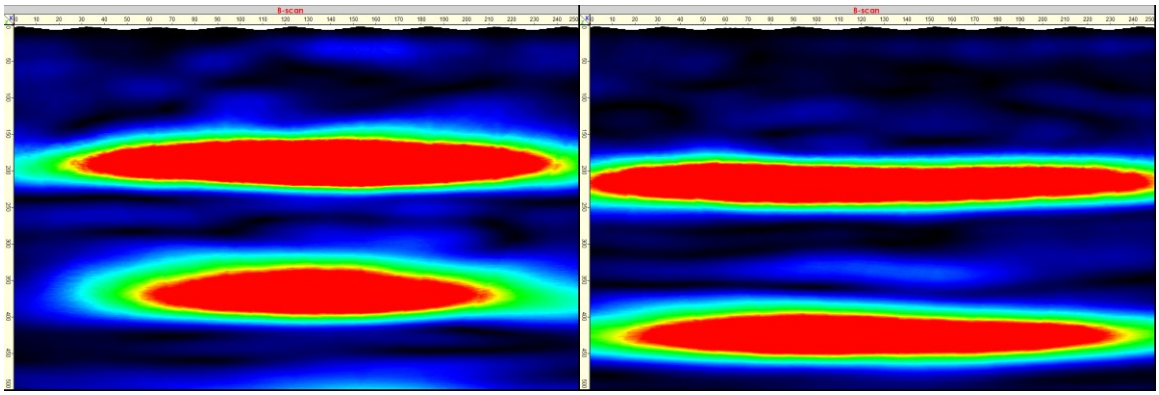

Figure 76. MIRA Plot for readings 238-2 and 4, Lower cement, Traffic Exposure

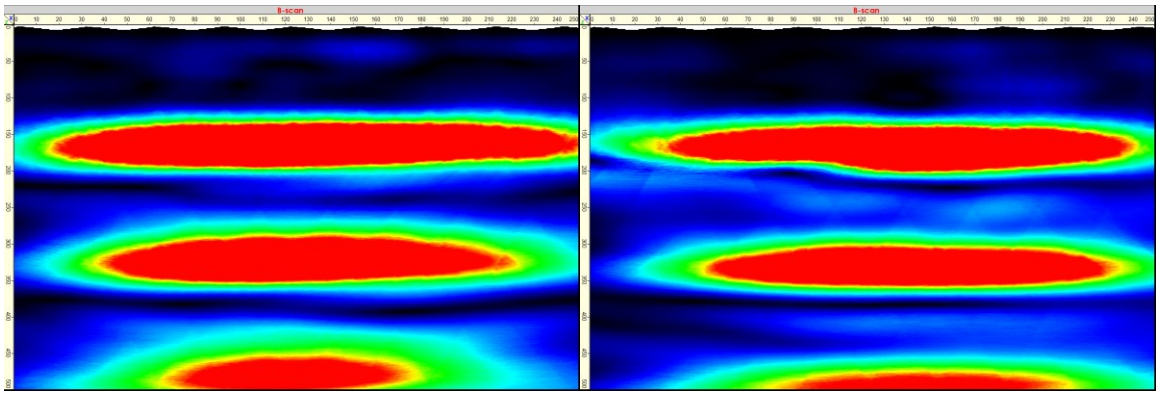

Figure 77. MIRA Plot for readings 524-2 and 4, Control, Environmental Exposure

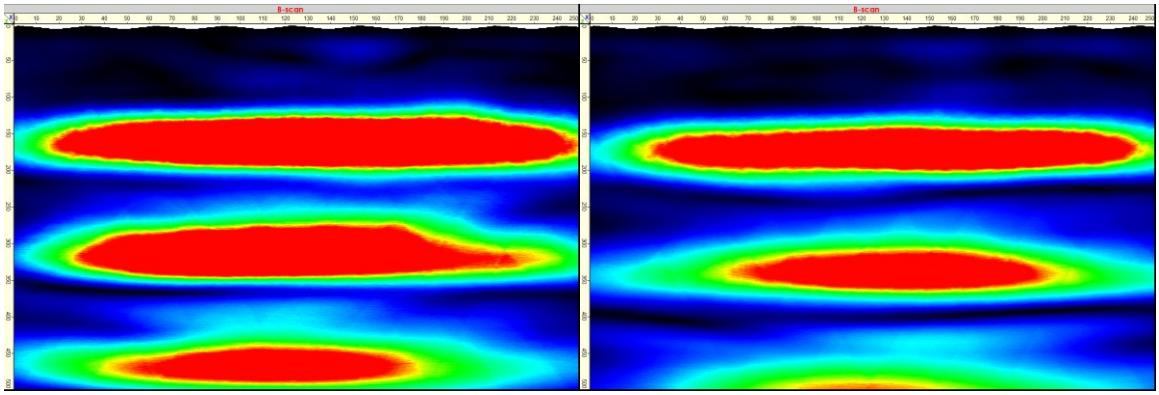

Figure 78. MIRA Plot for readings 524-1 and 3, Control, Traffic Exposure

The first red stripe indicates the depth of bottom of the concrete layers, which are consistent with design thicknesses. The second is the bottom of the base layers, all of which appear to be slightly thicker than designed, and the third in the control sections is likely the bottom of the sand layer. No other significant features are observed.

All of these data indicate that there is no signs of insufficient mixing, nor structural distress in the different sections.

CHAPTER 4: LONG TERM SERVICEABILITY AND ECONOMICS

4.1 ESTIMATED MAINTENANCE PERIOD FOR LIFE CYCLE COST ANALYSIS

Life cycle cost analysis (LCCA) started to be used by state agencies in the 1950s for cost evaluations and to compare proposed pavement systems (AASHTO 1960). LCCA is a form of economic analysis used to evaluate long-term economic efficiency among alternative investment options. Different pavement types, qualities of pavement, effects on the motoring public, and maintenance and rehabilitation costs should be considered in this type of analysis (Wilde et al. 1999).

Economic analysis focuses on the relationship between construction, maintenance, and rehabilitation costs; timings of costs; and discount rates employed. Once all costs and their timings have been determined, future costs are discounted to the base year and added to the initial cost to determine the net present value (NPV) for the LCCA alternatives. The basic NPV equation for discounting discrete future amounts at various points in time back to some base year is as follows (West et al. 2013):

$$NPV = Initial\ Construction\ Cost + \sum_{k=1}^{N} Rehabilitaion\ Cost_k \left[\frac{1}{(1+i)^n k}\right] - Salvage\ Value \left[\frac{1}{(1+i)^n k}\right] \quad (10)$$

Where i= discount rate and n= year of expenditure.

The LCCA period is the period over which future costs are evaluated. This period should be long enough to reflect long-term cost differences associated with reasonable design strategies. The analysis period should generally be long enough to see at least one maintenance or major rehabilitation activity over the pavement life, and the period can also be selected based on the requirements of the department of transportation. Figure 79 demonstrates the lifecycles of two different pavements over an analysis period; Alternative A has a higher initial cost but lower maintenance expenses than Alternative B.

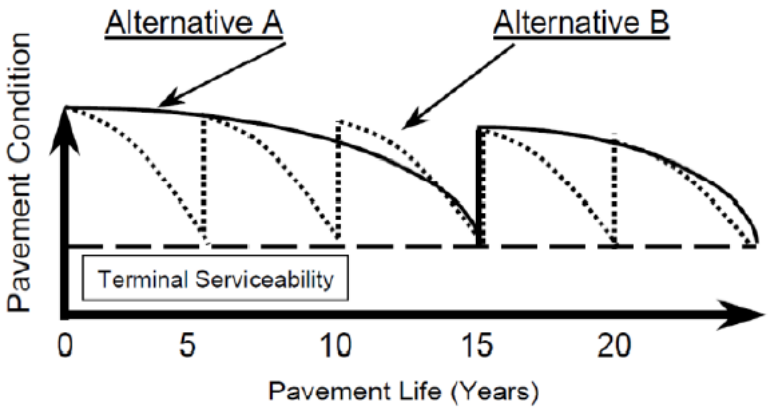

Figure 79. Lifecycles of two pavements over an analysis period (Walls and Smith 1998)

Routine annual maintenance costs usually do not change significantly and have a marginal effect on the total NPV of pavements compared to initial construction or major rehabilitation costs, particularly when discounted over 30- to 40-year analysis periods.

Salvage value represents the value of an investment alternative at the end of the analysis period. Residual value and residual serviceable life are two essential components of salvage value.

Residual value refers to the net value from recycling the pavement material. The differential residual values among pavement design strategies are usually not very significant and tend to have little effect on LCCA results when discounted over the entire analysis period.

Residual serviceable life represents the more significant component of salvage value and is the remaining life in a pavement alternative at the end of the analysis period. Residual serviceable life is primarily used to account for differences in remaining pavement life between alternative pavement design strategies at the end of the analysis period.

Figure 80 depicts the entire pavement cost stream over the analysis period, including initial construction, minor and routine maintenance, and major rehabilitation costs, as well as salvage value at the end of the period.

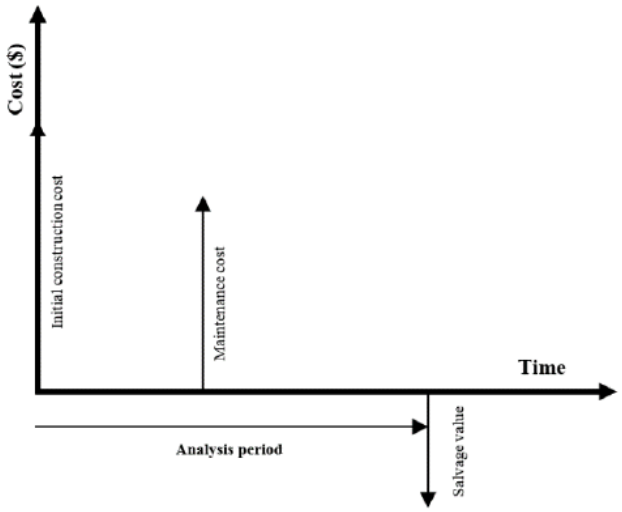

Figure 80. Cost stream over the lifecycle of a pavement (Vosoughi et al. 2017)

All of these values should be estimated and discounted to calculate NPV in the base year. Then, using the NPV, alternatives can be compared with each other.

So far the data obtained from testing concrete mixtures in fresh and hardened states are similar for both cells. The LTE data and dynamic loading data are not flagging any significant differences between the two cells either. IRI is a performance parameter of a pavement that can be used to study how the pavement behaves over the analysis.

The threshold value at which the pavement is assumed to have failed is 172 in. per mile. Maintenance should be conducted well before the pavement reaches the threshold value because delayed maintenance significantly increases maintenance costs. Therefore, it is assumed that major maintenance is required when the IRI value of the pavement reaches a specific threshold. This threshold can be assumed as 130 and 140 in. per mile for pavements with 1,500 and 400 AADTT, respectively, because a higher IRI value is acceptable for county roads with lower traffic levels (Vosoughi et al. 2017).

The smoothness of the pavement would be significantly improved after conducting major maintenance, so it is assumed that the IRI value will decrease to half (65 and 70 in. per mile for pavements with 1,500 and 400 AADTT, respectively). The IRI value after maintenance may be lower than the initial value because maintenance may mitigate some of the initial curling and warping that may occur at very early ages.

Even though no strong correlations could be established, the regression equations previously presented in Figure 39 were employed to obtain estimations of the time when the IRI values reach critical limits that necessitate maintenance.

A maintenance criteria of IRI= 140 in./mile is assumed in this study. It is also assumed that a pavement cast with either of the experimental mixtures will be initially constructed in a long enough stretch to enable achieving initial IRI of 65 in./mile. Considering the slopes of the lines obtained for right wheel

path at inside lanes of the investigated cells, the following rates can be considered for variation in IRI values over time:

- Cell 138: an increase rate of 0.437 in./mile/month
- Cell 238: an increase rate of 0.348 in./mile/month

These values correspond to maintenance at 14.5 and 18.0 years from construction, if mixtures prepared with low and lower cementitious materials content are used for pavement construction, respectively, as schematically shown in Figure 81.

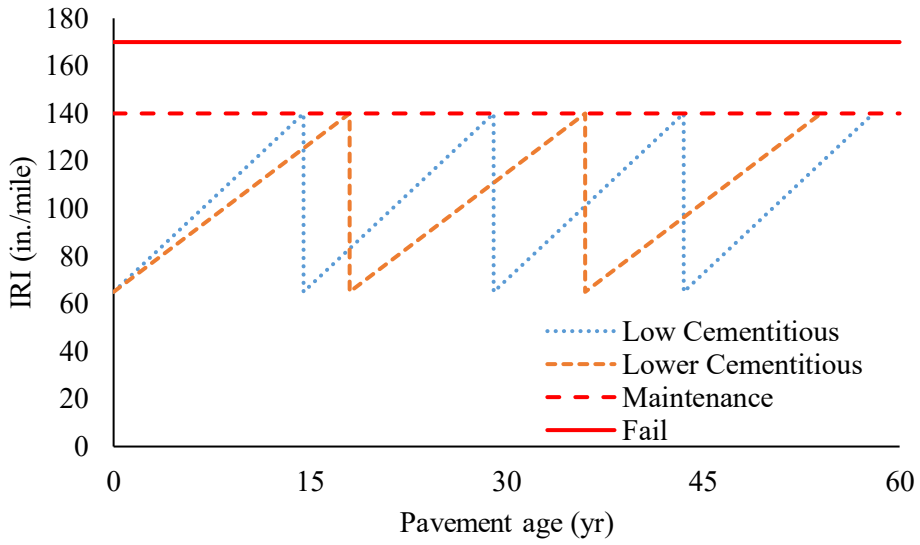

Figure 81. Lifecycle of pavements with low AADTT

Assuming a design life of 50 years, four major maintenance activities will be required for the pavement prepared with low cementitious materials content. Three major maintenance activities will be required for the pavement prepared with lower cementitious materials content during the same period. This was not estimated for the reference cell, as the variation in IRI over time was not following a logical trend (reduction in IRI over time was observed for inside lane cell 524).

4.2 SUSTAINABILITY- CARBON FOOTPRINT

Cement production is one of the major contributors to industrial CO_2 release worldwide, and a significant source of emissions in concrete production. Reducing the cementitious materials content therefore can reduce the carbon footprint of concrete mixtures significantly. Recommendations provided by Khayat & Sadati (2017) were considered for determining the emissions due to the use of cement and fly ash:

- Emission rate for ordinary portland cement: 2115 lb./ton or 1.06 lb./lb.
- Emission rate for fly ash : 205 lb./ton or 0.103 lb./lb.

This means that the CO_2 emissions per cubic yard of concrete due to cementitious materials for mixtures investigated in this study are:

- Reference mixture (cell 524): (400*1.06) + (170*0.103) = 442 lb./yd^3
- Low cementitious materials content (cell 138): (375*1.06) + (125*0.103) = 410 lb./yd^3 meaning a reduction of 7.2%.
- Lower cementitious materials content (cell 238): (353*1.06) + (117*0.103) = 386 lb./yd^3 meaning a reduction of 12.7%.

CHAPTER 5: RECOMMENDATIONS FOR CONCRETE MIXTURES WITH REDUCED CEMENTITIOUS MATERIALS CONTENT

5.1 MIXTURE PROPORTIONING METHODOLOGY

Summary of findings previously discussed in the literature review report of this project suggest the fact that SCMs type and replacement rate, use of admixtures, and aggregate system affect the binder content in a concrete mixture.

Paste quality needs to be tailored to the specific requirements of the project, to avoid issues with transport properties, freeze and thaw durability, and strength gain. SCMs are generally recommended as a partial replacement for Portland cement to achieve the desired engineering properties. Selection of a proper SCM type and dosage is a compromise between obtaining the benefits desired, such as increased resistance to alkali silica reaction, reduced water demand for a given consistency, and improved durability, and limiting negative effects such as shrinkage and risk of cracking. SCM types and dosages have varied effects on properties such as water demand and air content.

The w/cm and properties of the air-void system are also of great importance to secure desired fresh and hardened properties. The authors believe that the current MnDOT recommendations on w/cm and fresh air content are also suitable for mixtures with reduced cementitious materials content;

- Maximum w/cm of 0.40 with fly ash or 0.42 (with slag/ternary)
- Target air content of 7%

In addition, and based on the fresh and hardened concrete test data previously presented in Chapter 3, a SAM number of no more than 0.25 is recommended to ensure quality of air void system in fresh state.

As previously stated in Chapter 2, selection of an optimized aggregate skeleton is the key factor in successful design of concrete mixtures with reduced cementitious materials content. Concrete mixture proportioning is focused on meeting the basic performance specifications of a mixture and producing the most economical concrete. One way to reduce cost is to use as little cementitious paste as possible without compromising the engineering properties. Aggregate properties (e.g., gradation, surface texture, shape, and size) have a strong impact on system workability (Cook et al. 2016, Dhir et al. 2006, Alexander and Mindess 2005).

Enough paste is needed in paving mixtures to fill the voids available between the aggregate particles, coat the aggregate particles, and lubricate the aggregates to provide a desired workability (Kennedy 1940). The aggregate system can therefore strongly influence how much paste is required to achieve desired performance.

The concrete mixture proportioning method proposed by Taylor et al. (2015) defines three decisions: (1) selection of a combined aggregate system, (2) selection of paste quality, and (3) selection of paste quantity. The design procedure is based on evaluating and selecting the paste and aggregate systems

separately, followed by an analysis of the interaction between them (Taylor et al. 2015). The fundamental philosophy is that the paste quality primarily controls long-term performance (assuming durable aggregates), while the paste quantity and the aggregate system are mainly responsible for the workability of the fresh concrete as previously summarized in Table 7.

As previously stated, the aggregate and paste systems have the greatest effects on the concrete performance properties. An excess of paste content, especially binder content, may adversely affect the shrinkage and permeability of concrete mixtures and result in durability issues. However, sufficient paste content is needed to provide a level of workability that is suitable for pavement concrete mixtures. The minimum paste content should be determined based on the voids in the combined aggregate system used in the mixture.

The quantitative parameter, paste volume to voids volume in a combined aggregate ratio (V_{paste}/V_{voids}), was developed for this mix design method in order to correlate the performance of a mixture to the paste volume for a given aggregate system. The V_{paste}/V_{voids} ratio is calculated by calculating the paste volume of the concrete mixture and dividing that value by the volume of voids between the combined compacted aggregates. The paste volume includes the volume of water, cementitious materials content, and air in the system. The voids refer to the space between the compacted combined aggregates, which is determined in accordance with ASTM C29. A ratio of 100% indicates that all of the voids available in the combined aggregate system are filled with paste, with no excess (Taylor et al. 2015).

As discussed in previous publications of the research team (Taylor et al. 2015, Wang et al. 2018), it is believed that the “Tarantula Curve” which is an improved version of the individual percentage retained (IPR) chart (Richardson 2005, ACI 302 2004), is a suitable technique for optimizing the aggregate combination intended for use in concrete pavement mixtures. The tarantula curve describes an envelope that reports the desirable amount of materials retained on each sieve, as shown in Figure 82 (Ley and Cook 2014). The aim is to combine the individual aggregates available so that the combined system is within the envelope and as close to the center of the envelope as possible.

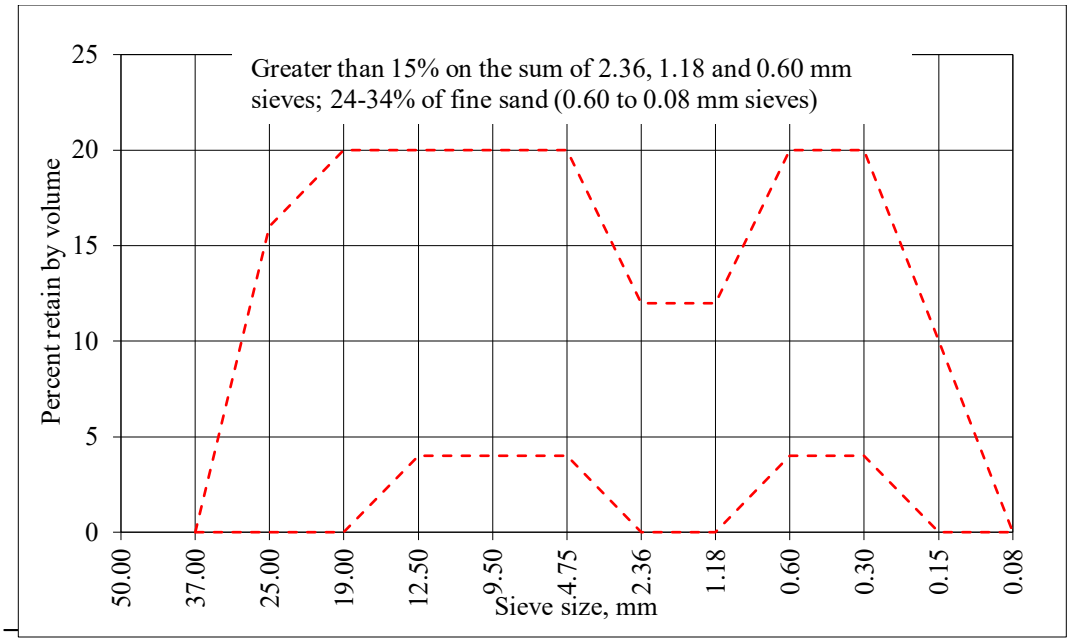

Figure 82. Tarantula curve

Additional requirements of this method include the following:

- The total volume of coarse sand (#8 to #30) must be a minimum of 15%.
- The total volume of fine sand (#30 to #200) must be within 24% and 34%.
- The flat or elongated coarse aggregate must be limited to 15% or less at a ratio of 1:3, according to ASTM D4791.

As previously shown in Figure 10, the aggregate combination used for concrete production in this research meets the criteria of tarantula envelop. In other words, the incorporated aggregate system provides the potential for reduction in cementitious materials content without compromising the quality.

In order to minimize binder content, it is recommended that the quantitative parameter V_{paste}/V_{voids}, developed by Wang et al. (2018), be used to correlate a mixture's performance with its paste volume for a given aggregate system. The suggested minimum V_{paste}/V_{voids} values for different SCMs and performance properties are provided in Table 8. These values can serve as a starting point for optimizing cementitious materials content in pavement mix design applications.

As previously shown in Table 10, the concrete mixtures used for construction of the low cement sections in this study were proportioned with the following ratios of V_{paste}/V_{voids}:

- Cell 138 prepared with low cementitious materials content: V_{paste}/V_{voids} =146%
- Cell 138 prepared with low cementitious materials content: V_{paste}/V_{voids} =137%

Both mixtures met the recommendations presented in Table 7Table 8 for concrete proportioned with Class F fly ash. However, the data obtained in this study suggested some workability issues with concrete prepared with V_{paste}/V_{voids} of 137% used for construction of cell 238. One should however note that the workability issues were minimal and no specific problems were reported during the pavement construction. In addition, the hardened data obtained for both experimental mixtures were comparable, with no abnormalities that could be attributed to the reduced cementitious materials content in either of the mixtures. This was also the case for in-situ test results and serviceability data obtained through the 3-year performance monitoring.

In general, results obtained through this study suggest the fact that optimizing the aggregate combination based on the requirements of Tarantula envelop and selection of a proper value for the ratio of V_{paste}/V_{voids} can result in preparation of green concrete mixtures with reduced cementitious materials content and desirable engineering properties. One should note that the V_{paste}/V_{voids} ratio is tied to the characteristics of the combined aggregate system and should be evaluated in laboratory using trial concrete mixtures.

5.2 RECOMMENDED TEST METHODS FOR LOW CEMENT CONCRETE CHARACHTERIZATION

Results obtained through this study suggest that workability issues can arise when a very low cementitious materials content is selected. Proper evaluation tools will therefore be required to ensure detection of potential constructability issues. Of great importance is the use of workability test methods that capture the response of the fresh concrete mixture to vibration energy applied during the slip form paving. It is suggested to use the following two test methods both in the laboratory and in the field to investigate the constructability of low cement concrete mixtures:

- V-Kelly
- Box Test

These two tests were proved effective in detection of workability issues during the construction of pavement sections:

- The VKelly index of 0.50 in./$s^{0.5}$ obtained for mixture with lower cementitious content was slightly lower than the recommended minimum of 0.60 in./$s^{0.5}$. However, the mixture with low cementitious content used for cell 138 exhibited a VKelly index of 0.88 in./$s^{0.5}$, which was within the recommended range (Taylor et al. 2015).
- The box test indicated better workability for mixture with low cementitious materials content. An average visual rating of 1.0 was reported for this mixture, corresponding to less than 10 percent overall surface voids. The visual rating was between 2 and 3 for the concrete with lower cementitious content, indicating 30-50 percent overall surface voids (Cook et al. 2014).

Both these test methods flagged potentials for workability issue for concrete produced with lower cementitious materials content used for construction of cell 238. These observations were later manifested in shape of finishing issues and surface voids in cell 238 as previously shown in Chapter 3.

Results obtained through this study, along with the previous experience of the research team suggest that the mixtures exhibiting desired workability, established through VKelly and box Test, can be placed, consolidated, and finished utilizing traditional equipment and procedures.

Good correlations were observed between the SAM test results and hardened air void system data obtained for both mixtures. This suggests the fact that SAM test can be used as an effective means for investigating the F/T durability of low cement concrete mixtures intended for use in pavement construction. The average SAM numbers of 0.26 and 0.22 were obtained for the mixtures with "low" and "lower" cementitious materials contents, respectively. Both these mixtures exhibited spacing factor of 0.002 in. and specific surface area within the range of 1500±100 $in.^2/in.^3$.

Moreover, and as discussed in previous reports, the resistivity test data suggested proper performance of both concrete mixtures. So far, the field observations suggest proper durability of the two test sections, indicating agreement between durability test data and field observations. The investigated mixtures exhibited comparable resistivity, with 91-day values of about 25.0 kohm-cm, corresponding to "Very Low" risk of chloride ion penetration at 91 days as proposed by AASHTO PP 84.

Same observations were made with regards to early age strength development and long-term mechanical properties, were the test results indicated acceptable performance of investigated low cement mixtures with no potential issues that could jeopardize the long-term serviceability.

It is therefore suggested to employ the performance engineered concrete mixture (PEM) test methods introduced in AASHTO PP84 to evaluate the fresh and hardened properties of low cement concrete mixtures to ensure delivery of proper quality and construction of durable concrete pavements.

CHAPTER 6: SUMMARY OF FINDINGS

Based on the reported results, the following findings are noted:

1. Results obtained from the work indicated that all properties were acceptable in the 500 lb/yd^3 section. Workability was marginal in the mixture proportioned with 470 lb/yd^3, although in all other aspects, the section performed satisfactorily.

2. Data from testing using the MIRA indicate that there were no signs of insufficient mixing or structural distress in the different sections.

3. No signs of early age materials related distress were observed that could be attributed to the reduced cementitious materials content. Distress observed in cell 238 was attributed to segregation that exacerbated cracking adjacent to a transverse crack induced by a utility line.

4. Both test sections performed well with respect to IRI and LTE, and slightly better than the control section, largely due to differences in thickness and age.

5. Comparable wear depth was observed for all three sections. Surface macro texture measurements exhibited comparable numbers for all three cells, with a slightly higher rate of increase for the trafficked lane.

6. Results suggest that given a proper mixture proportioning methodology, it will be possible to develop environmentally friendly concrete mixtures with reduced cementitious materials content, reduced carbon footprint, and reduced cost, without any negative impacts on quality of construction and long-term durability.

7. A mixture proportioning methodology is suggested to provide long-lasting mixtures without excess cementitious materials in the mixture.

REFERENCES

AASHTO. 2017. *Standard Practice for Developing Performance Engineered Concrete Pavement Mixtures*. American Association of State Highway and Transportation Officials, Washington, DC.

AASHTO. 1960. *Road User Benefit Analyses for Highway Improvements*. American Association of State Highway Officials Committee on Planning and Design Policies, Washington, DC.

ACI. 2004. *Guide for Concrete Floor and Slab Construction* (ACI 302.1 R-04). American Concrete Institute, Farmington Hills, MI.

ACPA. 2007. *Concrete Pavement Field Reference–Pre-Paving* (EB237P). American Concrete Pavement Association, Skokie, IL.

Addis, B., & M. Alexander. 1990. *A Method of Proportioning Trial Mixes for High-Strength Concrete* (ACI SP 121). American Concrete Institute, Farmington Hills, MI.

Alexander, M., & S. Mindess. 2005. *Aggregates in Concrete*. CRC Press, Taylor & Francis Group, New York, NY.

American Association of State Highway and Transportation Officials (AASHTO). 2017. *Standard Method of Vibrating Kelly Ball (VKelly) Penetration in Fresh Portland Cement Concrete*. AASHTO TP 129. AASHTO, Washington, DC.

American Association of State Highway and Transportation Officials (AASHTO). 2017. *Developing Performance Engineered Concrete Pavement Mixtures*. AASHTO PP 84. AASHTO, Washington, DC.

American Association of State Highway and Transportation Officials (AASHTO). 2011. *Standard Method of Test for Surface Resistivity Indication of Concrete's Ability to Resist Chloride Ion Penetration* (AASHTO TP 95). AASHTO, Washington, DC.

American Association of State Highway and Transportation Officials (AASHTO). 2015. *Coefficient of Thermal Expansion of Hydraulic Cement Concrete* (AASHTO T 336). AASHTO, Washington, DC.

Arachchige, A. 2008. Influence of Cement Content on Corrosion Resistance. *Proceedings of the ICE – Construction Materials*, *161*(1), 31–39.

ASTM C150/C150M-17. 2017. *Standard Specification for Portland Cement*. ASTM International, West Conshohocken, PA.

ASTM C157/C157M-17. 2017. *Standard Test Method for length Change of Hardened Hydraulic-Cement Mortar and Concrete*. ASTM International, West Conshohocken, PA.

ASTM C1753/C1753M-15e1. 2015. *Standard Practice for Evaluating Early Hydration of Hydraulic Cementitious Mixtures Using Thermal Measurements*. ASTM International, West Conshohocken, PA.

ASTM C231/C231M-17a. 2017. *Standard Test Method for Air Content of Freshly Mixed Concrete by the Pressure Method*. ASTM International, West Conshohocken, PA.

ASTM C29/C29M-17a. 2017. *Standard Test Method for Bulk Density ("Unit Weight") and Voids in Aggregate*. ASTM International, West Conshohocken, PA.

ASTM C39/C39M-18. 2018. *Standard Test Method for Compressive Strength of Cylindrical Concrete Specimens*. ASTM International, West Conshohocken, PA.

ASTM C457/C457M-16. 2016. *Standard Test Method for Microscopical Determination of Parameters of the Air-Void System in Hardened Concrete*. ASTM International, West Conshohocken, PA.

ASTM C469/C469M-14. 2014. *Standard Test Method for Static Modulus of Elasticity and Poisson's Ratio of Concrete in Compression*. ASTM International, West Conshohocken, PA.

ASTM C618-17a. 2017. *Standard Specification for Coal Fly Ash and Raw or Calcined Natural Pozzolan for Use in Concrete*. ASTM International, West Conshohocken, PA.

ASTM D4791-19. 2019. *Standard Test Method for Flat Particles, Elongated Particles, or Flat and Elongated Particles in Coarse Aggregate*. ASTM International, West Conshohocken, PA.

ASTM D6391-11. 2011. *Standard Test Method for Field Measurement of Hydraulic Conductivity Using Borehole Infiltration.* ASTM International, West Conshohocken, PA.

ASTM E2583-07. 2015. *Standard Test Method for Measuring Deflections with a Light Weight Deflectometer (LWD)*. ASTM International, West Conshohocken, PA.

ASTM E950/E950M-09. 2018. *Standard Test Method for Measuring the Longitudinal Profile of Traveled Surfaces with an Accelerometer-Established Inertial Profiling Reference.* ASTM International, West Conshohocken, PA.

Bullard, J., M. D'Ambrosia, Z. Grasley, W. Hansen, N. Kidner, D. Lange, … & L. Woo. 2006. A Comparison of Test Methods for Early-Age Behavior of Cementitious Materials. Paper presented at Symposium on Advances in Concrete through Science and Engineering, March 13–16, Quebec, Canada.

Cook, D., Ghaeezadah, A., & Ley, T. 2014. A Workability Test for Slip Formed Concrete Pavements. *Construction and Building Materials, 68,* 376–383.

Cook, M., T. Ley, & A. Ghaeezadah. 2016. Effects of Aggregate Concepts on the Workability of Slip-Formed Concrete. *Journal of Materials in Civil Engineering*, *28*(10), 04016097-1–04016097-10.

Cordon, W. 1946. Entrained Air – A Factor in the Design of Concrete Mixes. *ACI Journal Proceedings*, *42*(6), 605–620.

Day, K. 2006. *Concrete Mix Design, Quality Control and Specifications*. Third Edition. CRC Press, Boca Raton, FL.

de Larrard, F. 1999. *Concrete Mixture Proportioning: A Scientific Approach*. CRC Press, Boca Raton, FL.

Dewar, J. 1999. *Computer Modeling of Concrete Mixtures*. CRC Press, Boca Raton, FL.

Dhir, R. K., M. J. McCarthy, S. Zhou, & P. A. J. Tittle. 2006. Discussion: Role of Cement Content in Specifications for Concrete Durability: Aggregate Type Influences. *Structures and Buildings, 159*(4), 229–242.

Fuller, W. & S. Thompson. 1907. The Laws of Proportioning Concrete. *Transactions of the American Society of Civil Engineers*, *59*, 67–143.

Gilkey, H. 1958. Re-Proportioning of Concrete Mixtures for Air Entrainment. *Journal of the American Concrete Institute*, *54*(2), 633–645.

Goltermann, P., Johansen, V., & Palbol, L. 1997. Packing of Aggregates: An Alternative Tool to Determine the Optimal Aggregate Mix. *ACI Materials Journal*, *94*(5), 435–443.

Hale, W. M., S. F. Freyne, T. D. Bush, Jr., & B. W. Russell. 2008. Properties of Concrete Mixtures Containing Slag Cement and Fly Ash for Use in Transportation Structures. *Construction and Building Materials*, *22*(9), 1990–2000.

Helmuth, R. 1987. *Fly Ash in Cement and Concrete* (SP040.01T). Portland Cement Association, Skokie, IL.

Hooton, R. D. 2000. Canadian Use of ground granulated blast-furnace slag as a Supplementary Cementing Material for Enhanced Performance of Concrete. *Canadian Journal of Civil Engineering*, 27(4), 754–760.

Illinois Department of Transportation (IDOT). 2012. *Standard Specifications for Road and Bridge Construction: Section 1020. Portland Cement Concrete*. IDOT, Springfield, IL.

Indiana Department of Transportation (INDOT). 2008. *Standard Specifications 2016–Section 500–Concrete Pavement*. INDOT, Indianapolis, IN.

Iowa Department of Transportation (Iowa DOT). 2008a. *Portland Cement (PC) Concrete Proportions* (IM 529). Iowa DOT, Ames, IA.

Iowa Department of Transportation (Iowa DOT). 2008b. *Standard Specifications with GS-01015 Revisions. Section 2301: Portland Cement Concrete Pavement*. Iowa DOT, Ames, IA.

JTG/T F50. 2011. Technical Specifications for Construction of Highway Bridge and Culvert. Highway and Transportation Industry Standard (Recommended). Ministry of Transportation, People's Republic of China.

Kansas Department of Transportation (KDOT). 2015. *Standard Specifications for State Road and Bridge Construction. Section 401: Concrete.* KDOT, Topeka, KS.

Kennedy, C. 1940. The Design of Concrete Mixes. *Journal of the American Concrete Institute, 36*(20), 373–400.

Kennedy, C. 1940. The Design of Concrete Mixes. Journal of the American Concrete Institute, *36*(2), 373–400.

Kennedy, T., G. Huber, E. Harrigan, R. Cominsky, C. Hughes, H. Quintus, & J. Moulthrop. 1994. *Superior Performing Asphalt Pavements (Superpave): The Product of SHRP Asphalt Research Program*. Strategic Highway Research Program, Washington, DC.

Khayat, K. H., & S. Sadati. (2017). High-volume recycled materials for sustainable pavement construction (No. cmr 17-006). Missouri. Dept. of Transportation, Jefferson City, MO.

Kosmatka, S., & M. Wilson. 2016. *Design and Control of Concrete Mixtures*, Sixteenth Edition. Portland Cement Association, Skokie, IL.

Ley, T. 2013. *Super Air Meter* (Tech Brief). National Concrete Pavement Technology Center, Ames, IA.

Ley, T., & D. Cook. 2014. *Aggregate Gradations for Concrete Pavement Mixtures. CP Road MAP Brief* (FHWA TPF-5-(286)). National Concrete Pavement Technology Center, Iowa State University, Ames, IA.

Ley, T., D. Cook, & G. Fick. 2012. *Concrete Pavement Mixture Design and Analysis (MDA): Effect of Aggregate Systems on Concrete Properties*. National Concrete Pavement Technology Center, Ames, IA.

Lura, P., B. Pease, G. Mazzotta, F. Rajabipour, & J. Weiss. 2007. Influence of Shrinkage-Reducing Admixtures on Evaporation, Settlement, and Plastic Shrinkage Cracking. *ACI Materials Journal*, *104*(2), 187–194.

Malhotra, V. M. & P. K. Mehta. 1996. Pozzolanic and Cementitious Materials. In *Advances in Concrete Technology*, Vol. 1. CRC Press, Boca Raton, FL

Mehta, P. & P. Monteiro. 2006. *Concrete Microstructure, Properties, and Materials*, Third Edition. McGraw-Hill Publishing Company, Inc., New York, NY.

Michigan Department of Transportation (MDOT). 2012. *Standard Specifications for Construction*. MDOT, Lansing, MI.

Minnesota Department of Transportation (MnDOT). 2013. Lightweight Internal Surface Analyzer – MnROAD Ride Measurement. MnDOT, St. Paul, MN. Retrieved from http://www.dot.state.mn.us/mnroad/data/pdfs/lisa.pdf

Minnesota Department of Transportation (MnDOT). 2013. MnROAD Semi Tractor Trailer. MnDOT, St. Paul, MN. Retrieved from http://www.dot.state.mn.us/mnroad/data/pdfs/semidescription.pdf

Minnesota Department of Transportation (MnDOT). 2013. Moisture Sensing Documentation. MnDOT, St. Paul, MN. Retrieved from http://www.dot.state.mn.us/mnroad/pdfs/Moisture%20Sensing%20at%20MnROAD(working%20document).pdf

Minnesota Department of Transportation (MnDOT). 2015. An Overview of Mn/DOT's Pavement Condition Rating Procedures and Indices. MnDOT, St. Paul, MN. Retrieved from https://www.dot.state.mn.us/materials/pvmtmgmtdocs/Rating_Overview_State_2015V.pdf

Minnesota Department of Transportation (MnDOT). 2016. Standard Specifications for Construction. Section 2301: Concrete Pavement. MnDOT, St. Paul, MN. Retrieved from https://www.dot.state.mn.us/materials/concretedocs/Section_3_2301_Specifications.pdf

Missouri Department of Transportation (MoDOT). 2016. Supplemental Specifications to 2004 Missouri Standard Specifications for Highway Construction. Section 500: Concrete. MoDOT, Jefferson City, MO.

Monical, J., C. Villani, Y. Farnam, E. Unal, & W. J. Weiss. 2016. *Using Low-Temperature Differential Scanning Calorimetry to Quantify Calcium Oxychloride Formation for Cementitious Materials in the Presence of Calcium Chloride*. *Advances in Civil Engineering Materials, 5*(1), 142-156.

Montgomery, D. C. 2008. *Design and Analysis of Experiments*, Seventh Edition. John Wiley & Sons Inc., New York.

National Stone, Sand, and Gravel Association. 2013. *The Aggregates Handbook*, Second Edition, Sheridan Books, Alexandria, VA.

New York State Department of Transportation (NYSDOT). 2016. Standard Specifications – Construction and Materials. NYSDOT, Albany, New York.

Obla, K. H. 2012. Optimizing Concrete Mixtures for Performance and Sustainability. Paper presented at 2012 International Concrete Sustainability Conference, May 8, Seattle, WA.

Ohio Department of Transportation (ODOT). 2008. 2008 Construction and Material Specifications: ITEM 499 Concrete General. ODOT, Columbus, OH. Retrieved from http://www.dot.state.oh.us/Divisions/ConstructionMgt/OnlineDocs/Pages/2008OnlineSpecBook.aspx.

Pennsylvania Department of Transportation (PennDOT). 2009. Specifications: Section 704 – Cement Concrete (Publication No.408/2007-4). PennDOT, Harrisburg, PA.

Pickett, G. 1947. Effect of Gypsum Content and Other Factors on Shrinkage of Concrete Prisms. *Journal* of the American Concrete Institute, 44(10), 149–176.

Powers, T. C. 1948. A Discussion of Cement Hydration in Relation to the Curing of Concrete. (Research and Development Laboratories Department Bulletin RX025). Portland Cement Association, Skokie, IL.

Rached, M., D. Fowler, & E. Koehler. 2010. Use of Aggregates to Reduce Cement Content in Concrete. Paper presented at the Second International Conference on Sustainable Construction Materials and Technologies, June 28–30, Ancona, Italy.

Richardson, D. 2005. *Aggregate Gradation Optimization—Literature Search*. Missouri Department of Transportation, Jefferson City, MO.

Richardson, D. 2005. *Aggregate Gradation Optimization—Literature Search*. Missouri Department of Transportation, Jefferson City, MO.

Rudy, A. 2009. Optimization of Mixture Proportions for Concrete Pavements - Influence of Supplementary Cementitious Materials, Paste Content and Aggregate Gradation (PhD dissertation), Purdue University, West Lafayette, IN.

Sadati, S., M. Arezoumandi, K. H. Khayat, & J. S. Volz. (2016). Shear Performance of Reinforced Concrete Beams Incorporating Recycled Concrete Aggregate and High-Volume Fly Ash. *Journal of Cleaner Production, 115,* 284-293.

Shilstone, J. M. 1990. Concrete Mixture Optimization. *Concrete International, 12*(6), 33–39.

Taylor, P. 2014. *The Use of Ternary Mixtures in Concrete* (Technical Report). National Concrete Pavement Technology Center, Iowa State University, Ames, IA

Taylor, P. & X. Wang. 2014. *Concrete Pavement Mixture Design and Analysis (MDA): Factors Influencing Drying Shrinkage*. National Concrete Pavement Technology Center, Iowa State University, Ames, IA.

Taylor, P., E. Yurdakul, X. Wang, & X. Wang. 2015. *Concrete Pavement Mixture Design and Analysis (MDA): An Innovative Approach to Proportioning Concrete Mixtures*. National Concrete Pavement Technology Center, Iowa State University, Ames, IA.

Taylor, P., F. Bektas, E. Yurdakul, & H. Ceylan. 2012. *Optimizing Cementitious Content in Concrete Mixtures for Required Performance*. National Concrete Pavement Technology Center, Iowa State University, Ames, IA.

Taylor, P., X. Wang, & X. Wang. 2015. *Concrete Pavement Mixture Design and Analysis (MDA): Development and Evaluation of Vibrating Kelly Ball Test (VKelly Test) for the Workability of Concrete*. National Concrete Pavement Technology Center, Ames, IA.

Tia, M., Y. Liu, & D. Brown. 2005. *Modulus of Elasticity, Creep and Shrinkage of Concrete*. Department of Civil & Coastal Engineering, University of Florida, Gainesville, FL.

Virginia Department of Transportation (VDOT). 2016. Road and Bridge Specifications: Section 217.02: Materials (pp. 201-221). VDOT, Richmond, VA.

Vosoughi, P., & P. Taylor. 2017. *Impacts of Internal Curing on the Performance of Concrete Materials in the Laboratory and the Field*. National Concrete Pavement Technology Center, Ames, IA.

Vosoughi, P., S. Tritsch, H. Ceylan, & P. C. Taylor. (2017). *Lifecycle Cost Analysis of Internally Cured Jointed Plain Concrete Pavement.* CPTech Center, Ames, IA.

Walls, J., III, & M, R. Smith. 1998. Life-Cycle Cost Analysis in Pavement Design: In Search of Better Decisions (Interim Technical Bulletin, FHWA-SA-98-079). Federal Highway Administration, Washington, DC.

Wang, X. 2011. Drying Shrinkage of Ternary Blends in Mortar and Concrete (Master's thesis), Iowa State University, Ames, IA.

Wang, X., K. Wang, F. Bektas, & P. Taylor. 2012. Drying Shrinkage of Ternary Blend Concrete in Transportation Structures. *Journal of Sustainable Cement-Based Materials*, 1(1–2), 56–66.

Wang, X., K. Wang, P. Taylor, & G. Morcous. 2014. Assessing Particle Packing Based Self-Consolidating Concrete Mix Design Method. *Construction and Building Materials*, *70,* 439–452.

Wang, X., P. Taylor, E. Yurdakul, & X. Wang. 2017. An Innovative Approach to Concrete Mixture Proportioning. Submitted to *ACI Materials Journal*.

Wang, X., P. Taylor, E. Yurdakul, & X. Wang. (2018). An Innovative Approach to Concrete Mixture Proportioning. *ACI Materials Journal, 115*(5), 749-759.

Wassermann, R., A. Katz, & A. Bentur. 2009. Minimum Cement Content Requirements: A Must or a Myth? *Materials and Structures*, *42*, 973–982.

West, R., N. Tran, M. Musselman, J. Skolnik, & M. Brooks. 2013. *A Review of the Alabama Department of Transportation's Policies and Procedures for Life-Cycle Cost Analysis for Pavement Type Selection*. National Center for Asphalt Technology at Auburn University, Auburn, AL.

Whiting, D. & W. Dziedzic. 1992. Effects of Conventional and High-Range Water Reducers on Concrete Properties (Research and Development Bulletin RD107). Portland Cement Association, Skokie, IL.

Wilde, W. J., S. Waalkes, & R. Harrison. 1999. *Life-Cycle Cost Analysis of Portland Cement Concrete Pavements.* Center for Transportation Research, University of Texas at Austin, Austin, TX.

Wisconsin Department of Transportation. (WisDOT). 2018. 2018 Standard Specifications: Sections 415 and 501. WisDOT, Madison, WI.

Yurdakul, E., P. Taylor, H. Ceylan, & F. Bektas. 2013. Effects of Paste-to-Voids Volume Ratio on the Performance of Concrete Mixtures. *Journal of Materials in Civil Engineering*, *25*(12), 1840–1851.

APPENDIX A: Temperature Sensor Data

Temperature data obtained at Station 9390.8:

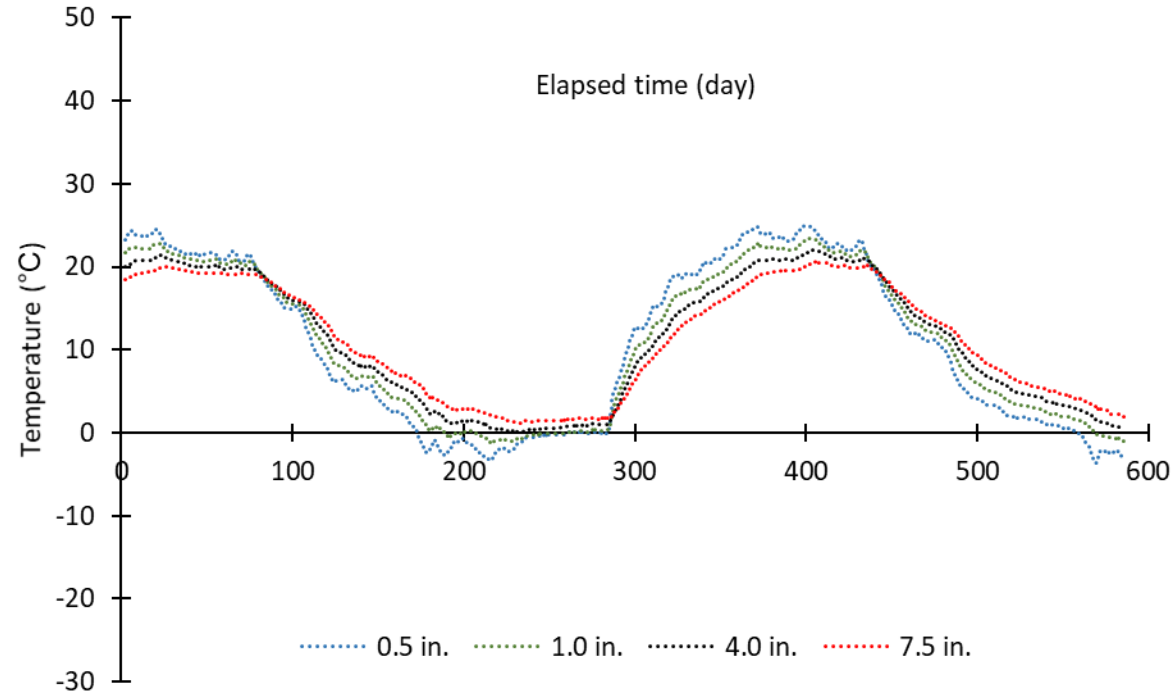

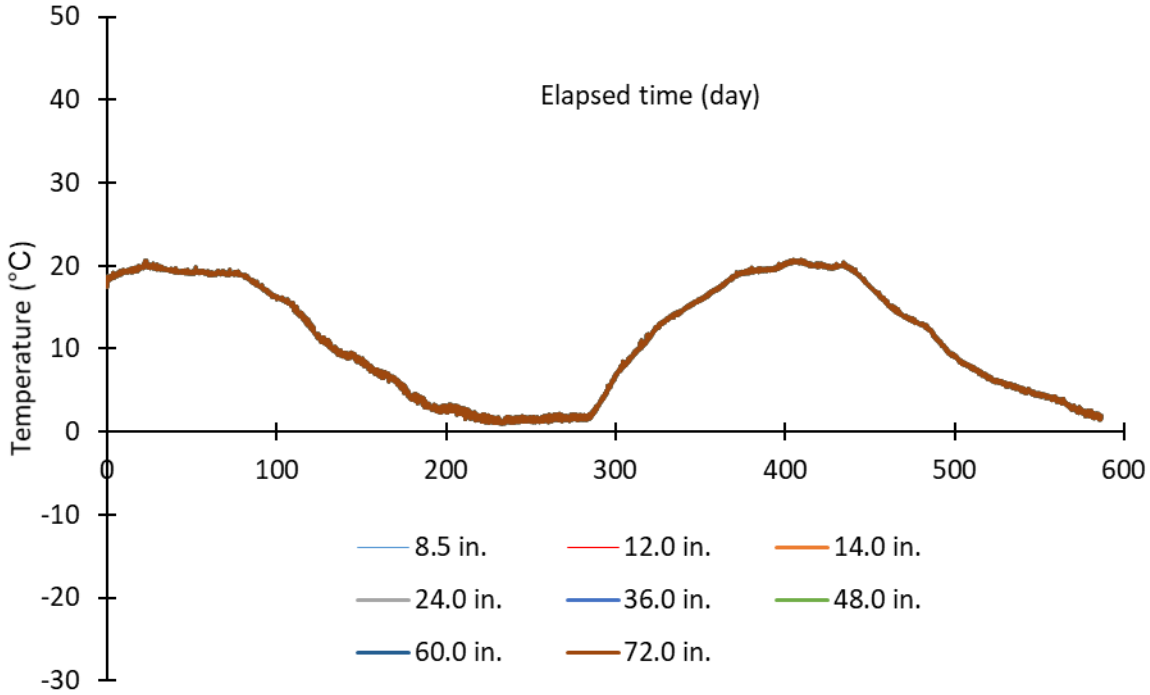

EW data obtained for sensors EC001 and EC002 embedded in concrete: